Rate Phenomena in Process Metallurgy

Viswanathan N. Nurni[a] and Bharath N. Ballal[b]
[a]Minerals and Metals Research Laboratory (MiMeR), Luleå University of Technology, Luleå, Sweden
[b]Centre of Excellence in Steel Technology (COEST), Department of Metallurgical Engineering and Materials Science, Indian Institute of Technology Bombay, Mumbai, India

NOMENCLATURE

$\vec{a}$ acceleration, $\mathrm{m\,s^{-2}}$

A area, $\mathrm{m^2}$

c sonic velocity, $\mathrm{m\,s^{-1}}$

C concentration, $\mathrm{mol\,m^{-3}}$

C specific heat capacity for condensed phases, $\mathrm{J\,kg^{-1}\,K^{-1}}$

C_1, C_2 integration constants

C_D discharge coefficient

C_p specific heat capacity at constant pressure, $\mathrm{J\,kg^{-1}\,K^{-1}}$

d diameter or distance, m

$\mathbb{D}$ mass diffusivity, $\mathrm{m^2\,s^{-1}}$

D diameter, m

D_b size of bubble, m

D_e equivalent diameter, m

D_p size of particles, m

D_{sph} diameter of sphere having equivalent volume, m

$\dot{E}$ rate of energy or power, W

$\hat{E}_f$ friction loss, $\mathrm{J\,kg^{-1}}$

E emissive power, $\mathrm{W\,m^{-2}}$

E energy, J

E_b emissive power of black surface at temperature T_b, $\mathrm{W\,m^{-2}}$

E^s energy in a system, J

F force, N

f_D D'Arcy's friction factor

f_F Fanning friction factor

F_{ij} view factor from surface "i" to "j"

g acceleration due to gravity, $\mathrm{m\,s^{-2}}$

$\dot{G}'''$ molar generation rate per unit volume, $\mathrm{mol\,s^{-1}\,m^{-3}}$

G mass flux, $\mathrm{kg\,m^{-2}\,s^{-1}}$

G total irradiation, $\mathrm{W\,m^{-2}}$

Gr Grashof number

Gz Graetz number

h height, m

h heat transfer coefficient, $\mathrm{W\,m^{-2}\,K^{-1}}$

h_{loc} local heat transfer coefficient, $\mathrm{W\,m^{-2}\,K^{-1}}$

$\hat{H}$ enthalpy per unit mass, $\mathrm{J\,kg^{-1}}$

H enthalpy, J

I intensity of radiation, $W\,m^{-2}\,m^{-1}\,sr^{-1}$

j diffusive mass flux in the mixture velocity frame, kg

J radiosity irradiation, $W\,m^{-2}$

J^* diffusive molar flux in the mixture velocity frame, kg

k D'Arcy's permeability, m^{-2}

k_f energy loss factor (friction loss)

k_m mass transfer coefficient, $m\,s^{-1}$

$\widehat{K.E}$ kinetic energy per unit mass, $J\,kg^{-1}$

L length, m

L_e equivalent length, m

L_{mf} length or height of fluidized bed at minimum fluidization, m

$\dot{m}$ mass flow rate, $kg\,s^{-1}$

m mass, kg

m_i mass fraction of species "i"

m^s mass in the system, kg

M molecular weight, $kg\,mol^{-1}$

Ma Mach number

n'' mass flux in the laboratory frame, kg

N'' molar flux in the laboratory frame, kg

Nu Nusselt number

$\mathbb{P}$ modified pressure, $\mathbb{P} = P + \rho gh$, where h is distance upward from a reference, Pa

P perimeter, m

P pressure, Pa

$\widehat{P.E}$ potential energy per unit mass, $J\,kg^{-1}$

Pr Prandtl number v/α

$\dot{q}$ rate of heat transfer, W

$\dot{q}_f$ rate of heat transfer through fin, W

$\dot{q}''$ heat flux, $W\,m^{-2}$

$\dot{q}''_x$ heat flux along x-coordinate, $W\,m^{-2}$

$\dot{Q}$ rate of heat (power), W

$\dot{Q}'''$ rate of thermal energy generation per unit volume, $W\,m^{-3}$

$\hat{Q}$ heat per unit mass, $J\,kg^{-1}$

r radial coordinate, m

r^* dimensionless radial coordinate

R radius, m

R thermal resistance, $K\,W^{-1}$

R universal gas constant, $J\,mol\,K^{-1}$

Ra Raleigh number

Re Reynolds number

Sc Schmidt number v/D

Sh Sherwood number

St Stanton number

t time, s

T temperature, K

T_0 initial temperature, K

T_∞ bulk temperature or temperature of approaching fluid, K

T_b bulk temperature, K

T_f film temperature, K

T_M melting temperature, K

T_s temperature at surface, K

$\hat{U}$ specific internal energy, J kg^{-1}

$\bar{v}$ average velocity, m s^{-1}

v velocity, m s^{-1}

v' fluctuating component of velocity in a turbulent flow, m s^{-1}

v^* mixture velocity, m s^{-1}

v_0 superficial velocity, m s^{-1}

v_∞ velocity of the approaching fluid, terminal velocity, m s^{-1}

v_b bubble velocity, m s^{-1}

v_{mf} superficial velocity at minimum fluidization, m s^{-1}

v_x velocity in x-direction, m s^{-1}

v_y y-component of velocity, m s^{-1}

v_z z-component of velocity, m s^{-1}

$\hat{v}_0$ unit vector along v_0, m s^{-1}

$\vec{v}_0$ superficial velocity vector, m s^{-1}

$\dot{V}$ volumetric flow rate, m

$\hat{V}$ specific volume, m^3 kg^{-1}

V volume, m^3

$\dot{W}$ rate of work, W

$\hat{W}$ work per unit mass, J kg^{-1}

x x-coordinate, m

x_i mole fraction of species "i"

y y-coordinate, m

z axial or z-coordinate, m

GREEK SYMBOLS

α radiation absorptivity

α thermal diffusivity, m^2 s^{-1}

β correction factor for kinetic energy in mechanical energy balance

γ adiabatic gas constant or heat capacity ratio

ΔH_M enthalpy of melting per unit mass, J kg^{-1}

Δr infinitesimal distance in r-coordinate, m

Δx infinitesimal distance in x-coordinate, m

Δy infinitesimal distance in y-coordinate, m

Δz infinitesimal distance in z-coordinate, m

δ boundary layer or film thickness, m

ε voidage in packed or fluidized bed

ε_b volume fraction of bubble phase in bubbling fluidized bed

ε_f effectiveness of a fin

ε_{mf} voidage at minimum fluidization

$\in$ emissivity

$\in$ mean roughness, m

$\in$ radiation: emissivity, m

κ thermal conductivity, W m^{-1} K^{-1}

κ_f film thermal conductivity, W m^{-1} K^{-1}

η_f efficiency of a fin

$\boldsymbol{\theta}$ dimensionless temperature difference

$\boldsymbol{\theta}$ polar angle in spherical coordinates

$\boldsymbol{\theta_0}$ dimensionless temperature difference at the center

$\boldsymbol{\mu}$ viscosity, Pa s

$\boldsymbol{\nu}$ kinematic viscosity, $\text{m}^2\,\text{s}^{-1}$

$\boldsymbol{\nu_T}$ turbulent kinematic viscosity, $\text{m}^2\,\text{s}^{-1}$

$\boldsymbol{\rho}$ density, kg m^{-3}

$\boldsymbol{\rho_s}$ density of solid, kg m^{-3}

$\boldsymbol{\rho_{solute}}$ mass concentration of solute, kg m^{-3}

$\boldsymbol{\sigma}$ Stefan–Boltzmann constant, $\text{W m}^{-2}\,\text{K}^{-4}$

$\boldsymbol{\tau_{rz}}$ shear stress or z-momentum flux transferred in r direction, N m^{-2}

$\boldsymbol{\tau_{yx}}$ shear stress or x-momentum flux transferred in y direction, N m^{-2}

$\boldsymbol{\dot{\phi}}$ rate of conservable entity, ϕ, entity s^{-1}

$\boldsymbol{\phi}$ any conservable entity or material property, entity

$\boldsymbol{\phi}$ azimuthal angle in spherical coordinates

$\boldsymbol{\phi}$ sphericity of particles

$\boldsymbol{\phi'''}$ any material property per unit volume, property m^{-3}

$\boldsymbol{\omega}$ solid angle, sr

4.1.1. INTRODUCTION

Process metallurgy is all about change: changing primary and secondary raw materials into valuable new materials, improving the quality of material products and process efficiencies, and reducing/eliminating the environment's impacts resulting from these changes. To bring about such desirable changes, it is necessary to understand what drives these processes as well as the rates at which these processes occur. This knowledge can be applied directly to control physical and chemical processes, or indirectly through improved design of equipment and technologies.

A process can be defined as that which brings about a change in the state of the system. The state of a system is defined using measurable properties that describe the system, such as density, pressure, temperature, and composition. An isolated system left to itself would eventually attain equilibrium, wherein the state of the system remains constant. A system at equilibrium can be altered through external factors imposed through the system boundary, such as work and/or transfer of mass and energy, so that the system seeks a new state of equilibrium. Therefore, a process can be viewed as the system response toward attaining equilibrium either left to itself (isolated systems) or being continuously altered through external means (closed and open systems). Using the principles of thermodynamics, which deal extensively with the definition of the state variables and equilibrium, the driving force for a process can be deduced by knowing how far away the current state of the system is from the state of equilibrium.

Thermodynamics does not, however, deal with rates at which processes occur. Rates are determined not only by the driving forces but also by the mechanisms of change and

resistances offered to change. To describe the rates of processes there is a need to understand and define how mass, work as well as energy are being exchanged through the system boundary with time as well as the rate at which the state of the system evolves toward equilibrium. Transport phenomena in conjunction with reaction kinetics deal with these aspects of processes. Through the system boundary, mass can be transferred by bulk flow or molecular mechanisms. Similarly, energy in the form of work, heat, or other forms can be exchanged through the system boundary. These aspects of transport of mass, momentum, and heat are dealt with together in this section as transport phenomena. The rates of processes involving chemical reactions are dealt in a separate section on reaction kinetics.

4.1.1.1. Importance of Transport Phenomena in Metallurgical Processing

Transport phenomena is an engineering science subject and are essential for understanding, designing, and operating most engineering processes. Therefore, it is an essential part of core curriculum of several engineering disciplines such as mechanical, civil, chemical, and materials engineering. The subject is dealt with in each case with a different emphasis in keeping the focus of the particular discipline. In this section, the importance of the subject for process metallurgy will be illustrated through a typical example of a packed bed reactor.

Consider a simple packed bed reactor shown in Figure 4.1.1. Hot gas is fed from the bottom of the reactor and is allowed to rise through the packed bed of particles, heating the bed. Gas flowing tortuously through the voids exerts a force on the particles, which in turn exerts an opposite force on the gas. To keep the gas flowing at a desired rate of throughput, therefore, a net force has to be exerted on the gas in the form of a pressure
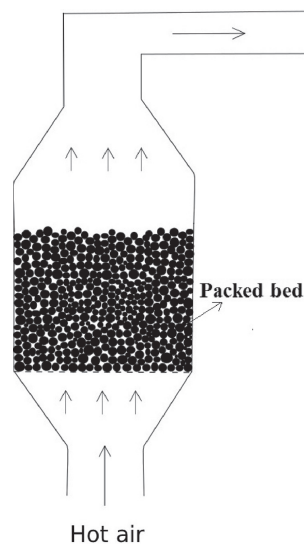

Figure 4.1.1 Example of a simple packed bed reactor.

difference across the bed. To estimate the required pressure difference, the forces acting on individual particles or an ensemble of them should be understood and quantified. Numerous detailed investigations have been carried out; the results of such investigations are rationalized through the principles of momentum transport.

As the hot gas flows up through the bed, the difference in temperature between the gas and the solid phases leads to thermal interactions, heat being transferred from the hot gases to the colder solids. This interaction, brought about at the basic level, by molecular phenomena, is dependent on the materials properties of the gas and the solid, on one hand, and the process conditions such as fluid flow, particle size and shape, and so on, on the other. The gas continuously cools as it moves up through the bed and the solid heats up. At the scale of the reactor, temperatures of the solids and the gas are seen to vary with time and position. Energy conservation principles have to be used to develop a methodology for predicting these changes in the context of heat transfers at the particle level. This understanding and these methodologies are rationalized into the principles of heat transfer.

In a reactor such as the blast furnace, the gases and the solids react chemically. Hot gas generated in front of the tuyeres located near the bottom of the furnace consists primarily of CO, H_2, and N_2. A mixture mainly of iron ores and coke forms the slowly descending packed bed of solids. Gas moves at great velocities covering a height of 25 m in 4–5 s. CO and H_2 in the gas chemically react with the solids resulting in the overall reduction of the ore to lower oxides and eventually in the formation of iron metal. The rates of the reduction processes determine evolution of the compositions of the solids and the gases. Since the ore exists as particles of considerable size (10–40 mm), the reductant specie, CO and H_2 have to be transferred from the flowing gas to the oxides deep within the particles. The rates of this transfer are determined by material properties and the process conditions such as flow velocities, particle size and shape, and the pore structure. The results of experimental and theoretical studies of all such phenomena are organized into the area of mass transfer. The rates of the chemical reactions at the reaction interface, between iron and its oxide, for example, are the subject matter of reaction kinetics.

In the blast furnace, there are many other processes taking place. For example, the reduced iron would ultimately melt lower down in the furnace due to the high temperatures in this region. Gangue materials from the ore and ash from coke, along with the added flux also melt down forming a slag. These two immiscible liquids trickle down the coke bed as drops and rivulets to collect at the bottom of the furnace to be taken out periodically/continuously. The rates of trickle flow of the liquid phases are important, since inadequate rates of trickling at high rates of production can lead to liquid accumulation in the bed and process break-down. To understand all these phenomena it is necessary to study transport phenomena.

Another example of a packed bed reactor is the iron ore-sintering machine, wherein air is made to flow down through a packed bed made of a mixture of ore, coke, and

limestone fines, by applying suction at the bottom. Once the coke at the top is ignited, the complex interchange of heat and mass between the gases and the solids results in the progressive movement of the flame front down through the bed. The high temperatures generated from combustion lead to incipient fusion in the solid particles and agglomeration to larger lumps, accompanied by complex reactions of reduction, oxidation, and slag formation. Though the process itself looks substantially different from the blast furnace process, the underlying phenomena have much similarity and are described by similar principles of transport phenomena and reaction kinetics.

Thus the principles of transport phenomena are integral to the design, operation, and control of engineering processes, and metallurgical processes are no exception.

4.1.1.2. Basic Methodologies in Transport Phenomena

Transport phenomena consist of broadly three important topics: momentum transfer or fluid dynamics, heat transfer, and mass transfer. The methodology used to describe transport phenomena consists of conservation equations, especially applied to open systems, coupled with constitutive relations describing the physics of specific phenomena. As these methodologies are nearly the same for fluid flow, heat transfer, or mass transfer, Bird *et al.* [1] integrated these topics and formulated a unified approach, which they termed transport phenomena. Since then, chemical engineers have preferred to treat these topics together in this fashion. Mechanical and civil engineers, however, regard these as three separate topics. Process metallurgists, along the lines of chemical engineers, have preferred the unified approach. In this section, the important concepts and methodologies generic to transport phenomena are discussed.

The concept of a continuum is the fundamental basis on which much of the subject of transport phenomena is developed. All materials, including fluids, are made of discrete atoms or molecules with large amount of void space between them. The continuum hypothesis, however, treats materials as continuous media and correspondingly properties are defined as varying spatially in a continuous manner. The hypothesis is valid only when a derivative of any material property, say ϕ, can be defined as

$$\phi''' = \frac{\mathrm{d}\phi}{\mathrm{d}V} = \lim_{\Delta V \to \lambda^3} \frac{\Delta \Phi}{\Delta V}$$

and that λ is small enough for this derivative to be meaningful in the scale of the macroscopic system under study, but is still large enough that the discreteness at the molecular level is averaged into a continuum. This approximation is almost always valid for the flow of liquids since the molecular dimensions are very small (the exception to this occurs for flow of liquids through channels of nanometer scale and below). In gases, the mean free path, i.e., the average distance traversed by a molecule between two consecutive collisions, should be small compared to the system dimensions, for example, the diameter of the pipe

through which the gas flows. If the mean free path is comparable to the scale of the system of interest, then the frequency of collisions of molecules with the walls of the system will be comparable to those among molecules themselves. Continuous variation of a property such as density across the cross section of the pipe then becomes meaningless. This phenomenon is characterized by Knudsen number (named in honor of the scientist Knudsen, for his contributions in this field). The Knudsen number is defined as the ratio of the mean free path of the gas molecules at a particular state of the system under study to the characteristic dimension of the system. In many engineering situations, the Knudsen number is very low and hence the system can be treated as a continuum. However, the Knudsen number can become significant, especially when considering the flow of gases under vacuum or in fine pores. In this chapter, only the continuum approach has been used. The reader may refer elsewhere [2] for other approaches.

The principle used to describe the conservation of mass, energy, momentum, etc., can be illustrated using the example of filling and draining of water in a tank. The variation of water level in the tank with time when both inlet and outlet valves are open can be calculated using the following simple equation of volume conservation.

The rate of change volume of water in the tank $=$ Volume flow rate in

$-$Volume flow rate out

This principle can be extended to any generic conservable entity say, ϕ, as

Rate of accumulation of ϕ $=$ Rate at which ϕ comes into the system$-$
Rate at which ϕ goes out of the system$+$ (4.1.1)
Rate at which ϕ is generated within the system

The example below illustrates the use of the principle for predicting changes in composition during change of ladle and grade in the continuous casting of steel.

Example 4.1.1

Figure 4.1.2 is a schematic of a continuous steel casting machine showing the ladle, the tundish, and the mold. The hot liquid steel is delivered in batches to the casting machine by the ladle. The tundish, the intermediate reservoir primarily for flow control, supplies liquid steel continuously to the mold through a nozzle. The continuous casting machine is operated without interruption even when an empty ladle is replaced by a newer ladle. If the steel in this new ladle is of different grade from the previous one, intermediate cast slabs have composition deviating significantly from both the desired grades.

Let a thin slab-casting machine operate at 5 m min^{-1} to produce slabs of cross section 1500 mm $\times$ 50 mm. The machine has a tundish with a capacity of 5 tonnes. Estimate the amount of slab to be discarded, if the operator accepts a variation of 20% in grade. Assume as a first approximation that the amount of metal in the tundish as well as the casting speed remains the same during the transition from one grade to the other. Additionally, assume
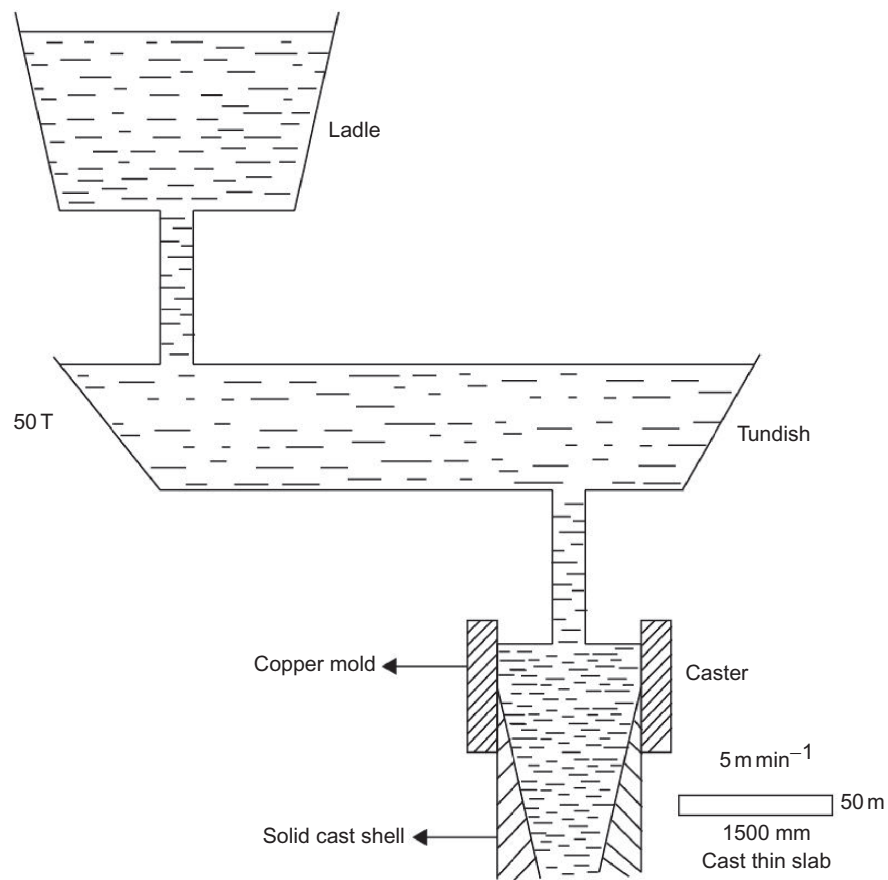
Figure 4.1.2 Schematic of a continuous metal caster.

that the tundish is well stirred and that the composition of the steel is uniform throughout the tundish at any instant of time.

Solution

Let us denote the composition of any particular solute in the steel by $\rho_{\text{solute},1}$ and $\rho_{\text{solute},2}$ (expressed as mass per unit volume of liquid steel) for grades 1 and 2, respectively. To find the mass of slab to be discarded, the variation of composition in the tundish, ρ_{solute}, with time should be examined. Since the composition in the tundish is uniform, the composition of steel that exits to the mold from the tundish at any instant of time would be the same as that in the tundish. If V is the volume of the liquid steel in the tundish and $\dot{V}$ the volumetric flow rate of steel flowing into as well as out of the tundish (both V and $\dot{V}$ are assumed to remain constant during ladle exchange), the conservation principle to the solute in the tundish yields,

$$V\frac{\mathrm{d}\rho_{\text{solute}}}{\mathrm{d}t} = \dot{V} \times \rho_{\text{solute,inlet}} - \dot{V} \times \rho_{\text{solute}}$$

Rate of accumulation of solute = Rate in : solute − Rate out : solute

The composition of the solute in the tundish changes as soon as the transition to grade 2 starts. At $t=0$, the composition of the solute in the tundish would be that corresponding to grade 1, i.e., $\rho_{\text{solute,1}}$. The composition of the liquid steel reaching the inlet of the tundish will remain that corresponding to grade 2, i.e., $t \geq 0$, $\rho_{\text{solute,inlet}} = \rho_{\text{solute,2}}$. Solution of the differential equation with the initial condition is

$$\frac{\rho_{\text{solute}} - \rho_{\text{solute,2}}}{\rho_{\text{solute,1}} - \rho_{\text{solute,2}}} = \exp\left(-\frac{\dot{V}}{V}t\right)$$

As per the problem posed, a composition (C) variation up to $0.8\rho_{\text{solute,1}} + 0.2\rho_{\text{solute,2}}$ is accepted as grade 1 and correspondingly $0.2\rho_{\text{solute,1}} + 0.8\rho_{\text{solute,2}}$ is accepted as grade 2. These correspond to $\frac{\rho_{\text{solute}} - \rho_{\text{solute,2}}}{\rho_{\text{solute,1}} - \rho_{\text{solute,2}}}$ being 0.8 and 0.2, respectively. Hence, from the solution of the differential equation, the time duration when $\frac{\rho_{\text{solute}} - \rho_{\text{solute,2}}}{\rho_{\text{solute,1}} - \rho_{\text{solute,2}}}$ changes from 0.8 to 0.2 can be calculated knowing the volume of the steel in the tundish and the volumetric flow rate of steel through the tundish. For a liquid steel of 5 tonnes, the volume will be approximately 7.1 m^3 and flow rate of liquid steel can be estimated from the casting speed and cross section of slab as 0.00625 m^3 s^{-1}. Thus, the time period over which the composition of liquid steel in the tundish will be unacceptable is about 1570 s and the corresponding weight of slab to be discarded is 69 tonnes.

The generic conservation Equation (4.1.1) is now examined more closely for a system with a finite volume and definite boundaries. Boundaries are those through which the system interacts with the surroundings. The term on the left-hand side represents the accumulation of the conservable entity, ϕ, in the system. Generally, the entity to be conserved is expressed as a quantity per unit volume of the system. For example, in case of mass conservation, the mass per unit volume, density (ρ), can be used in the conservation expression. Similarly, momentum per unit volume (ρv), enthalpy per unit volume (ρH), and species density of any species "i" (ρ_i) can be used in the conservation equations for momentum, heat, and species "i," respectively, in a system. The first two terms together on the right-hand side of Equation (4.1.1) denote the net amount of entity ϕ entering the system. Conservable entity is transported through the system boundary generally by two mechanisms. One, by virtue of the bulk movement of material through the boundary, the associated momentum, enthalpy, or species in the material are transported along with it. This is termed as advective transport. Second, there can be transfer of conservable entity, even in the absence of the macroscopic transport because of molecular or atomic interactions in the material. For example, heat

can be transported through the system boundary without having any bulk movement of materials through the boundary. Such transport is termed as diffusive transport. This transport originating from molecular or atomic interactions is specific to a particular material as well as to the entity being transported. Therefore, this diffusive transport is defined using constitutive laws, such as, Fourier's law of heat conduction. The last term in the conservation Equation (4.1.1) denotes the bulk generation term, generally expressed as the rate of generation per unit volume of the system. In case of conservation of heat, it may denote heat liberated due to bulk reaction, or dissipation of mechanical energy to internal energy. Similarly, there may be body forces acting on the system due to gravity, electromagnetic field, etc., leading to generation of momentum according to Newton's second law of motion. Physics specific to these interactions are described quantitatively by the generation terms.

The principle of conservation can be applied at various scales depending on the information required. The simple example from continuous casting discussed above illustrates the conservation principle being applied in a macroscopic scale. For a flow of fluid through a pipe, if only the pressure drop required to maintain a particular flow rate is desired, the mechanical energy conservation principle is applied at the scale of pipe. The effect of finer details of flows is accounted for through empirical correlations, permitting fast and cost-effective solution to engineering design problems. However, if the details of the flow profile in the system are required, the conservation equations need to be applied at an infinitesimal or differential scale. Such formulations for real systems often lead to nonlinear partial differential equations, which necessitate sophisticated numerical techniques to obtain solutions.

4.1.2. MOMENTUM TRANSFER

A large number of transport processes involve fluids: liquids and gases. In comparison to rigid solids, fluids can flow, i.e., velocity variations can occur within the body of the fluid. Flow of the fluid has large influence on transport of heat and mass. In transport phenomena, therefore, description of flow becomes an integral part of analysis of most processes.

A packet of fluid in a flow field can be viewed as that carrying momentum or as being characterized by its kinetic energy. Flow takes place under the influence of forces acting on it. The fluid flow can be analyzed either by performing momentum balances, considering forces as those that generate momentum according to Newton's second law of motion or by performing energy balances according to first law of thermodynamics considering the work done by the forces on the system. Apart from forces due to external factors, such as pressure and gravity, internal forces resisting flow variations develop within the body of the fluid due to "viscous" phenomena. The Laws of motion and the relationships describing the viscous phenomena are the constitutive equations needed for fluid flow descriptions.

4.1.3. FLOW DESCRIPTION

Elastic solids resist a shear force by a shear deformation, i.e., a shear stress resisting the external force is developed within the body due to the deformation, till a stable equilibrium is reached. A simple fluid cannot resist a shear force by a static deformation; it continues to deform. The fluid develops a resisting shear stress by the rate of deformation and comes to a dynamic equilibrium (there are complex fluids that can resist shear elastically up to some limiting value). This implies that a static fluid cannot have any shear stresses present in it; only normal stresses are present. It can be proved using simple force balance that this normal stress is the same irrespective of direction and hence is described by a scalar entity called pressure (the reader can find the proof in any text book on fluid mechanics). The normal force on any surface is calculated by the product of pressure and surface area, the latter being a vector.

Some of the terminologies used to describe fluid flow are given below.

4.1.3.1. Steady and Unsteady Flows

A system is at steady state when all the properties at any point (some of these such as velocity to be defined with respect to a frame of reference) in the system remain constant with respect to time. If this condition is not satisfied, the system is said to be unsteady or in a transient state. In general, a property is a function of space and time, i.e., $\phi(x,y,z,t)$. For a steady-state process, the partial derivative $\frac{\partial \phi}{\partial t}$ remains constant everywhere in the system.

4.1.3.2. Uniform and Nonuniform Flows

Flow is uniform if properties associated with flow, such as velocity, momentum, and density, are the same everywhere, at any instant of time. That is, partial derivatives with respect to spatial coordinates are zero. Evidently, uniform flows can be unsteady, and steady flows can be nonuniform.

A flow that is uniform with respect to all the three coordinates gives a rigid body motion. More often, the definition refers to uniformity with respect to one or two coordinates, as for example, "uniform across the cross section."

4.1.3.3. Streak Lines, Particle Paths, and Stream Lines

Flows are often visualized, experimentally or in graphical descriptions, through lines of flow. These lines are dependent on the view point or the experimental method of visualization. One can visualize a flow by continuous release of a visual trace into the flowing fluid from a point fixed in space. Each packet of tracer emanating from the point at successive times forms a continuous line. If an "instantaneous" photograph of this

is taken, a streak line is obtained. A thin smoke trail from a chimney top in slowly moving air is an example.

Another way of visualization is to release a single neutrally buoyant tracer particle into the flow from any point at a given instant of time. The particle will move along with the fluid tracing a path in the flow field. This can be captured experimentally with time-lapse photography, i.e., by keeping the aperture of the camera open for a length of time. These lines are called particle paths. In a steady flow, streak lines and particle paths superimpose on each other. This need not be the case for unsteady flows.

In contrast to these two observable lines, the streamline is a mathematical construction: it is a continuous line for which tangent at every point gives the direction of velocity. Evidently there is no flow across a streamline (in two-dimensional (2D) view) or across a stream surface formed by series of stream lines. Streamlines cannot be visualized, except in the case of steady flows where it is identical to the streak lines and particle paths.

4.1.3.4. Eulerian and Lagrangian Points of View

Since properties at a point depend on the coordinates of the point, and coordinates depend on the frame of reference, expressions of flow descriptions can be different in different frames of reference. Frames of reference can be arbitrary. Two types are of specific interest.

A Eulerian frame is one that is fixed with respect to the laboratory and the fluid flows relative to it. This is the familiar frame of reference. Fluid flow past a given fixed point, and therefore a property at that point refers to different fluid elements at different times. In the Lagrangian view point, the frame of reference moves along with the fluid element. A property at a point with respect to this frame of reference refers to the same fluid particle over time.

These two view points are equivalent and are related to each other through the fluid velocity vector. Selection of either of them depends on convenience. Take the example of a bubble rising up steadily in a fluid. The flow around the bubble can be described from a Eulerian frame of reference fixed with respect to the container, or a Lagrangian frame fixed to the leading point on the bubble. The former view point will describe the flow as unsteady, whereas the Lagrangian frame depicts steady flow in the neighborhood of the bubble.

4.1.3.5. Laminar and Turbulent Flows

One of the most influential scientific papers on fluid dynamics is by Reynolds [3,4]. In his classic experiment (the experimental set up is still preserved at the Manchester University, United Kingdom), he injected dye into a stream of water flowing through a pipe. His observations have been reproduced from his original paper in Figure 4.1.3.

Below a critical velocity, he observed laminar flow where the dye streak remained straight. Above the critical velocity, the flow exhibited a transition state where the
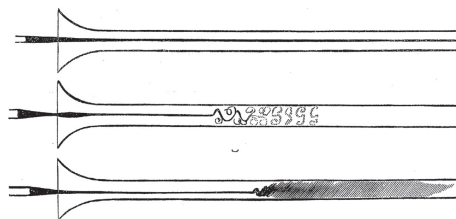
Figure 4.1.3 Reynolds' experimental observations [3].

dye streak became wavy. At high flow velocities, the dye mixed significantly with the water within a short distance and this is termed as turbulent flow.

Thus, flow of a fluid can take place in two distinct regimes depending on the intensity of flow and system geometry: laminar and turbulent. At low velocities, the flow seems to be "orderly": tracer particles traveling along smooth lines seem to indicate the flow consists of layers (lamella) sliding past each other. This is laminar flow. As the flow rate is increased, however, the flow becomes "turbulent": the particles seem to travel in random paths, though the overall direction of travel is in the direction of mean flow. The flow consists of "eddies," fluid packets of various sizes making circular motion; it is difficult to visualize the flow using streak lines, since the tracer quickly dissipates due to the eddies. Whether the flow is laminar, turbulent, or in a transition regime between the two is determined by a characteristic dimensionless number called the Reynolds number, Re (see Section 4.1.8 for further discussion).

$$Re = \frac{\rho VL}{\mu}$$

where V is the characteristic velocity, L is a dimension characterizing the system size, ρ and μ are the fluid density and viscosity, respectively. Over a small range of Re values, the flow changes from laminar flow (low Re) to turbulent flow.

Reynolds in his experiments of flow through tubes found that the critical velocity beyond which flow changes from laminar to turbulent corresponds to a Reynolds number of approximately 2000. Most flows of engineering interest are turbulent. More discussions on these aspects are presented in later sections (Section 4.1.15.1).

4.1.3.6. Incompressible and Compressible Flows

The densities of fluids change with pressure, i.e., all real fluids are compressible. However, for many engineering flows, the change in density due to change in pressure during flow is small enough to be neglected. Such flows are classified as incompressible flows. The incompressible flow approximation leads to large simplifications. Using some simple reasoning, the conditions where a flow can be considered incompressible can be determined.

In a flowing fluid with velocity varying between 0 and V, the pressure variation is of the order of $\frac{\rho V^2}{2}$ (description on this term derived from energy balance is presented in Section 4.1.4). The relative density change expected in ideal gases under isothermal conditions is therefore:

$$\frac{|\Delta\rho|}{\rho} = \frac{|\Delta P|}{P} \approx \frac{1}{2}\frac{\rho v^2}{P} = \frac{1}{2}\frac{\rho v^2}{\rho RT/M} \tag{4.1.2}$$

The velocity of sound under isothermal conditions is given by $c = \sqrt{\frac{RT}{M}}$ and hence,

$$\frac{\Delta P}{P} \approx \frac{1}{2}\frac{v^2}{c^2} = \frac{1}{2}Ma^2 \tag{4.1.3}$$

where the ratio of the velocity of the fluid to the speed of sound is termed the Mach number, Ma. For a $\frac{\Delta\rho}{\rho}$ of 0.05, i.e., for a 5% change in density, the value of Mach number is approximately 0.3. Thus, for speeds where $Ma < 0.3$, the change in density will be $<5\%$, and assuming the fluid to be incompressible is a reasonable engineering approximation. The orders of magnitude of the associated errors remain the same in non-isothermal flows too. Once fluid velocities reach values beyond that corresponding to Mach number of 0.3, the change in density due to pressure difference becomes significant. In such flows, the equation of state, which relates the density with pressure and temperature, must be considered. Generally in such flows, a change in density results in significant change in temperature and it is necessary to examine both flow and heat transfer together to arrive at a better understanding. If the velocities are less than that of sound in the fluid, $Ma < 1$, they are termed as subsonic flows and those beyond the velocity of sound are classified as supersonic flows. In process metallurgy, most of the flows are incompressible. However, in some processes, such as basic oxygen furnace (BOF) wherein supersonic nozzles are used to inject oxygen into the liquid steel, the gas flows are compressible. Throughout this section, most of the flows discussed are incompressible; a separate section has been devoted to compressible flows with specific focus on the supersonic nozzle for oxygen injection in BOF.

4.1.4. OVERALL ENERGY BALANCE

In order to perform the overall energy balance in a flowing fluid system, it is generally necessary to consider the following energies associated with the fluid: (1) the kinetic energy arising out of flow velocities, (2) the potential energy due to the gravitational field, and (3) the internal energy. In addition, the system can exchange energies with the surroundings through the boundary as work done against pressure, other forms of work through pumps and turbines, or as heat. Other forms of energies, such as
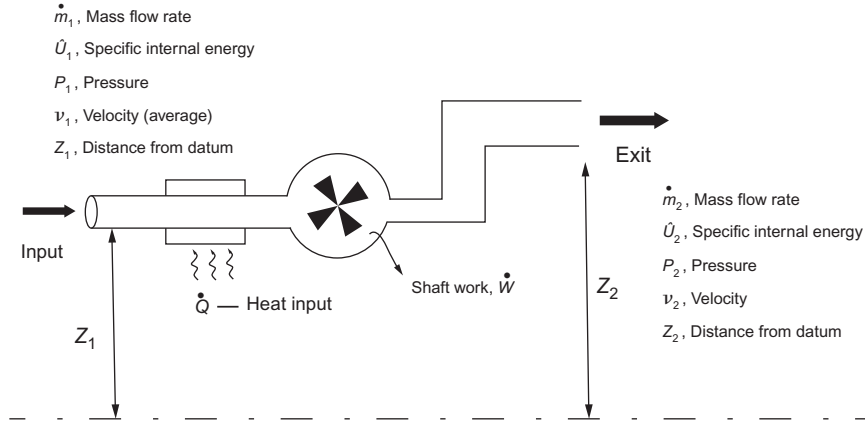
Figure 4.1.4 Schematic of a flowing system performing shaft work using a heat source.

chemical, electrical, and magnetic, can be further added depending on the system; for brevity, these additional terms are not considered in the present discussions.

Let us consider a general system shown in Figure 4.1.4, wherein a fluid enters and leaves the system at mass flow rates of $\dot{m}_1$ and $\dot{m}_2$, respectively (there can be multiple inlets and outlets, without loss of generality). The fluid carries with it internal energy, kinetic energy, and potential energy. At the inlet and the outlet P–V kind of work needs to be done to push the fluid through the boundaries. The fluid also performs shaft work continuously at the rate of $\dot{W}$ on the surroundings (for example, in driving a turbine). During its transit through the system, the fluid receives heat at the rate of $\dot{Q}$ from the surroundings. Let P_i, $\hat{U}_i$, v_i, and ρ_i represent pressure, specific internal energy (internal energy per unit mass), velocity, and density at any point "i." Let z represent the height.

If E_T represents the total energy of the system at any instant of time, then conservation equation gives,

$$
\frac{\mathrm{d}E_T}{\mathrm{d}t} = \overbrace{\dot{m}_1\left(\hat{U}_1 + \frac{1}{2}\frac{v_1^2}{\beta_1} + gz_1\right) - \dot{m}_2\left(\hat{U}_2 + \frac{1}{2}\frac{v_2^2}{\beta_2} + gz_2\right)}^{\text{Net advective energy input}}
$$
$$
+ \underbrace{\frac{P_1\dot{m}_1}{\rho_1} - \frac{P_2\dot{m}_2}{\rho_2}}_{P-V\ \text{work}} + \overbrace{\dot{Q}}^{\text{Heat input}} - \overbrace{\dot{W}_S}^{\text{Shaft work}} \qquad (4.1.4)
$$

If the system is at steady state, LHS is zero, and $\dot{m}_1 = \dot{m}_2 = \dot{m}$. Then, after dividing by $\dot{m}$,

$$
\left(\hat{U}_2 - \hat{U}_1\right) + \left(\frac{1}{2}\frac{v_2^2}{\beta_2} - \frac{1}{2}\frac{v_1^2}{\beta_1}\right) + (gz_2 - gz_1) + \left(\frac{P_2}{\rho_2} - \frac{P_1}{\rho_1}\right) - \hat{Q} + \hat{W}_S = 0 \qquad (4.1.5)
$$

where $\hat{Q} = \frac{\dot{Q}}{\dot{m}}$ and $\hat{W}_S = \frac{\dot{W}_S}{\dot{m}}$. The terms in the above equation have units of J kg^{-1}. Let us look at some of these terms closely.
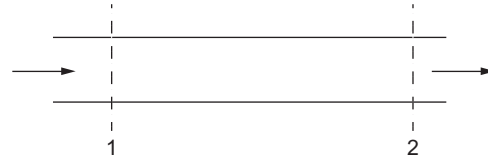
Internal energy is the energy associated with a mass of fluid excluding its kinetic and potential energies. Normally internal energy change manifests itself in the form of temperature change and is calculated as sensible heat using specific heat C_v. Energy can also be stored in the system by phase change and chemical reactions.

Potential energy per unit mass with respect to a datum is gz.

Kinetic energy per unit mass is $\frac{1}{2}v^2$. If the velocity across a cross section is uniform at $\overline{v}$, the total kinetic energy flow across the cross section is $\frac{\dot{m}\overline{v}^2}{2}$. If the flow, however, is non-uniform with the velocity averaged over the area of cross section A being $\overline{v}$, then the total kinetic energy crossing the section is $\int_A \frac{v^2}{2}(v\rho dA)$. This term is represented as $\frac{1}{2\beta}\dot{m}\overline{v}^2$, where β is the correction factor that accounts for nonuniformity in flow. Most engineering flows in conduits are turbulent and the flow is nearly uniform except very close to the boundaries, and therefore $\beta \approx 1$. In laminar flow, β is significantly lower than 1; for steady flow through circular pipes $\beta = 0.5$.

Equation (4.1.5) describes the conservation principle from an Eulerian view point, i.e., the system is fixed with respect to the laboratory, and counting is done at the boundary. One would like to use such an equation for design purposes: to estimate, for example, the pressure drop that needs to be applied across a length of piping to maintain a desired flow rate of water. The presence of an internal energy term here, however, is inconvenient. In most engineering situations, one is neither interested in specifying the internal energy changes and the associated temperature changes, nor in tracking them; these are often very small anyway. Neglecting the term, however, can give meaningless solutions, as the following example illustrates.

Consider flow of an incompressible fluid such as water through a horizontal pipe of constant cross section (see Figure 4.1.5). Let the wall be adiabatic $\left(\widehat{Q} = 0\right)$ and no shaft work is done inside the pipe between sections 1 and 2 ($\hat{W}_S = 0$). Since the fluid is incompressible ($\rho_1 = \rho_2$), flow rate and average velocities are constant ($\dot{m}_1 = \dot{m}_2 = \dot{m}$, $\overline{v}_1 = \overline{v}_2$). Then Equation (4.1.5) gives

$$\left(\frac{P_2}{\rho_2} - \frac{P_1}{\rho_1}\right) = \left(\hat{U}_2 - \hat{U}_1\right)$$

Figure 4.1.5 Flow through a straight pipe.

It is known that a pressure difference must be applied to maintain a flow in a pipe to counter the viscous resistances. This work done against the pressure difference is converted irreversibly into an increase in the internal energy, which manifests itself as a barely perceptible rise in temperature. Unless this rise in temperature is measured, it is not possible to estimate the pressure difference needed to maintain a desired flow rate.

The increase in internal energy arises from the irreversible conversion of mechanical energy to internal energy, due to the viscous phenomena. The viscous phenomena, as discussed later, are related to the details of the flow field inside the system, and an equation developed by measurements at the boundary cannot capture this phenomenon. To do this, a Lagrangian approach must be used: consider a packet of fluid as a "closed system" and perform an energy balance on it as it travels from the inlet to the outlet.

Let the packet of fluid be of unit mass, having internal energy $\hat{U}_1$ and $\hat{U}_2$, and density ρ_1 and ρ_2, at the inlet and outlet, respectively. Due to change in density, this packet would have changed its volume and therefore performed P–V work on its surroundings. If the heat input $\dot{Q}$ in the system has been distributed uniformly, the packet would have received a heat of $\hat{Q}$.

Though the first law of thermodynamics is about conservation of total energy, scientists concerned with material behavior often restrict themselves to internal energy alone, ignoring the contributions from kinetic and potential energies as follows

$$\hat{U}_2 - \hat{U}_1 = \hat{Q} - \hat{W}_{P-V} = \hat{Q} - \int_1^2 P \, d\hat{V} = \hat{Q} - \int_1^2 P \, d\left(\frac{1}{\rho}\right) \qquad (4.1.6)$$

where, $\hat{V}$ is the specific volume or reciprocal of the density, ρ, and the P–V work has been assumed to be reversible.

This assumption works fine in cases where the mechanical energies are only associated with the position and movement of the system as a whole, and remain uncoupled with the internal energy of the material. If there are relative movements within the system itself, however, there is dissipation of mechanical energy to internal energy, and in a balance written for internal energy alone this should appear as a generation term. If the rate of conversion of mechanical energy into internal energy (per unit mass) within the body of the fluid is $\hat{E}_f$, Equation (4.1.6) is modified as:

$$\hat{U}_2 - \hat{U}_1 = \hat{Q} - \int_1^2 P \, d\left(\frac{1}{\rho}\right) + \hat{E}_f \qquad (4.1.7)$$

Substituting Equation (4.1.7) into Equation (4.1.5), and noting that $\frac{P_2}{\rho_2} - \frac{P_1}{\rho_1} = \int_1^2 d\left(\frac{P}{\rho}\right)$, the following expression is obtained.

$$\frac{1}{2}\frac{v_2^2}{\beta_2} - \frac{1}{2}\frac{v_1^2}{\beta_1} + g(z_2 - z_1) + \int_1^2 \left(\frac{1}{\rho}\right) dP + \hat{W} + \hat{E}_f = 0 \qquad (4.1.8)$$

If $\hat{E}_f$ can be estimated from the details of the flow, Equation (4.1.8) is an extremely useful equation for design and analysis. This is the generalized form of the overall or the integral energy balance equation.

For laminar flows, depending on the system geometry and the fluid, flow details (flow structures) can be predicted from first principles. However, as the velocities become larger, these structures become quite complex and manifest as turbulence. Prediction of these turbulent flow structures from first principles is still an ongoing active research topic for the scientific community. For many systems of engineering interest, however, a large body of experimental data exists, and these have been coded into empirical equations for $\hat{E}_f$, using the principles of dimensional analysis and similarity.

In addition, a few remarks need to be made regarding the term, $\int_1^2 \frac{1}{\rho} dP$ in Equation (4.1.8). This term, generally termed as flow work, is path dependent. For incompressible fluids, the density does not change during flow, and hence this term becomes $\frac{\Delta P}{\rho}$. However, for compressible flows, the path by which the compression–expansion takes place needs to be defined. Idealized paths, such as isothermal or adiabatic, are frequently used to describe many compressible flows. In a later section, design of a supersonic nozzle for steel-making operations is discussed using such a simplified analysis.

As a first approximation, many systems can be analyzed by neglecting the friction loss term, i.e., $\hat{E}_f$ in Equation (4.1.8). In thermodynamic terminology, friction loss is an irreversible phenomenon. Hence, a flowing system without having friction losses is an idealized system and can be termed as a reversible system. For an incompressible fluid flowing without having any friction loss and shaft work, Equation (4.1.8) can be rewritten as

$$\frac{1}{2}v_2^2 + gz_2 + \frac{P_2}{\rho} = \frac{1}{2}v_1^2 + gz_1 + \frac{P_1}{\rho} \qquad (4.1.9)$$

This equation is the well-known Bernoulli's equation, named after the famous scientist Bernoulli.

The mechanical energy balance equation can also be written in differential form as

$$v\frac{dv}{\beta} + g\,dz + \frac{1}{\rho}dP + d\hat{W} + d\hat{E}_f = 0 \qquad (4.1.10)$$

Let us look at a simple application of this equation in a continuous caster. In order to make clean steel, it is essential that oxygen pick-up into the liquid steel is minimized. Any dissolved oxygen in steel can result in inclusions or porosity in the cast product that can have adverse effect on further processing of solid steel as well as on the mechanical properties of the end product.
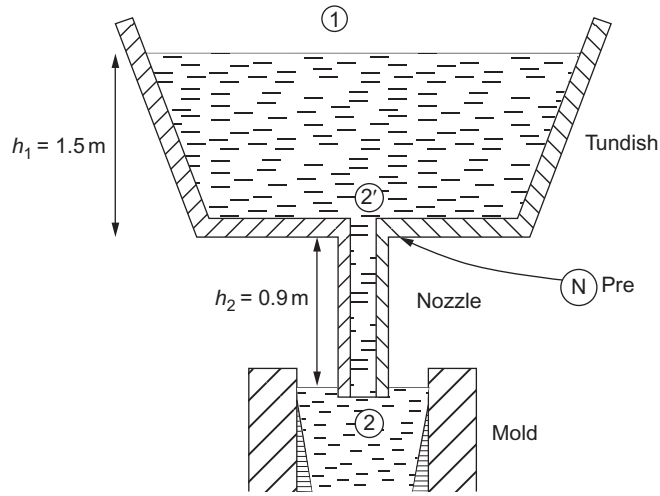
Figure 4.1.6 Schematic showing flow of liquid steel through a nozzle from a tundish to a caster.

Example 4.1.2

Figure 4.1.6 shows a schematic of flow of liquid steel from a tundish to a mold through a submerged entry nozzle. Estimate the velocity of the liquid steel at the exit of the nozzle and the pressure at the neck where the tundish meets the nozzle (shown as N in the figure). Neglect friction losses. Comment on the results [5].

Solution

In order to estimate the exit velocity of liquid steel at the tip of the nozzle, we need to apply Bernoulli's equation between the levels of liquid steel in the tundish and the tip of the nozzle. Let us denote them by 1 and 2, respectively. The pressure at location 1 is atmospheric. If only a negligible length of the nozzle (compared to its total length) is dipped into the liquid metal in the mold, one can assume pressure at 2 also to be atmospheric. Since the tundish area is large compared to the nozzle area, the kinetic energy contribution at 1 compared to that at 2 can be neglected. If frictional losses are also neglected ($\hat{E}_f = 0$), Equation (4.1.9) gives,

$$\frac{1}{2}v_2^2 + g(-(h_1 + h_2) - 0) = 0,$$
$$\text{i.e.,} v_2 = \sqrt{2g(h_1 + h_2)}$$

(It may be noted that the velocity at the exit corresponds to the free fall velocity from a height of $h_1 + h_2$. This is the consequence of neglecting friction). Let us denote the section at the neck by $2'$. From mass balance, the velocity of liquid steel just below the neck should be the same as that at the exit (location 2). Applying Bernoulli's equation between location $2'$ and 2 will therefore give

$$0 + \frac{P_2 - P_{2'}}{\rho} + g(-h_2 - 0) = 0$$

$$P_{2'} = P_2 - \rho g h_2$$

P_2 being atmospheric pressure, the pressure $P_{2'}$ is below the atmospheric pressure.

Comment: The neck area, sometimes with slide gates, consists of joints. Further, the nozzle components are refractory materials that are often porous. A negative pressure at the neck therefore can lead to aspiration of air leading to inclusions in the product. In Al-killed steel, the residual aluminum can react with this air depositing Al_2O_3 on the nozzle, progressively narrowing down the opening, which ultimately leads to choking.

The Bernoulli equation has been used in designing many flow-measuring devices such as the Venturi meter, orifice meter, and Pitot tube. The Venturi meter (Figure 4.1.7) works on the principle that on flow through a pipe, a change in fluid velocity due to change in cross section of the tube leads to a corresponding change in pressure.

The meter consists of converging, straight, and diverging sections. Pressure taps are placed just before the converging section and at the throat, where the area of cross section for the flow is the least. Applying mass balance and energy balance (Bernoulli's equation) between these two sections for turbulent flow of an incompressible fluid will give

$$\frac{\pi D^2}{4} \rho v_A = \frac{\pi d^2}{4} \rho v_B \tag{4.1.11}$$

$$\frac{P_A}{\rho} + \frac{1}{2} v_A^2 = \frac{P_B}{\rho} + \frac{1}{2} v_B^2 \tag{4.1.12}$$

where v_A and v_B refer to fluid velocities at the initial and throat sections, respectively. From the above two equations, volume flow rate $\left(\dot{V} \right)$ can be deduced as

$$\dot{V} = \frac{\pi d^2}{4} v_B = C_D \frac{\pi d^2}{4} \sqrt{\frac{\frac{2(P_A - P_B)}{\rho}}{\left[1 - \frac{d^4}{D^4} \right]}} \tag{4.1.13}$$
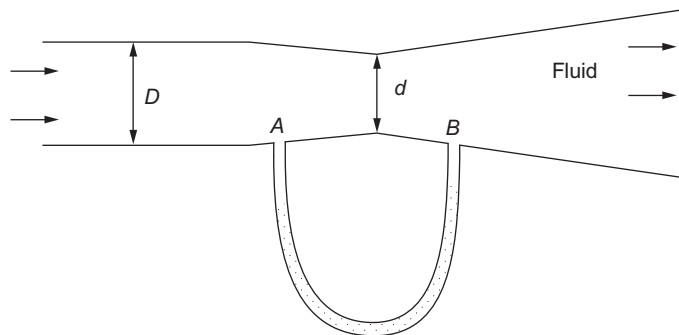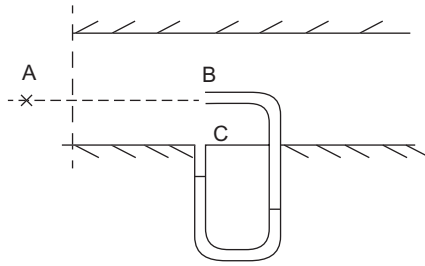

Figure 4.1.7 Schematic of a Venturi meter.

Figure 4.1.8 Schematic of a Pitot tube.

where a factor C_D, discharge coefficient, is introduced to account for the assumption of zero frictional effects. For making accurate measurements, the Venturi should be calibrated against known flows and C_D determined. Fortunately, experiments have shown [6] that the calibration factor generally ranges between 0.95 for cast ventures and almost 1 for well-designed machined ventures. To minimize friction losses arising from recirculating zones in the diverging section, the diverging angle should be kept small.

The Pitot tube is another relatively simple measuring device that can measure velocity in a flowing fluid. A schematic of a Pitot tube (named after French scientist from seventeenth century) measuring the velocity at a point B in a pipe is shown in Figure 4.1.8.

In the absence of the Pitot tube, velocity at the point of interest, B, is the same as at a point A upstream. When the Pitot tube is placed with its opening normal to the flow direction, the fluid is brought to rest at B along the centerline (note that the fluid inside the Pitot tube is static). On an infinitesimal stream tube, enveloping the centerline between points A and B, the Bernoulli equation is applied:

$$P_B = P_A + \frac{1}{2}\rho v^2 \tag{4.1.14}$$

The pressure at A and pressure at B away from the tube (or the pressure in the absence of the Pitot tube) are nearly the same, if the pipe is large enough compared to the Pitot tube. This pressure can then be measured at C, and is called the static pressure at B. The pressure at the opening at B is the combined effect of the static pressure and the effect of bringing the fluid to rest. It is called the total pressure. The difference $P_B - P_A = P_B - P_C = \frac{1}{2}\rho v^2$, called the dynamic pressure, is measured by the manometer.

Pitot tube is an absolute velocity-measuring device. This can be used without calibration to a maximum accuracy of $\pm 2\%$, unless the flow is compressible. Care should be taken to see that the total pressure opening is normal to the flow and the static pressure opening is parallel to the flow.

The static and total pressure openings can be combined to a single device called the Pitot–static tube as shown in Figure 4.1.9. Due to its geometry and large size, disturbance to the flow is large; Pitot–static tube should be calibrated before use as a measurement device.
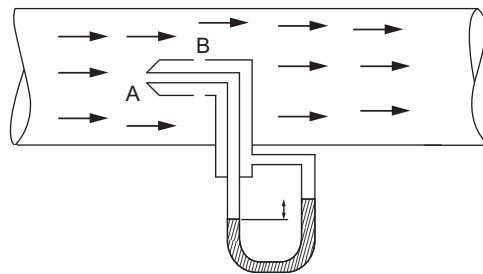
Figure 4.1.9 Schematic of a Pitot static tube.

4.1.5. THE CONCEPT OF VISCOSITY

In general, scientific methodology for explaining any new phenomenon is to seek a "law" that can give a generalized description of experimental observations, especially when carried out on simple systems where a particular phenomenon of interest is isolated from the rest. Subsequently, the law is applied in conjunction with other existing laws to describe the observations in complex systems. In the last section, we saw that in order to obtain the energy term corresponding to friction losses (conversion of mechanical energy to internal energy), it is necessary to look at the internal structure of the flow itself.

The irreversible process is a consequence of the work that needs to be done against forces developed within the fluid resisting relative motion between adjoining regions. Consider, for example, a fluid between two large parallel plates at a distance "d" apart (see Figure 4.1.10). To maintain the velocity, v, of the top plate constant with respect to the stationary bottom plate, a constant force, F, must be applied. Work done by this force does not result in any acceleration (increase in momentum); it is dissipated as internal energy. The analogous situation is the constant motion of a book dragged along the table top, leading to heating of the two surfaces that are touching each other.

The law that relates the force needed to keep the fluid in relative motion is called the Newton's law of viscosity, named after Sir Issac Newton. Using this law, a unique
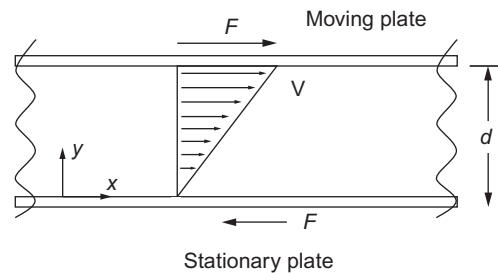

Figure 4.1.10 Flow profile of a fluid between two plates, one stationary and the other moving with a constant velocity, v.

property of the fluid called the coefficient of viscosity or simply viscosity is defined. Newton's law of viscosity can be described in simple terms using the system shown in Figure 4.1.10.

The area of each plate in contact with the fluid is A. Then the force, F, needed to maintain the upper plate in steady motion is:

$$F \propto A \frac{v}{d}$$

If the plates and the fluid are in steady motion, and the bottom plate needs to be held with an opposite force $-F$ to keep it from moving, a steady force should have been exerted by the fluid on the plates. How does this come about?

One of the fundamental properties of fluid is that it does not slip past a solid surface or an adjoining fluid packet (this is called the no–slip condition). Hence, when the top plate is set suddenly in motion at a velocity, v, the fluid next to it is also set into motion at the same velocity. The relative motion of this fluid layer with the adjoining layer below leads to an internal stress within the fluid, leading to dragging of the next layer, and so on. Finally, the fluid would develop a velocity gradient as shown, leading to the opposite force applied to the bottom plate.

The internal shear stress is opposite to the applied force pair as shown in Figure 4.1.11 and this can be expressed as

$$\tau_{yx} \propto -\frac{F}{A}$$
$$\propto -\frac{v}{d}$$
$$= -\mu \frac{v}{d}$$

In a general case where the velocity gradient is not constant, the shear stress at any point is defined as

$$\tau_{yx} = -\mu \frac{dv_x}{dy} \tag{4.1.15}$$
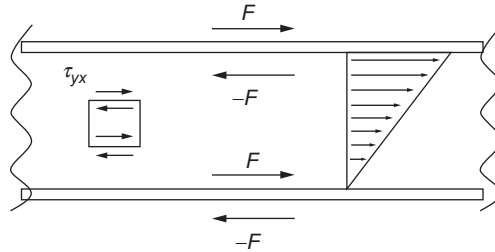
Figure 4.1.11 Forces acting on the plate and the fluid layers: flow of a fluid between two plates, one stationary and the other moving with a constant velocity, v.

This is the Newton's law of viscosity. The proportionality constant μ is called the coefficient of absolute viscosity, or simply viscosity, and is the property of the fluid.

τ_{yx}, the internal shear stress, when +ve can be interpreted as a force in the +ve x-direction being applied by a fluid layer normal to the xy plane at lesser y to the one above or as a force in the −ve x-direction being applied by a fluid layer at larger y to the one below. In solid mechanics, opposite sign convention is often used. Bird *et al.* [1], in their unified approach toward momentum, mass, and heat transfer, interpreted τ_{yx} as momentum flux. The force acting on the fluid at the top surface can be viewed as generating momentum (Newton's second law of motion). Since momentum cannot be accommodated at a surface (it has no volume), it has to be transported away. So the x-momentum generated at the top surface is transported down the velocity gradient. Finally, at the bottom, the momentum flux is neutralized by the negative momentum generated by a negative force on the bottom plate. For the case in Figure 4.1.11, the velocity gradient is +ve, and therefore τ_{yx} is negative: a +ve x-momentum transported in the −ve y-direction. A +ve value of τ_{yx} can indicate either flux of +ve x-momentum flux in the +ve direction or −ve x-momentum transported in the −ve y direction.

In the SI system, the units of viscosity are Pa s, and in CGS, it is poise. The ratio of viscosity to density is termed as kinematic viscosity. In the CGS system, the unit of kinematic viscosity is Stokes, in honor of a great scientist during Newton's era. In the SI system, unit is m^2/s.

The viscosities of condensed fluids such as liquids, slurries, and pastes are determined experimentally. The viscosities of gases and gas mixtures can be estimated to a reasonable degree of accuracy using kinetic theory of gases [1]. Study of kinetic theory also gives an insight to the molecular origin of the viscous phenomena.

Gases generally obey Newton's law of viscosity. Experiments have shown that only simple fluids obey Newton's law of viscosity. For complex fluids, such as slurries, polymeric solutions, gum, pastes, and metallic mixtures consisting both liquid and solid phases in the freezing range, the line correlating the shear stress and the velocity gradient (shear rate) is either not a straight line or does not pass through the origin. The flow behavior of such fluids is termed as rheology and is not discussed here. The reader may refer other sources for more information [7].

In Section 4.1.1.2, it was stated that a full description of a phenomenon needs a conservation equation, for example, conservation of momentum as well as constitutive equations describing the physics behind the underlying flow phenomena. Newton's law of viscosity forms one of the prime constitutive relationships for momentum transfer. The approach of Bird *et al.* [1] in viewing τ_{yx} as momentum flux due to a velocity gradient (and therefore a gradient of momentum) makes Equation 4.1.15 analogous to the constitutive equations in the other two-rate phenomena: Fourier's law of heat conduction in heat transfer and Fick's law of diffusion in mass transfer. This permits the three-rate processes to be treated in a unified fashion.

4.1.6. STEADY-STATE FULLY DEVELOPED LAMINAR FLOW THROUGH A STRAIGHT PIPE

Flow of fluids through pipes and conduits are quite common not only in engineering applications, but also in many natural systems. In fact the famous eighteenth century French scientist Jean Léonard Marie Poiseuille performed extensive experiments on the flow of distilled water through capillaries to understand the flow of blood. He discovered a functional relationship between the volumetric flow rate, the length and the diameter of the tube, and the pressure differential. Later, in 1860, Eduard Hagenbach derived Poiseuille's relation. The relation is therefore named Hagen–Poiseuille's law [8]. The derivation of this relationship is discussed below.

Consider a steady flow of liquid through a pipe as shown in Figure 4.1.12a. The fluid enters the pipe from a larger reservoir as illustrated in the figure. Let us also assume that just outside the inlet of the smaller pipe, the flow is almost uniform. As soon as the fluid layer reaches the inner wall of the pipe, its velocity becomes zero (no-slip condition). As the fluid moves farther into the pipe, more and more layers closer to the walls start decelerating due to viscous momentum transport. In other words, as the fluid moves farther into the pipe, the fluid layers starting from the wall are progressively affected by the presence of the wall. Since the volumetric flow rate of the incompressible fluid is being maintained (steady state), the velocity of fluid layers in the vicinity of the axis of the pipe progressively
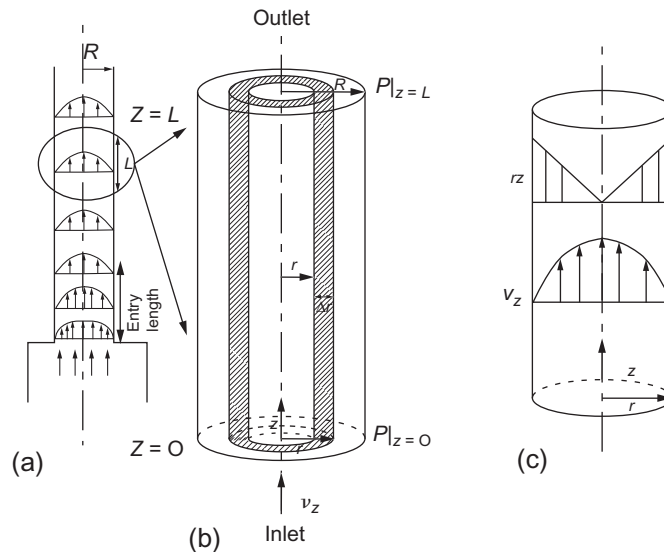
Figure 4.1.12 Steady laminar compressible flow through a vertical pipe: schematic of the (a) flow profiles, (b) shell or infinitesimal control volume, and (c) velocity and viscous momentum flux profiles.

increases. The schematic of the velocity profiles at different locations along the length of the pipe from the entry point are shown in Figure 4.1.12a. Further downstream, the affected region of the flow reaches the center and does not change further downstream. Flow in this region is termed as fully developed: the velocity is no longer a function of axial distance. Very close to the exit, the profile again relaxes: it changes to suit the exit conditions. The distance the fluid needs to travel before it attains a fully developed profile is termed as the entry length. Similarly, the length near the exit where the profile changes axially is the exit length. The region in between is the fully developed flow region. In the fully developed region, the velocity at any point is a function of radial position alone. The streamlines are therefore parallel to the axis. Mass balance would then demand the radial and azimuthal velocities (v_r and v_θ) be zero. The flow is said to be one dimensional (1D): only one component of the velocity is nonzero, and it changes in one direction only.

As already stated earlier, the flow is steady, laminar, and fully developed. In order to obtain the detailed description of the flow, mass and momentum balances are undertaken on a differential control volume and subsequently the appropriate differential equation is obtained. Since the problem is axi-symmetric, i.e., there is no variation of flow parameters along the circumferential direction. Let us consider a small annular shell of radius, r, length, Δz, and thickness, Δr as illustrated in Figure 4.1.12b.

To perform the mass balance for the fluid flowing through this shell (at steady state, the fluid entering the shell must be equal to that leaving the shell). The curved surfaces are parallel to the streamlines and there is no flow through them, and therefore:

$$\left(2\pi r\Delta r v_z\rho\right)\big|_{z=z} = \left(2\pi r\Delta r v_z\rho\right)\big|_{z=z+\Delta z}$$

Thus, v_z is independent of z for constant ρ and depends only on r, i.e., $v_z = f(r)$ as was already known.

Let us perform a momentum balance. As the flow is in the z-direction, it is only necessary to perform the balance of the z-component of momentum. The z-momentum balance will have the following terms.

The advective momentum entering the control volume from the bottom by virtue of fluid motion is the product of mass flow rate and velocity: $(2\pi r\Delta r)\rho(v_z v_z)\big|_{z=z,r=r+\Delta r/2}$ at $z=z, r=r+\Delta r/2$. Similarly, the advective momentum leaving the control volume from the top at $z=z+\Delta z, r=r+\Delta r/2$ is $2\pi r\Delta r\rho(v_z v_z)\big|_{z=z,r=r+\Delta r/2}$.

At the curved surfaces at r and $r+\Delta r$, there are no advective fluxes. Since there are velocity gradients across these surfaces, z-momentum fluxes across the surfaces, or equivalently viscous forces in the z-direction act on these surfaces. τ_{rz} represents the z-viscous momentum flux transferred along the r direction. Therefore, the viscous momentum enters the shell at $r=r$ at the rate of $\tau_{rz}\big|_{z=z+\Delta z/2,r=r}\,2\pi r\Delta z$. This can also be seen as the force that fluid at lesser r exerts on the shell along z-direction because of viscous friction. Similarly, the rate at which viscous momentum leaves the shell at $r=r+\Delta r$ is

$\tau_{rz}|_{z+\Delta z/2, r=r+\Delta r}\, 2\pi(r+\Delta r)\Delta z$. This is the force that fluid at r more than $r+\Delta r$ exerts on the shell along negative z-direction.

The force due to pressure at the inlet is $P|_{z=z, r=r+\Delta r/2}\, 2\pi r\Delta r$, and at the outlet is $-P|_{z=z+\Delta z, r=r+\Delta r/2}\, 2\pi r\Delta r$.

The gravitational body force is $2\pi r\Delta r\Delta z\rho(-g)$. In the general case of an inclined tube, g_z is used (z-component of gravity in place of $-g$).

As the system is at steady state, by conservation of momentum (refer to Section 4.1.1.2):

$$2\pi r\Delta r\rho\left\{ (v_z v_z)|_{z=z, r=r+\Delta r/2} - (v_z v_z)|_{z=z+\Delta z, r=r+\Delta r/2} \right\}$$
$$+\tau_{rz}|_{z+\Delta z/2, r=r}\, 2\pi r\Delta z - \tau_{rz}|_{z+\Delta z/2, r=r+\Delta r}\, 2\pi(r+\Delta r)\Delta z$$
$$+2\pi r\Delta r\left(P|_{z=z, r=r+\Delta r/2} - P|_{z=z+\Delta z, r=r+\Delta r/2} \right) - 2\pi r\Delta r\Delta z\rho g = 0$$

By mass conservation, $v_z|_z = v_z|_{z+\Delta z}$, and therefore the first term is zero. Dividing the above equation by the volume of the shell, $2\pi r\Delta r\Delta z$ and taking the limit as $\Delta r\to 0$,

$$-\frac{1}{r}\frac{\rho}{\partial r}(r\tau_{rz}) - \frac{dP}{dz} - \rho g = 0 \qquad (4.1.16)$$

There is no component of velocity in the radial direction and hence, by performing radial momentum balance, we obtain

$$-\frac{\partial P}{\partial r} = 0 \qquad (4.1.17)$$

Similarly there is no variation of pressure in the θ-direction. Pressure P is a function of z alone.

Substituting Newton's law of viscosity, Equation (4.1.15), into Equation (4.1.16),

$$\frac{1}{r}\frac{\partial}{\partial r}\left(r\mu\frac{\partial v_z}{\partial r} \right) - \frac{dP}{dz} - \rho g = 0 \qquad (4.1.18)$$

Since the flow under consideration is fully developed, flow in a region between two sections at z_1 and z_2, and that between z_2 and z_3 are exactly identical and therefore $\frac{dP}{dz}$ should be independent of z and can be written as $\frac{P_{z=L}-P_{z=0}}{L}$. If so Equation (4.1.18) can be considered as an ordinary differential equation and can be written as,

$$\frac{1}{r}\frac{d}{dr}\left(r\mu\frac{dv_z}{dr} \right) + \frac{P_{z=0}-P_{z=L}}{L} - \rho g = 0 \qquad (4.1.19)$$

Integrating the above equation,

$$v_z = -\left(\frac{P_{z=0}-P_{z=L}}{L} - \rho g \right)\frac{r^2}{4\mu} + C_1\ln(r) + C_2 \qquad (4.1.20)$$

where C_1 and C_2 are the integration constants that need to be determined using appropriate boundary conditions.

Boundary condition 1: Since velocities have to be finite anywhere inside the tube including the center, $r=0$, the constant C_1 has to be zero.

Boundary condition 2: As mentioned earlier, there is no slip between the solid surface and the fluid adjacent to it and therefore at $r=R$, $v_z=0$

Using the boundary conditions,

$$v_z = \frac{P_{z=0} - P_{z=L} - \rho g L}{4\mu L}\left(R^2 - r^2\right) \tag{4.1.21}$$

Defining a new quantity called the modified pressure, $\mathbb{P} = P - \rho g_z z$, where g_z is the component of gravity in the z-direction. In the present case, $g_z = -g$, and therefore $P + \rho g z$ (see footnote[1]), then, Equation (4.1.21) can be written as

$$v_z = \frac{\mathbb{P}_{z=0} - \mathbb{P}_{z=L}}{4\mu L} R^2 \left(1 - \frac{r^2}{R^2}\right) \tag{4.1.22}$$

The schematic profiles of the velocity and the viscous momentum flux (shear stress) are shown in Figure 4.1.12c. The velocity profile is parabolic with the maximum at the center and the viscous momentum flux is linear having the maximum at the wall.

From the velocity profiles, the volumetric flow rate is determined by integration:

$$\dot{V} = \int_0^R v_z(r)\, 2\pi r\, \mathrm{d}r = \frac{(\mathbb{P}_{z=0} - \mathbb{P}_{z=L})\pi R^4}{8\mu L} \tag{4.1.23}$$

This is the famous Hagen–Poiseuille's equation. The average velocity of the fluid, denoted by $\bar{v}$, is easily obtained by dividing the volumetric flow rate by the area of cross section.

$$\bar{v} = \frac{(\mathbb{P}_{z=0} - \mathbb{P}_{z=L})R^2}{8\mu L} \tag{4.1.24}$$

Application of overall energy balance equation (Equation 4.1.8) for fully developed incompressible flow ($\bar{v}_1 = \bar{v}_2$), in a tube,

$$g(z_2 - z_1) + \frac{P_2 - P_1}{\rho} + \hat{E}_f = 0,$$
$$\text{i.e.,} \frac{\mathbb{P}_1 - \mathbb{P}_2}{\rho} = \hat{E}_f \tag{4.1.25}$$

---

[1] Pressure varies in a static fluid as $P = P|_{z=0} + \rho g_z z$ (Pascal's law). Hence, $\mathbb{P} = P - \rho g_z z = P|_{z=0}$, everywhere. Variation in $\mathbb{P}$ therefore is the variation of pressure beyond the static fluid pressure variation, and this is the driving force for flow.

Substituting for $(\mathbb{P}_1 - \mathbb{P}_2)$ from Equation (4.1.24)

$$\hat{E}_f = \frac{8\mu v L}{\rho R^2} \tag{4.1.26}$$

Hence, the total work done per unit time in the section is $\dot{m} \cdot \hat{E}_f = \rho \cdot \pi R^2 \cdot \overline{v} \cdot \hat{E}_f = 8\pi\mu\overline{v}^2 L$. Interestingly, it can be shown that:

$$\left(\tau_{rz}\big|_{r=R} \cdot 2\pi R L\right)\overline{v} = -\mu\frac{dv_z}{dr}\bigg|_{r=R} \cdot 2\pi R L \cdot \overline{v} = 8\pi\mu\overline{v}^2 L \tag{4.1.27}$$

The energy loss due to friction can be seen as the work done to move the fluid at a velocity $\overline{v}$ against the viscous forces at the pipe walls. This, however, should not be interpreted to mean that all dissipation takes place at the pipe/fluid interface. Dissipation is due to work against the shear force in the bulk and is given as $\mu\left(\frac{\partial v}{\partial r}\right)^2$ per unit volume. Integration of this term over the volume would give Equation (4.1.27).

It is now possible to calculate the kinetic energy per unit mass in the mechanical energy balance equation (Equation 4.1.8) for laminar flow through pipe. The kinetic energy flow through an infinitesimal area formed by a ring with radii r and $r + \Delta r$:

$$\text{K.E. per unit mass} = \frac{\int_0^R (2\pi r \, dr)(\rho v_z(r))\left(\frac{1}{2}v_z^2(r)\right)}{\rho\dot{V}} = \frac{\overline{v}^2}{2\beta} \tag{4.1.28}$$

The above equation gives $\beta = \frac{1}{2}$ for fully developed laminar flow through circular tubes.

From the above example, it can be seen that for laminar flows, the *first principle approach*, i.e., the basic constitutive equation for flow in conjunction with mass and momentum conservation, can be used to arrive at the detailed flow structure and then to deduce the energy loss due to friction in the system. When the flow becomes unstable and subsequently manifests as turbulent flow, however, predicting the flow structures from *first principles* is not possible for most engineering systems. An empirical approach is therefore necessary. Experiments are performed on each system of interest. Experimental effort as well as data organization is optimized using the similarity approach, based on the Buckingham Π theorem as described in the next section.

4.1.7. BUCKINGHAM Π THEOREM AND ITS APPLICATION TO TRANSPORT PHENOMENA

The Buckingham Π theorem is a theorem in dimensional analysis. A process or a phenomenon can be described by a set of variables based on its physics. The nature of

these variables is captured in their dimensional representations in terms of a few indepen-dent dimensions. These dimensional representations indicate the interrelationships between the variables. Due to these interrelationships, the degrees of freedom of a process are phenomenon constrained by the principle of dimensional homogeneity: each term in a function relating several variables should have the same dimension for it to be physically meaningful.

Let a process be described by n variables; $X_1, X-2, \ldots X_n$. A general polynomial representation would be

$$X_n = \sum_i C_i X_1^{m_{1,i}} X_2^{m_{2,i}} \ldots X_{n-1}^{m_{n-1,i}}$$

C_is are arbitrary constants and $m_{1,i}, m_{2,i} \ldots m_{n-1,i}$ are arbitrary exponents. One may obtain these exponents as well as the constants C_i using regression analysis of the data obtained through experiments. The principle of dimensional homogeneity stipulates that each of the terms on both sides of the equations should have the same dimensions. In other words, if all the variables $(X_1, X_2, \ldots X_n)$ are expressed in their fundamental dimensions and substituted in the proposed power law, the exponents of each of the fun-damental dimension should be the same in all terms.

This constraint is expressed formally in the Buckingham Π theorem: if there are "n" variables identified to describe a particular phenomenon in a system and if all these "n" variables can be expressed using "k" fundamental dimensions such as mass, length, time, and charge, then one can form "$n-k$" independent dimensionless numbers. Fur-ther, suppose these dimensionless numbers are denoted as $\Pi_1, \Pi_2 \ldots \Pi_{n-k}$, then one can write a mathematical relation $f(\Pi_1, \Pi_2 \ldots \Pi_{n-k}) = 0$ to describe the phenomena in the system.

The dimensionless numbers can be obtained using power law relation,

$$\Pi_p = X_1^{p_1} X_2^{p_2} \ldots X_n^{p_n}$$

Though the choice of these exponents is arbitrary, generally, one would like to choose these exponents as integers and in such a way that the dimensionless numbers represent some physically meaningful entity. Please note that the dimensionless numbers need to be independent of each other. With a given set of variables one may be able to form a large number of dimensionless variables (product of two or more dimensionless numbers would also be dimensionless). Which set of mutually independent Πs are to be selected depends on the phenomenon under study.

The Buckingham Π theorem reduces the number of experiments to be conducted for studying a particular phenomenon in a system substantially. Let us say, one has identified "n" variables that describe the phenomena of interest and decides to choose 10 levels for each of the "n" variables for experimentation. Then, one needs to perform 10^n experiments to cover the whole spectrum of planned experiments. However, if k is the number of fundamental

dimensions, experiments need to be conducted only with $n - k$ dimensionless numbers as dictated by the theorem, and thereby, the number of experiments reduces to 10^{n-k}. Additionally, the amount of information needed to report the experimental data and correlations developed on that data through tables, charts, or equations also reduce substantially. In transport phenomena, therefore, the numerous experimental data as well as correlations developed based on experimental data are reported using dimensionless numbers.

Another consequence of this theorem is that in two geometrically similar systems, if all the dimensionless numbers corresponding to a particular phenomenon of interest are identical, then the systems are similar as far as that phenomenon is concerned. In other words, in both systems, identical mathematical relations among the dimensionless variables hold good in describing the phenomenon of interest. This has been used extensively in studying many process metallurgical systems using, what is termed as, physical models, which are built on a laboratory scale to study a particular phenomenon. For example, water models at the laboratory scale have been used to understand mixing of steel in Basic Oxygen Furnace (BOF), Electric Arc Furnace (EAF), and ladles and to understand flow phenomena and subsequent to control liquid steel flow in tundish and continuous casting molds.

4.1.8. REYNOLDS NUMBER

In Section 4.1.3, the experiment by Reynolds was discussed. In a given flow system, laminar flow is maintained only at low velocities. Beyond some critical velocity, which is characteristic of a particular system, the flow becomes unstable and with further increase, manifests as turbulent flow. The dimensionless number that is used to characterize the transitions from laminar to unstable and further to turbulent flow is the Reynolds number:

$$Re_L = \frac{\rho \bar{v} L}{\mu} \tag{4.1.29}$$

where $\bar{v}$ is the characteristic velocity that characterizes the strength of the flow and L is the characteristic length for the system. One can interpret the Reynolds number as the ratio of advective momentum flux or inertial force to the viscous momentum flux or viscous force. The advective momentum flux is the product of the mass flux and the velocity and is given by $(\rho \bar{v}) \bar{v}$. Similarly, the viscous momentum flux or stress is given by $\tau = \mu \frac{\bar{v}}{L}$. It must be noted that the characteristic length is used to characterize the velocity gradients. For flow through pipes, the characteristic velocity chosen is the average velocity of the fluid through the pipe and as the velocity gradients are primarily along the radial direction, the characteristic length chosen is the diameter of the tube. Similarly, for flow around a sphere, the velocity of the approaching fluid far away from the sphere and the diameter of the sphere are chosen as characteristic velocity and length, respectively. Experiments in numerous systems have shown that for geometrically similar systems, the

Reynolds number characterizes the nature of the flow. For flow through pipes, one can maintain laminar flow under normal circumstances for Reynolds number up to approximately 2000. At *Re* values above 5000–10,000, the flow becomes fully turbulent. In the intermediate region, the flow is said to be in transition: flow keeps alternating between laminar and turbulent states. The transitions depend on disturbances. If the inner surface of the pipe is smooth and if one maintains experimental conditions with extreme care so as to minimize the vibrations and disturbances in the incoming flow to the pipe, the transition from laminar flow can be delayed till the Reynolds number reaches values much beyond 2000.

4.1.9. FRICTION FACTOR FOR FLOW THROUGH PIPES

As has been said earlier in Section 4.1.6, the energy term corresponding to friction in flowing fluids through pipes can be deduced from first principles only for laminar flows. Once the flow becomes unstable, one needs to rely on empirical correlations developed using experimental data. So, let us look at the application of the Buckingham Π theorem in understanding flow through a pipe.

The first step is to identify the variables that would affect the flow phenomenon through the pipe. They are:

(1) Diameter of the pipe, D

(2) Length of the pipe, L

(3) Surface roughness of the pipe. This is characterized by the average height of the asperities, and let it be denoted as ϵ

(4) The density of the fluid, ρ

(5) The viscosity of the fluid, μ

(6) The pressure difference one needs to maintain across the length of the pipe, $\Delta \mathbb{P}$. (The modified pressure has been used so that the pressure difference accounts only for the frictional losses eliminating the gravitational term)

(7) The average velocity of the fluid through the pipe, v.

There are seven variables and these can be expressed using three fundamental dimensions, namely, mass, length, and time. Therefore, as per the theorem, one can have four independent dimensionless numbers. The dimensionless numbers that specify the geometry of the system are $\frac{L}{D}$ and $\frac{\epsilon}{D}$. As mentioned earlier, the Reynolds number for the system can be defined as $\frac{\rho v D}{\mu}$. The pressure difference, $\Delta \mathbb{P}$ can be made dimensionless by the characteristic dynamic pressure, namely, $\frac{1}{2}\rho v^2$. Thus, the flow phenomena through the pipe can be described using the following equation

$$f\left(\frac{\Delta \mathbb{P}}{\frac{1}{2}\rho v^2}, Re_D, \frac{L}{D}, \frac{\epsilon}{D}\right) = 0 \tag{4.1.30}$$

The dimensionless number $\dfrac{\Delta\mathbb{P}}{\rho v^2}$ is referred to as the Euler number.

The relationship for flow through pipes can then be written as:

$$\frac{\Delta\mathbb{P}}{\rho v^2} = f\left(\frac{L}{D},\frac{\epsilon}{D},Re_D\right) \tag{4.1.31}$$

For fully developed flow, the pressure drop is linearly dependent on length, since any two sections of equal length should show equal pressure drop. One can therefore write

$$\frac{\frac{\Delta\mathbb{P}}{\rho v^2}}{\frac{L}{D}} = f\left(\frac{\epsilon}{D},Re_D\right) \tag{4.1.32}$$

The function f in the above equation is also dimensionless and can be used to characterize the flow in place of the Euler number.

$$f_D\left(\frac{\epsilon}{D},Re_D\right) = \frac{\frac{\Delta\mathbb{P}}{(1/2)\rho v^2}}{\frac{L}{D}} \tag{4.1.33}$$

is called the D'Arcy–Weisbach's or simply D'Arcy's friction factor popular among mechanical engineers. Chemical engineers use a slightly different form and call it the Fanning friction factor f_F:

$$f_F = \frac{\frac{\Delta\mathbb{P}}{\rho v^2}}{\frac{2L}{D}} \tag{4.1.34}$$

Evidently, $4f_F = f_D$.[2]

The above dimensional analysis has been made without the assumption of the nature of the flow. It is therefore valid for both flows, i.e., the friction factor for incompressible fully developed flow in circular tubes is dependent only on the Reynolds number, Re, and the relative roughness $\frac{\epsilon}{D}$. In the case of the entrance or exit regime where the flow changes along the axial direction, the friction factor is dependent on $\frac{L}{D}$ too. Extensive experimental data have been compiled into dimensionless forms and have been presented in graphical or equation forms. Figure 4.1.13 gives a graph of the Fanning friction factor, f_F, as a function of Reynolds number and relative roughness [9,10]. One may note that the friction factor is independent of roughness in the laminar regions and can be obtained from Equation (4.1.24) as:

---

[2] Fanning friction factor is normally defined with respect to force of friction:

$$F_{\text{friction}} = \frac{\pi D^2}{4}\cdot\Delta\mathbb{P} = (\pi DL)\left(\frac{1}{2}\rho v^2\right)f_F$$

where πDL represents the wetted area on which the friction force, F_{friction} acts and $\frac{1}{2}\rho v^2$ gives the characteristic kinetic energy (or dynamic pressure).
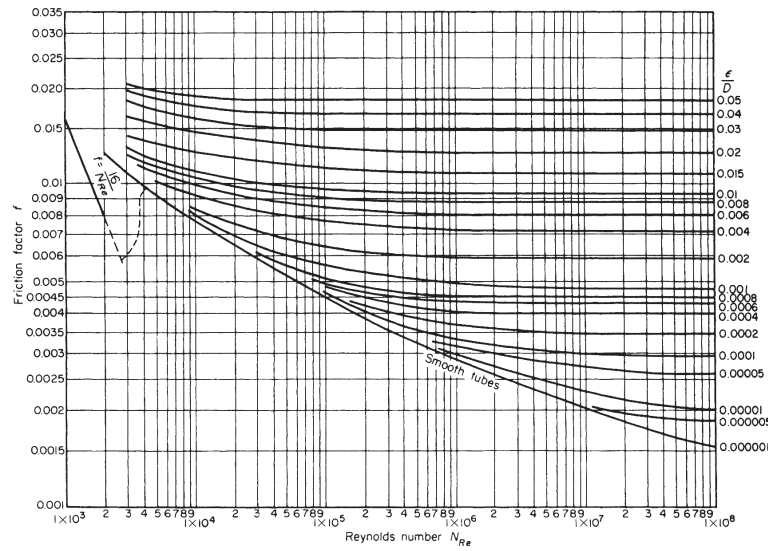
Figure 4.1.13 Fanning friction factor chart for pipe flow [9].

$$f_F = \frac{16}{Re_D} \tag{4.1.35}$$

This corresponds to $\hat{E}_f = \frac{\Delta\mathbb{P}}{\rho} = \frac{8\mu v^2}{\rho R^2}$ given by Equation (4.1.26).

In the transition region, it has been observed that the pressure drop does not remain stable; it keeps fluctuating. This is marked with dotted lines and generally is not suitable for engineering applications due to its unpredictability. In the turbulent region, the friction factor values are stable and vary depending on the Reynolds number and the relative roughness. One can clearly see that the dependence of Reynolds number on friction factor decreases with increasing Reynolds number. Dependence also decreases with increasing roughness.

Instead of graphical representation, correlations in the form of algebraic equations are also available to estimate the friction factor through pipes in the turbulent region. The most widely used correlation is by Colebrook [11]

$$\frac{1}{\sqrt{f_F}} = -4\log\left(\frac{1}{3.7}\frac{\epsilon}{D} + \frac{1.255}{Re_D\sqrt{f_F}}\right) \quad \text{Turbulent flow, for } Re_D > 4000 \tag{4.1.36}$$

There is also a more recent correlation by Churchill [12], which has the advantage of estimating the friction factor directly as the equation is explicit unlike the previous one

$$\frac{1}{\sqrt{f_F}} = -4\log\left(0.27\frac{\epsilon}{D} + \left(\frac{7}{Re_D}\right)^{0.9}\right) \quad \text{Turbulent flow, for } Re_D > 4000 \tag{4.1.37}$$

Table 4.1.1 Values of Surface Roughness for Various Materials [9]

Material Surface Roughness	mm
Drawn tubing (brass, lead, glass, and the like)	0.00152
Commercial steel or wrought iron	0.0457
Asphalted cast iron	0.122
Galvanized iron	0.152
Cast iron	0.259
Wood stove	0.183–0.914
Concrete	0.305–3.05
Riveted steel	0.914–9.14

For turbulent flow through hydraulically smooth pipes ($\epsilon \rightarrow 0$), up to Re_D of 10^5, one can also use the simpler expression by Blasius [13]

$$f_F = \frac{0.0791}{Re_D^{0.25}} \quad \text{Turbulent flow, smooth pipes, for } Re_D < 10^5 \tag{4.1.38}$$

Typical, surface roughness values of materials of commercial pipes are shown in Table 4.1.1. The roughness values shown in the table correspond to newly manufactured pipes. Colebrook [11] found that a simple linear relation can reasonably represent the increase in roughness because of corrosion and scale deposition.

The energy term corresponding to friction losses, $\hat{E}_f$, in a pipe is related to the friction factor as follows

$$\hat{E}_f = 2\frac{L}{D}v^2 f_F \tag{4.1.39}$$

4.1.9.1. Friction Losses from Pipe Fittings

In a piping system, there are always pipe fittings such as bends, valves, and couplings besides straight sections. One needs to account for the additional friction losses due to these fittings. Friction losses are also associated with entry lengths and exit conditions. One of the ways of quantifying these additional friction losses is through an equivalent length of a straight pipe giving the same friction loss as that with the pipe fitting. For geometrically similar pipe fittings, irrespective of their actual dimensions, the friction losses can be expressed using an equivalent length to diameter ratio $\left(\frac{L_e}{D}\right)$. Some typical values obtained from experimental measurements are tabulated in Table 4.1.2 for common pipe fittings.

Table 4.1.2 Equivalent Pipe Length to Diameter Ratio for Some Common Pipe Fittings (Turbulent Flow) [14]

Pipe Fitting	$\dfrac{L_e}{D}$
Globe valve, wide open	~ 300
Angle valve, wide open	~ 170
Gate valve, wide open	~ 7
3/4 Open	~ 40
1/2 Open	~ 200
1/4 Open	~ 900
90° Elbow, standard	30
Long radius	20
45° Elbow, standard	15
Tee, used as elbow, entering the stem	90
Tee, used as elbow, entering one of two side arms	60
Tee, straight through	20
180° Close return bend	75
Ordinary entrance (pipe flush with the wall of the vessel)	16
Borda entrance (pipe protruding into vessel)	30
Rounded entrance, union, coupling	Negligible
Sudden enlargement from d to D	
Turbulent flow in d	$\dfrac{1}{4f_{F,ind}}\left[1-\dfrac{d^2}{D^2}\right]^2$
Sudden contraction from D to d	
Turbulent flow in d	$\dfrac{1}{10f_{F,ind}}\left[1.25-\dfrac{d^2}{D^2}\right]$

Often in flow systems, there may be elements for which defining an equivalent length is not convenient. A chamber in the flow line filled with pebbles for mixing of fluids or a water-cooled mold with complex geometry are examples. These need experimental determinations of pressure drop. The data are then stored as an energy loss factor k_f using the following equation:

$$\Delta P = \frac{1}{2}\rho v^2 k_f \tag{4.1.40}$$

In highly turbulent flows, k_f remains relatively independent of Re.

4.1.9.2. Estimation of Friction Factor for Flow Through Conduits Having Noncircular Cross Section

For turbulent flow through conduits having noncircular cross sections, one can approximate the friction loss by representing the conduit as a circular pipe having an equivalent diameter, D_e defined as:

$$D_e = 4(\text{Hydraulic radius}) = 4\left(\frac{\text{Area of cross section}}{\text{Wetted perimeter}}\right) \qquad (4.1.41)$$

For example, for a conduit having a square cross section with side a, the equivalent diameter, D_e, for calculating the friction loss will be a.

Example 4.1.3

Oxygen is being delivered to a steel melt shop (SMS) at the rate of $400\,\mathrm{Nm}^3\,\mathrm{min}^{-1}$ through a 50 m long, 100-mm piping from a reservoir at the oxygen plant. The piping has five 90° bends of standard radius. In addition, one gate valve and one globe valve are placed in the pipeline. If the delivery pressure at the SMS should be 10^6 Pa (gauge pressure), what should be the minimum pressure at the reservoir with the valves fully open? Pipes are made of galvanized iron. The viscosity of oxygen at room temperature (300 K) is 20.2×10^{-6} Pa s. Density of oxygen at STP is $1.4\,\mathrm{kg\,m}^{-3}$.

Solution

First one needs to identify whether the flow can be approximated as being incompressible. For that, let us find the Mach number (Ma). The pressure will be minimum at the exit and therefore the velocity is maximum at this section. For a temperature of 300 K and pressure of 10^6 Pa, the volumetric flow rate is

$$\dot{V} = \frac{400\left(\frac{300}{273}\right)\left(\frac{1.013}{11}\right)}{60} = 0.67\,\mathrm{m}^3\,\mathrm{s}^{-1}$$

the velocity, v, is

$$v = \frac{\dot{V}}{\pi\frac{D^2}{4}} = 85\,\mathrm{m\,s}^{-1}$$

The velocity of sound under adiabatic condition is given by $c = \sqrt{\frac{\gamma RT}{M}}$, which for oxygen gives $330\,\mathrm{m\,s}^{-1}$. Thus the Mach number is $\frac{85}{330} = 0.26$. As the Mach number is <0.3, one can approximate the flow as incompressible.

The Reynolds number for the flow is independent of pressure for isothermal flow:

$$Re_D = \frac{\rho v D}{\mu} = \frac{14.11 \times 85 \times 0.1}{20.2 \times 10^{-6}} = 5.8 \times 10^6$$

From Table 4.1.1, the relative roughness for the pipe is $\frac{0.152}{100} = 0.00152$. For this roughness, the flow is completely turbulent and the friction factor is independent of Reynolds number (see Figure 4.1.13). The Fanning friction factor, f_F, is approximately as 0.0055.

Though the flow is considered incompressible, one needs to estimate the density and velocity at some mean pressure for the entire tube. Let us assume that the upstream pressure is 1.4×10^6 Pa (absolute), and the average pressure is 1.2×10^6 Pa (absolute). Thus, the average density and the average velocity for the flow are 16.6 kg m^{-1} and 78 m s^{-1}, respectively.

The equivalent length for the piping system can be calculated using values given in Table 4.1.2:

$$\sum \frac{L}{D} = \left(\frac{L}{D}\right)_{\text{Straight pipe}} + 5\left(\frac{L_e}{D}\right)_{\text{Elbow}} + \left(\frac{L_e}{D}\right)_{\text{Gate value}} + \left(\frac{L_e}{D}\right)_{\text{Globe value}}$$

$$\sum \frac{L}{D} = 500 + 5 \times 30 + 7 + 300 = 957$$

Applying mechanical energy balance, Equation (4.1.8)

$$\frac{v^2}{2} + \frac{P_2 - P_1}{\rho} + 2 \times 0.0055 \times 957 v^2 = 0$$

$$\therefore P_1 - P_2 = \Delta P = 0.95 \times 10^6 \text{ Pa}$$

Here ΔP is comparable to P. Our assumption of the average pressure being 1.2×10^6 Pa is erroneous. One needs to iteratively improve the solution by trial and error. This leads to the value of P_1 to be 1.88×10^6 pa.

Example 4.1.4
A schematic of a continuous casting mold is shown in Figure 4.1.14. One side of the continuous casting mold face has the dimensions of 1 m height and 2 m width. The hot face made of copper is backed by a steel plate with a gap of 20 mm in between. The designer specifies that cooling water should be passed in the gap between the two plates at a velocity of at least 10 m s^{-1}, from the bottom to the top.
• What is the pressure drop across the mold?
• What is the theoretical pump rating for supplying water to this mold, discounting losses in supply pipes, entrance, exit, etc.? Assume the surfaces to be hydraulically smooth.

Solution
In the above problem, the flow of water is through a rectangular duct. As the flow rate is quite large, the flow is expected to be turbulent. Therefore, one can conveniently represent the conduit by a circular pipe having equivalent diameter given by Equation (4.1.41)

$$D_e = 4 \times \frac{2 \times 20 \times 10^{-3}}{2 \times (2 + 20 \times 10^{-3})} = 0.0396 \text{m}$$
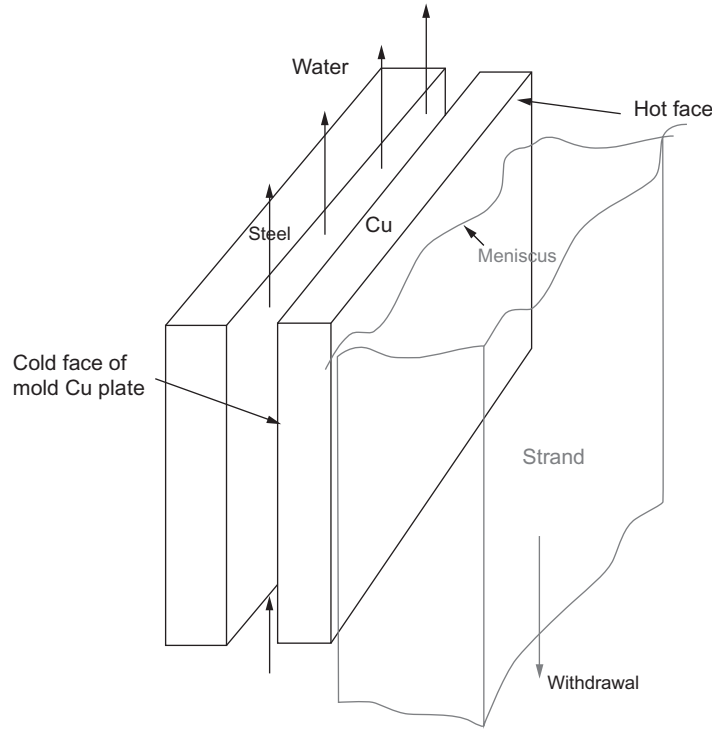
Schematic showing water cooling in a slab mold

Figure 4.1.14 Continuous casting mold: water flow.

The viscosity of water at room temperature is approximately 0.001 Pa s. Hence, the Reynolds number for the flow is

$$Re_D = \frac{1000 \times 10 \times 0.0396}{0.001} = 3.96 \times 10^5$$

Using Churchill's (refer to Equation 4.1.37) relation for friction factor,

$$f_F = 6.3 \times 10^{-4}$$

Applying the mechanical energy balance equation (Equation 4.1.8) between inlet of water at the bottom of the mold and the exit at the top,

$$\frac{P_2 - P_1}{\rho} + g(z_2 - z_1) + 2 f_F \frac{L}{D} v^2 = 0$$
$$\frac{P_2 - P_1}{1000} + g(1) + 2 \times 6.3 \times 10^{-4} \frac{1}{0.0396} 10^2 = 0$$
$$P_1 - P_2 = 13 \text{kPa}$$

The work done per unit time to maintain the pressure drop and the flow on both sides of the mold

$$(P_1 - P_2)(Av) = 13 \times 2 \times 2 \times 20 \times 10^{-3} \times 10 = 10.4 \text{kW}$$

Comment: Molds used in practice normally have a series of slits along its width, with water distributor at the top and bottom. Supply pipes are connected to these distributors. The overall geometry is fairly complex, and one may have to generate data for equivalent lengths or energy loss factors. Pressure drop through the overall system may be substantially higher.

4.1.10. FLOW THROUGH PACKED BEDS

As mentioned in the introductory section, understanding flow through packed beds is very important for design and operation of numerous metallurgical processes. Simple examples of packed beds include rock piles, sand filters, and a soil bed. A predominant part of the interior of a working blast furnace consists of a packed bed of iron ore and coke at the top with gas flowing through it and a packed bed of coke at the bottom with gas and liquids flowing through it. Similarly, a sinter bed for iron ore sintering or a bed of pellets for induration are packed beds. Leaching operations can also be performed in a reactor where the leachant is allowed to flow through a packed bed of mineral particles.

While designing a packed bed reactor, a process engineer desires to calculate the pressure difference that needs to be applied to maintain a desired flow rate through the bed. One would also like to know how this relation between the pressure drop and the flow rate changes depending on the properties of the packed bed. While describing flow through packed beds, a term called "superficial velocity" is often used. This refers to the flow rate per unit area of cross section of the reactor (in the absence of the particles). Please note that the fluid flows only through the voids between particles in the bed and the actual area available for the fluid to flow is a fraction of the cross-sectional area of the reactor.

The methodology commonly adopted in developing relationships for complex systems like flow through packed beds is to approximate the system by a comparatively simpler system that is amenable to analysis. The hypothesis is that the functional relationship developed for the simple systems is applicable to the complex system under consideration with a few empirical corrections. In the case of packed beds, two approaches have been adopted: (1) considering the flow of fluid through the voids in the packed bed as flow through a bundle of tubes and (2) considering the system as flow around particles submerged in a fluid. The tube-bundle theory has been adopted here for developing the governing equation.
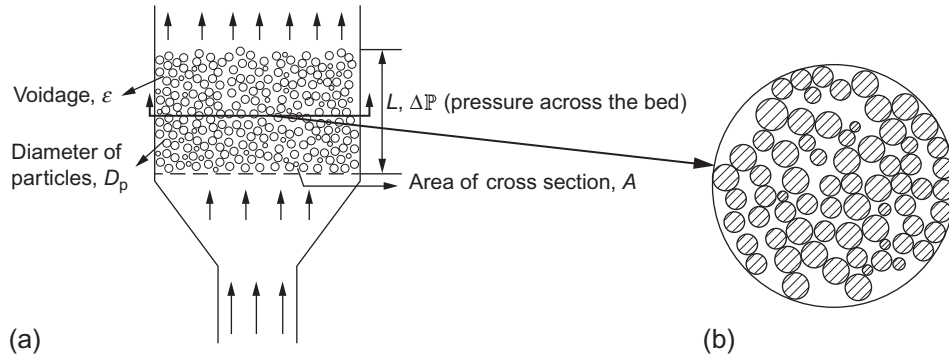
Figure 4.1.15 (a) A simple packed column or bed and (b) cross section of the bed.

Consider the simple case of a packed bed made from randomly packed uniform-sized spherical particles in a container as shown in Figure 4.1.15. The two important bulk characteristics of such a packed bed are the average volume fraction of voids, ε, and the diameter of the particles, D_p. The voidage in a randomly packed bed is reasonably uniform, except near the wall where it is higher. Experiments have shown that this wall region extends to a distance of $3D_p - 5D_p$ from the wall [15]. Let us, therefore, consider a case where the cross-sectional dimension of the reactor is much larger than the diameter of the particle, so that the effect of the wall is negligible.

The basic idea behind the tube-bundle theory is to estimate an equivalent diameter for the bundle of tubes that gives the same pressure drop for the desired flow rate, i.e., the tube that gives the same friction loss as that for the flow through the bed. The equivalent diameter for noncircular conduit cross sections is given by

$$D_e = 4 \times \frac{\text{Area of cross section for the flow}}{\text{Wetted perimeter for the flow}}$$

Figure 4.1.15b shows a schematic cross-section of the bed. The nonhatched area is the area available for flow. The sum of the boundaries of the particles is the wetted perimeter. When bed diameter is large enough, the length along the wall can be neglected.

Let us multiply the denominator and numerator of the RHS of this equation by an infinitesimal bed height dL.

$$
\begin{aligned}
D_e &= 4 \times \frac{\text{Area of cross section for the flow} \times dL}{\text{Wetted perimeter for the flow} \times dL} \\
&= 4 \times \frac{\text{Volume of the voids in height } dL \text{ of this bed}}{\text{Surface of area of particle in height } dL \text{ of this bed}}
\end{aligned}
$$

Since the bed is macroscopically uniform, the above relationship should hold for any thin slice of the bed. Hence the equation can be rewritten as

$$D_e = 4 \times \frac{\text{Volume of the voids in height } L \text{ of this bed}}{\text{Surface of area of particle in height } L \text{ of this bed}}$$

Suppose, ε denotes the average fraction of voidage in the bed and D_p denotes the diameter of the particles that constitute the packed bed, and A denotes the cross-sectional area of the packed bed column as shown in the figure, then

$$\text{Volume of the voids in the bed} = \varepsilon AL$$
$$\text{Number of particles in the bed} = \frac{(1-\varepsilon)AL}{\frac{1}{6}\pi D_p^3}$$
$$\text{Surface of area of particle in the bed} = \text{Number of particles in the bed}$$
$$\times \text{Surface area of one particle}$$
$$= \frac{(1-\varepsilon)AL}{\frac{1}{6}\pi D_p^3}\left(\pi D_p^2\right) = \frac{6(1-\varepsilon)}{D_p}AL \qquad (4.1.42)$$
$$\therefore D_e = 4\frac{\varepsilon AL}{\frac{6(1-\varepsilon)}{D_p}AL} = 4\frac{\varepsilon D_p}{6(1-\varepsilon)}$$

The actual average velocity $\bar{v}$ through the voids is related to the superficial velocity, v_0:

$$\bar{v} = \frac{v_0}{\varepsilon} \qquad (4.1.43)$$

Using Equations (4.1.42) and (4.1.43) in the equation for flow through a tube (Equation 4.1.34):

$$\frac{\Delta\mathbb{P}}{\rho} = \frac{4L}{D_e}\cdot\frac{\bar{v}^2}{2}\cdot f_F = \frac{2L}{D_e}\cdot\frac{v_0^2}{\varepsilon^2}\cdot f_F \qquad (4.1.44)$$

The value of f_F is dependent on Re for the flow and the "roughness" of the tube. The Reynolds number for tubes is given by

$$Re = \frac{\rho\bar{v}D_e}{\mu} = \frac{\rho v_0 D_e}{\varepsilon\mu} = \frac{4}{6}\frac{\rho v_0 D_p}{(1-\varepsilon)\mu}$$

For laminar flow in tubes, $f_F = \frac{16}{Re}$. From Equation (4.1.44), one obtains

$$\frac{\Delta\mathbb{P}}{L} = \frac{72\mu(1-\varepsilon)^2}{D_p^2\varepsilon^3}v_0$$

This equation is now empirically corrected for the assumption of a straight tube and fully developed flow by replacing the constant 72 to 150 to obtain,

$$\frac{\Delta\mathbb{P}}{L} = \frac{150\mu(1-\varepsilon)^2}{D_p^2\varepsilon^3}v_0 \qquad (4.1.45)$$

In his paper on packed beds, Ergun [16] attributes the above equation to Blake and Kozeny and calls it the Blake–Kozeny equation. Much earlier, in the 1850s, the French scientist D'Arcy had observed, in flow through sand beds, a linear dependence of the pressure drop on v_0 and μ and proposed what is now known as D'Arcy's equation:

$$\frac{\Delta \mathbb{P}}{L} = k\mu v_0 \tag{4.1.46}$$

where k is called the specific permeability of the bed.

Reynolds number for packed beds is defined as [3]

$$Re_E = \frac{\rho v_0 D_p}{(1 - \varepsilon)\mu} \tag{4.1.47}$$

Equation (4.1.45) for the pressure drop is valid for $Re_E \lesssim 10$.

At much larger values of Re_E, the flow becomes fully turbulent. For flow through tubes, f_F becomes independent of Re_E if the roughness of the tube is very high (see Figure 4.1.13). Flow channels in a packed bed of particles can reasonably be viewed as a very rough tube. Therefore, the pressure equation becomes

$$\frac{\Delta \mathbb{P}}{L} = \frac{2}{D_e} \cdot \frac{\rho v_0^2}{\varepsilon^2} \cdot f_F = 3f_F \frac{(1 - \varepsilon)}{D_p \varepsilon^3} \rho v_0^2$$

The constant $(3f_F)$ is now empirically determined and is found to be 1.75 giving

$$\frac{\Delta \mathbb{P}}{L} = 1.75 \frac{(1 - \varepsilon)}{D_p \varepsilon^3} \rho v_0^2 \tag{4.1.48}$$

Ergun [16] calls it the Burke–Plummer equation. The above equation is valid for $Re_E \gtrsim 1000$, when flow everywhere in the bed is expected to be turbulent.

In the range of $10 < Re_E < 1000$, the flow can be mixed. Since flow through a packed bed involves several openings of different sizes between particles, the flow can be laminar, turbulent, or in transition simultaneously at different places in the bed, in this intermediate range of Reynolds numbers. Ergun [16] found empirically that summing the terms on the RHS of Equation (4.1.45) and Equation (4.1.48) predicts the pressure drop to a reasonable accuracy:

$$\frac{\Delta \mathbb{P}}{L} = \frac{150\mu(1 - \varepsilon)^2}{D_p^2 \varepsilon^3} v_0 + \frac{1.75\rho(1 - \varepsilon)}{\varepsilon^3 D_p} v_0^2 \tag{4.1.49}$$

This equation is called the Ergun equation and is used extensively for packed bed flow analysis over the entire Re range. One can rewrite this equation as:

---

[3] Note that the constant $\frac{4}{6}$ that occurred in the definition earlier is dropped since transition values for Re are anyway determined experimentally for each geometric system.

$$\frac{\Delta\mathbb{P}}{\rho v_0^2}\frac{D}{L}\frac{\varepsilon^3}{1-\varepsilon}=\frac{150\mu(1-\varepsilon)}{D_\mathrm{p}\rho v_0}+1.75=\frac{150}{Re_\mathrm{E}}+1.75 \qquad (4.1.50)$$

The first term on the left is the definition of a friction factor for packed beds. Hence:

$$f_{\mathrm{F,packed\ bed}}=\frac{150}{Re_\mathrm{E}}+1.75 \qquad (4.1.51)$$

Data from experiments plotted as $\log(f_{\mathrm{F,packed\ bed}})$ versus $\log(Re_\mathrm{E})$ show a straight line with a slope of -1 for $Re\lesssim10$, and a constant value for $Re\gtrsim1000$ and a smooth curve connecting these two straight lines in between [1].

The above expression has been deduced for a packed bed having spherical particles with uniform size. However, in reality, the industrial packed beds are made of particles having different shapes and sizes and even completely different materials, such as iron ore and coke in blast furnace. Thus, detailed characterization of the packed bed is required. For nonspherical particles, there may be different ways of defining particle sizes. However, one needs to adopt an appropriate one as far as flow through packed bed is concerned. Two important measures of a particle that affect the flow are its volume and surface area. Thus, the size and shape of particles in a packed bed are characterized using these measures.

The size of the particle is defined by the size of equivalent sphere having the same volume of that of the particle, i.e.,

$$D_\mathrm{sph}=\text{Diameter of sphere having the same volume as that of the particle} \qquad (4.1.52)$$

In order to account for the surface area of the particle, a parameter called sphericity, ϕ, is defined as

$$\phi=\frac{\text{Surface area of the sphere having equivalent volume of the particle}}{\text{Surface area of the particle}} \qquad (4.1.53)$$

Sphericity of some of the commonly shaped particles is listed in Table 4.1.3.

The particle size, D_p, used in Ergun equation (Equation 4.1.49) is, then, given by

$$D_\mathrm{p}=\phi\times D_\mathrm{sph} \qquad (4.1.54)$$

For the estimation of D_p from standard screen size, the reader may refer to Ref. [14].

If there is a size distribution of particles, the average size that can be used for flow through packed bed is

$$\overline{D}_\mathrm{p}=\frac{1}{\sum_i\left(\dfrac{\xi_i}{D_{\mathrm{p},i}}\right)} \qquad (4.1.55)$$

Table 4.1.3 Sphericity of Particles [14,17]

Particle Shape	Sphericity, ϕ
Sphere	1.00
Cube	0.81
Cylinder	
$h=d$	0.87
$5h=d$	0.70
$10h=$ d	0.58
Disks	
$3h=d$	0.76
$6h=d$	0.60
$10h=d$	0.47
Old beach sand	As high as 0.86
Young river sand	As low as 0.53
Average for various types of sand	0.75
Crushed solids	0.5–0.7
Granular particles	0.7–0.8
Wheat	0.85
Raschig rings	0.26–0.53

where ξ_i is the volume fraction of particles of size $D_{p,i}$.

In many metallurgical processes, the bed characteristics change spatially. In a blast furnace, for example, the packed bed consists of layers of ore and coke. Further, due to softening of iron-bearing layers at the bottom part of the furnace, the voidage in this layer reduces to very small values and the gas flows only through the coke layer. There can also be variation in the bed characteristic due to particle breakage, physico-chemical changes, size-segregation, etc. In such situations, the Ergun equation (Equation 4.1.49) can be written in a differential form and bed characteristics are allowed to change spatially so that detailed flow behavior can be obtained. Please note the word detailed in the current context refers only to a flow behavior averaged over several particles in the bed, not to the scale of each single particle. This also implies that the macroscopic bed characteristics such as bed voidage and particle size are also averaged over several particles locally to represent their spatial distribution.

When the flow in a packed bed is three-dimensional (3D), the Ergun equation (Equation 4.49) can be interpreted as a relationship between the local pressure drop per unit length and the superficial velocity aligned along the flow direction. For an arbitrarily selected coordinate system, velocity needs to be defined as a vector, $\vec{v_0}$ and the Ergun equation in vector form can be written as

$$\nabla \mathbb{P} = -\left(\frac{150.0\mu(1-\varepsilon)^2}{D_p^2\varepsilon^3} + \frac{1.75\rho(1-\varepsilon)}{\varepsilon^3 D_p}|\vec{v_0}|\right)\vec{v_0} \qquad (4.1.56)$$

Example 4.1.5
In a pellet-hardening unit, the flow rate of air at 1000 K is 5×10^{-3} m^3 s^{-1} and the size of the spherically shaped pellets is 4 mm. Pellets are filled to a depth of 250 mm. The cross-sectional area is 0.185 m^2. If the void fraction is 0.4, calculate the pressure drop needed to maintain the flow in mm of water. The density of air at 1000 K is 0.43 kg m^{-3} and its viscosity is 30×10^{-6} Pa s.

Solution
Ergun equation (Equation 4.1.49) needs to be used to find the pressure drop across the bed:

$$\frac{\Delta \mathbb{P}}{L} = \frac{150\mu(1-\varepsilon)^2}{D_p^2\varepsilon^3}v_0 + \frac{1.75\rho(1-\varepsilon)}{\varepsilon^3 D_p}v_0^2$$

The superficial velocity, $v_0 = 5 \times 10^{-3}/0.185 = 0.027$ m s^{-1}. Substituting this in the Ergun equation yields $\frac{\Delta \mathbb{P}}{L} = 44.00$ and hence $\Delta \mathbb{P} = 11 Pa = 1.1$mm of water.

It can be easily verified that only the first term in the Ergun equation is significant, since the superficial velocity is so small.

Example 4.1.6
The quality of cement greatly depends on the surface area of particles per unit mass of cement (specific surface area). Since the pressure drop in packed beds primarily depends on this property, one can design a simple packed-bed apparatus for determining the quality of cement powder. Figure 4.1.16 shows a schematic of such an apparatus. The apparatus consists of a glass bulb, valves to control air flow, manometer, and an appropriately designed container wherein desired amount of cement can be placed to make a packed bed.

Initially by opening the valve A, air is filled in the glass bulb to a predetermined pressure that can be measured using the manometer. Subsequently, valve A is closed and valve B is opened to allow the air to pass through the packed bed. As the air is removed from the bulb, the pressure decreases. Therefore, the pressure drop across the bed progressively decreases with a corresponding decrease in the flow rate through the cement bed and hence the rate of depletion of pressure in the bulb. This rate of depletion depends on
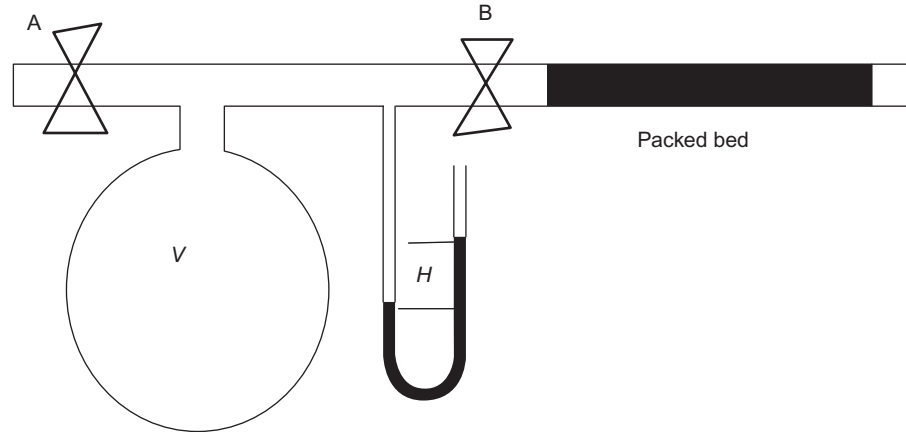
Figure 4.1.16 A schematic of a cement testing apparatus.

the resistance that the packed bed offers, which in turn depends on the bed characteristics. Flow rate through the cement bed is small enough to consider only the first term in the Ergun's equation. We need to obtain a relationship for the pressure in the bed as a function of time, from which the bed characteristics may be estimated.

Solution
According to the Ergun equation at low flow rates, the superficial velocity through the bed is proportional to the pressure drop across the bed. As the bed is expected to offer much more resistance than pipe and fittings, it is reasonable to assume that difference in pressure between that inside the bulb and that at the exit can be attributed completely to the packed bed. If $F_1 v_0$ represents the first term in the Ergun Equation (4.1.49), then,

$$P_{\text{bulb}} - P_0 = \Delta P_{\text{bulb}} = F_1 v_0 L \tag{4.1.57}$$

Please note that it has been assumed that any small change in pressure drop across the cement bed would result in instantaneous change in superficial velocity as well. This is quite reasonable as the characteristic time to attain steady-state velocity is much shorter than the characteristic time for the depletion of pressure inside the bulb.

The unsteady mass balance from the bulb can be written as

$$V_{\text{bulb}} \frac{\mathrm{d}(\rho_{\text{bulb}})}{\mathrm{d}t} = -\rho_{\text{average}} \times A_{\text{bed}} v_0 \tag{4.1.58}$$

where V_{bulb} denotes the volume of the bulb, ρ_{bulb} the density of air inside the bulb, and ρ_{average} the average density of the air while flowing through the cement bed. Applying ideal gas law, the above equation becomes,

$$V_{\text{bulb}} \frac{\mathrm{d}(P_0 + \Delta P_{\text{bulb}})M/(RT)}{\mathrm{d}t} = -(P_0 + \Delta P_{\text{bulb}}/2)M/(RT) \times A_{\text{bed}} v_0 \tag{4.1.59}$$

$$V_{\text{bulb}} \frac{\text{d}(\Delta P_{\text{bulb}})}{\text{d}t} = -(P_0 + \Delta P_{\text{bulb}}/2)^* A_{\text{bed}} v_0 \tag{4.1.60}$$

Substituting from Equation (4.1.57) for v_0,

$$V_{\text{bulb}} \frac{\text{d}(\Delta P_{\text{bulb}})}{\text{d}t} = -(P_0 + \Delta P_{\text{bulb}}/2)^* A_{\text{bed}} \frac{\Delta P_{\text{bulb}}}{F_1} \tag{4.1.61}$$

If $\Delta P_{\text{bulb}} \ll P_0$, the second-order term on the right-hand side of the above equation can be neglected and hence,

$$V_{\text{bulb}} \frac{\text{d}(\Delta P_{\text{bulb}})}{\text{d}t} = -P_0 A_{\text{bed}} \frac{\Delta P_{\text{bulb}}}{F_1} \tag{4.1.62}$$

The solution of this equation for an initial pressure difference ΔP_{bulb}^0 will be

$$\Delta P_{\text{bulb}} = \Delta P_{\text{bulb}}^0 \exp\left(-\frac{P_0 A_{\text{bed}}}{F_1 V_{\text{bulb}}} t\right) \tag{4.1.63}$$

The slope of the line in the graph $\log(\Delta P)$ vs. time permits the calculation of F_1, which is equal to $\dfrac{150.0\mu(1-\varepsilon)^2}{D_{\text{p}}^2 \varepsilon^3}$. Knowing μ_{air} and ε, one can estimate the particle size, D_{p}

4.1.11. FLUIDIZED BEDS

As upward flow rate of a fluid through a packed bed is increased, there is an increase in the pressure drop across the bed too. Eventually, the net force due to the pressure drop would equal that of the weight of the bed. Beyond this point, the particles that were static in the bed start moving and eventually with further increase in gas flow rate become suspended in the fluid; this is termed fluidization. Once fluidized, the suspension behaves like a fluid. For example, if the bed is tilted, the top surface remains horizontal. Further, the suspension can be transferred from one container to another in a manner similar to that with fluids. This suspension is named as fluidized bed. In case of liquid–solid systems, once fluidized, increase in superficial velocity results in a uniform increase in suspension volume as the voidage in the bed increases. This is termed particulate fluidization. In case of gas–solid systems, once fluidized, increase in superficial velocity can result in non-uniform expansion of the suspension containing bubble-like regions devoid of any particles. This state is termed bubbling fluidization and the bed is called a bubbling bed. The superficial velocity at the point of change from a packed bed to a fluidized bed is termed the minimum fluidization velocity, v_{mf}. These fluidization phenomena are illustrated in the schematics in Figure 4.1.17.

The change in pressure drop as well as the bed voidage with increase in superficial velocity is illustrated in Figure 4.1.18. When the bed is static, the pressure drop increases
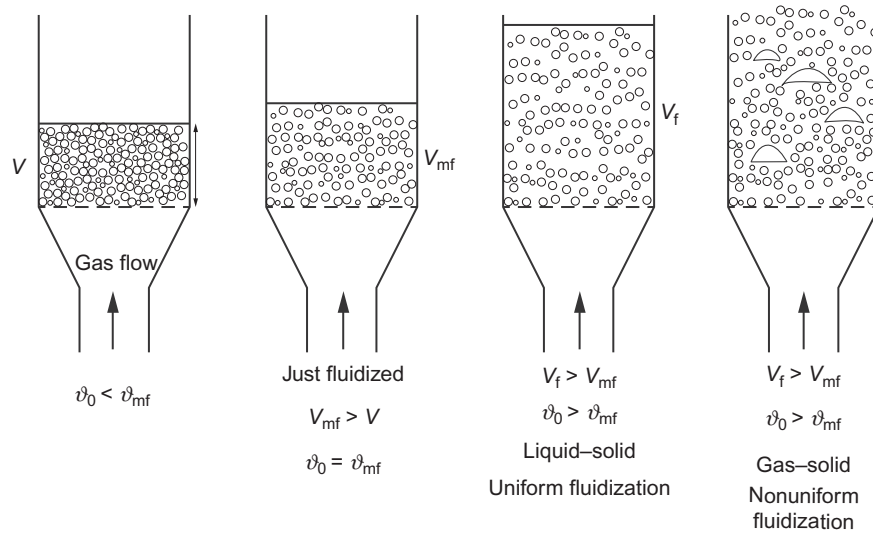
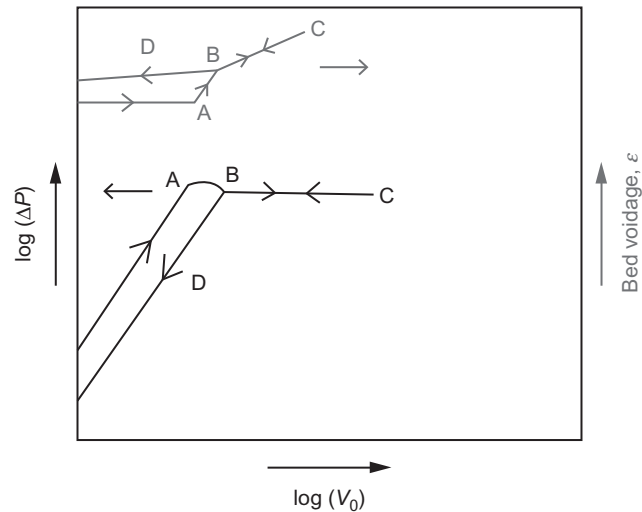**Figure 4.1.17** A schematic of fluidization phenomena.

Figure 4.1.18 A schematic of variation of pressure and bed voidage during fluidization.

with increase in superficial velocity in a manner predicted by the Ergun equation. Increase in superficial velocity beyond the point where the pressure drop counterbalances the weight of the bed results in fluidization. In the fluidization region, the pressure across the bed remains constant, just balancing the weight of the bed in the fluid. The void fraction and, therefore, the height of the bed should correspondingly increase (Figure 4.1.17).

In real systems, the bed might have been initially packed tightly interlocking the particles. Hence, the pressure in this packed condition may rise initially to a point A before the particles become free to move. As soon as the particles are released, the pressure drop settles back to the steady value corresponding to the fluidized bed (point B). If the superficial velocity is reduced from C, the bed settles down to a packed bed at point B with higher voidage than that when it was formed while filling. The pressure drop follows the path CBD. This difference in voidage often arises due to higher impact forces during bed formation or due to vibratory compaction.

4.1.11.1. Minimum Fluidization Velocity, v_{mf}

The minimum fluidization velocity can be estimated, since at this point the bed still remains packed, but the force arising from the pressure drop just balances the weight of the bed. As the pressure drop across the bed is given by the Ergun equation (4.1.49), the force balance at v_{mf} can be written as

$$AL(1-\varepsilon_{mf})(\rho_s - \rho)g = \Delta \mathbb{P} A$$

$$= AL\left(\frac{150.0\mu(1-\varepsilon_{mf})^2}{D_p^2\varepsilon_{mf}^3}v_{mf} + \frac{1.75\rho(1-\varepsilon_{mf})}{\varepsilon_{mf}^3 D_p}v_{mf}^2\right) \qquad (4.1.64)$$

As mentioned before, the voidage corresponding to the minimum fluidization (ε_{mf}) needs to be determined experimentally by slowly allowing the bed to settle from a fluidized state to a static one. Wen and Yu [18] found empirically that for a variety of systems, ε_{mf} can be correlated with sphericity, ϕ, using the following equations

$$\frac{1}{\phi\varepsilon_{mf}^3} \approx 14 \quad \text{and} \quad \frac{1-\varepsilon_{mf}}{\phi^2\varepsilon_{mf}^3} \approx 11 \qquad (4.1.65)$$

Substituting the above equations along with Equation (4.1.54) in Equation (4.1.65), the expression for estimating the minimum fluidization velocity can be written as,

$$\frac{D_{sph}v_{mf}\rho}{\mu} = \left(33.7^2 + \frac{0.0408D_{sph}^3\rho(\rho_s - \rho)g}{\mu^2}\right)^{0.5} - 33.7 \qquad (4.1.66)$$

4.1.11.2. Voidage in Particulate Fluidized Bed

As illustrated in Figure 4.1.18, the pressure drop across the bed remains more or less constant in the fluidization regime. One can assume that the Ergun's equation is still valid in the fluidized bed, but with varying voidage (ε) in the bed. In other words, the voidage is dependent on the superficial velocity. Since the pressure drop across the bed is equal to the apparent bed weight, one can write:

$$(1-\varepsilon)(\rho_s-\rho)g = \frac{150.0\mu(1-\varepsilon)^2}{D_p^2\varepsilon^3}v_0 + \frac{1.75\rho(1-\varepsilon)}{\varepsilon^3 D_p}v_0^2 \qquad (4.1.67)$$

In principle, the voidage in the fluidized bed (ε) can be determined by solving the above implicit nonlinear equation for a given superficial velocity, v_0. However, experimental investigations have indicated that the voidage measured in the bed is less than that predicted by the above equation. This may be due to the fact that the resistance offered by the bed on the gas flow changes with changing voidage in the bed.

Attempts have therefore been made for obtaining empirical correlations to predict the voidage in particulate fluidized beds with increasing superficial velocity. One such correlation based on a simple power law is proposed by Lewis *et al.* [19]:

$$v_0 = \varepsilon^m \qquad (4.1.68)$$

where the exponent m is obtained from a plot of m vs. Re_{D_p} as given in Figure 4.1.19 [20].

4.1.11.3. Voidage in Bubbling Fluidized Bed [21]

The bubbling fluidized bed also expands with increasing superficial velocity through the bed. Interestingly, experiments have shown that the primary contribution to this expansion comes from the bubble phase rather than relatively dense particulate–fluid phase. In other words, the voidage in the dense phase can be assumed as not increasing significantly with increasing superficial velocity, and the volume of gas flowing through this dense phase remains almost the same.

If ε_b represents the volume fraction of the bubble, v_b the bubble velocity, and v_{mf} is superficial velocity at the minimum fluidization point, then in a bubbling fluidized bed

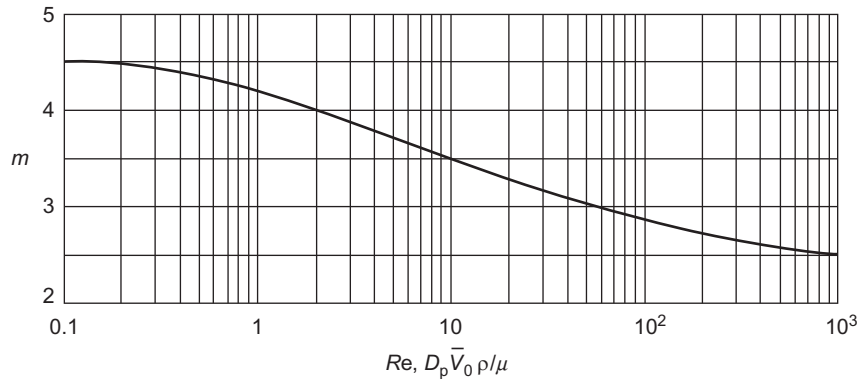$$v_0 = \varepsilon_b v_b + (1-\varepsilon_b)v_{mf} \qquad (4.1.69)$$

Figure 4.1.19 Exponent m in correlation for bed voidage in particulate fluidized bed [20].

The average velocity of the bubble, v_b, has been empirically correlated to the bubble size, D_b, as [21]

$$v_b = 0.711\sqrt{gD_b} \tag{4.1.70}$$

Experiments have also shown that large bubbles are generally mushroom shaped rather than spherical and for such cases D_b calculated based on bubble volume holds quite well.

Since the volume of the dense phase in a bubbling fluidized bed remains the same, the height of the fluidized bed, L, can be related to that at the minimum fluidization, L_{mf} as

$$L_{mf} = L(1 - \varepsilon_b) \tag{4.1.71}$$

4.1.12. FLOW AROUND PARTICLES

In many metallurgical processing systems, solid particles, liquid droplets, or gas bubbles dispersed in a fluid medium are common, e.g., solid particles in a liquid medium in sedimentation processes, solid particles in a gas medium in pneumatic screening processes and pneumatic transport of granular materials, solid or liquid inclusions in liquid metal, solid particles or liquid droplets in a spray-forming process, and gas bubbles in gas-stirred liquid metals. In all such systems where there is a relative movement between the dispersed phase and the continuous fluid medium, the movement of the particle is governed by the drag force arising from the viscosity of the fluid, the buoyancy force, and the gravitational force. Additional forces may also exist in the system such as those arising from electrostatic, magnetic, or electromagnetic phenomena. Even though these additional forces are not considered in the current section, these can be easily added to the governing equation.

In general, the governing equation for a dispersed phase of mass, m, moving in a fluid medium can be described using Newton's law of motion as

$$m\vec{a} = \vec{F}_{\text{Drag}} + \vec{F}_{\text{Buoyancy}} + m\vec{g} \tag{4.1.72}$$

where $\vec{a}$ is the acceleration of the dispersed phase.

For the case wherein the movement of the particle as well as the net force acting on the dispersed phase is either along the gravitational direction or against it, the above vectorial equation reduces to a simple scalar equation. When the dispersed phase has an axis of symmetry or a plane of symmetry parallel to the direction of its movement and has no rotational motion, the drag force acts exactly opposite to the direction of the movement of the particle. If not, the drag force need not be in line with its direction of movement resulting in what is termed as lift forces in addition to the drag forces. In many

metallurgical systems, the shape of the second phase may be approximated to a spherical shape using an appropriate sphericity factor discussed earlier and its motion as well as forces acting on it can be considered to be acting opposite to the flow direction. In the current section, only such cases are discussed.

For the case where the movement of the dispersed phase is along the gravitational direction (example: sedimentation of an ore particle in a liquid media), the force balance equation reduces to

$$ma = -F_{\text{Drag}} - F_{\text{Buoyancy}} + m\vec{g} \qquad (4.1.73)$$

and for the case where the movement of the dispersed phase is opposite to the gravitational direction (example: bubble rising in a fluid),

$$ma = -F_{\text{Drag}} + F_{\text{Buoyancy}} - m\vec{g} \qquad (4.1.74)$$

In both these cases, as the velocity of particle increases, the drag force opposing the motion increases as well. Eventually, the dispersed phase may reach a point where the net force acting on it becomes zero. Then, the dispersed phase attains a constant velocity, termed the terminal velocity. The concept of terminal velocity has been found to be quite useful in designing sedimentation systems, pneumatic screening processes, flotation of inclusions in liquid steel, etc.

In order to determine the net drag force acting on an object submerged in a flowing fluid, the concept of the friction factor is used. The definition of Fanning friction factor developed for flow through conduits using forces is extended to flows around submerged objects, also termed as external flows:

$$F_{\text{Drag}} = A\left(\frac{1}{2}\rho v_\infty^2\right)f_{\text{F}} \qquad (4.1.75)$$

where A is the characteristic area, typically taken as the projected area of the solid on a plane perpendicular to the velocity of the approaching fluid, v_∞, ρ is the density of the fluid and f_{F} is the Fanning friction factor. For a spherical object of diameter D_{p}, the above equation becomes

$$F_{\text{Drag}} = \left(\frac{\pi D_{\text{p}}^2}{4}\right)\left(\frac{1}{2}\rho v_\infty^2\right)f_{\text{F}} \qquad (4.1.76)$$

Using Buckingham's Π theorem, it can be easily proved that the friction factor, f_{F}, will be a function of the Reynolds number, Re_D. The Reynolds number Re_D is defined using the characteristic velocity v_∞ and the characteristic dimension, D_{p}.

Numerous studies, especially on the flow of fluids around spheres, have been carried out by many researchers. The important flow features from these studies are illustrated in Figure 4.1.20. Please note that a situation in which a spherical particle is seen to be
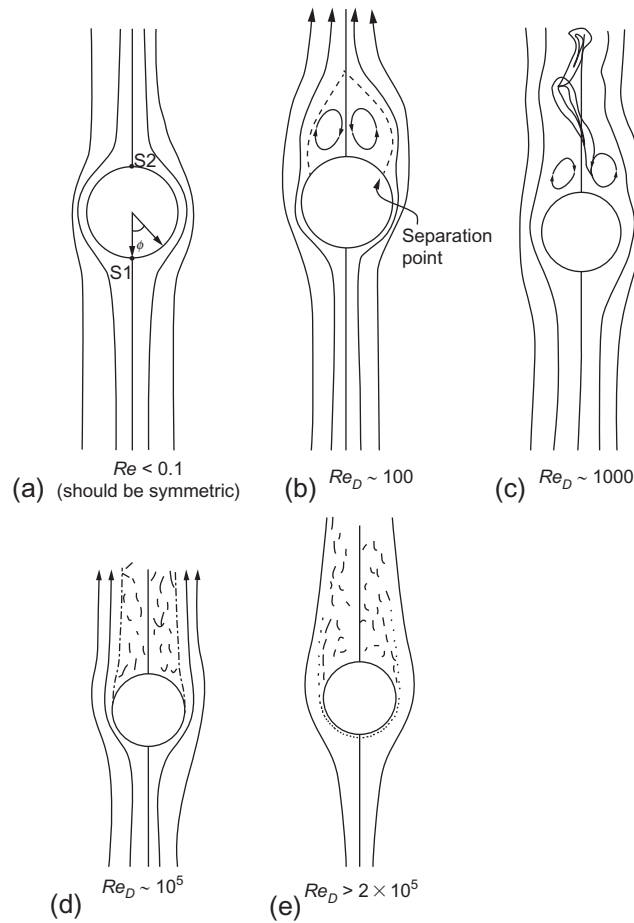
Figure 4.1.20 Schematic illustration of flow around a sphere.

moving in a fluid medium in the laboratory frame of reference can also be viewed as fluid moving around a stationary spherical particle if the frame of reference is attached to the moving particle.

At very low velocities ($Re_D < 0.1$), the viscous forces dominate over the inertial forces. As illustrated in the schematic (see Figure 4.1.20a), the flow lines are almost symmetrical on the front and the back side of the sphere. Stokes [22] obtained an analytical solution for the differential momentum balance equations along with the equation of continuity, for the asymptotic limit wherein the velocity is so small that one can neglect the advective momentum term (the differential momentum balance equations and the continuity equation are described in Section 4.1.14.2). Flows at such low velocities are termed as creeping flows. From the analytical expression, Stokes [22] found that

the net drag force acting on the sphere in the direction opposite to the flow direction has contributions both from the pressure and the tangential force (arising from the fluid velocity gradients at the surface of the sphere) acting on the surface of the sphere. The net force acting on the particle arising from the pressure is given by $\pi\mu D_p v_\infty$ and that from the tangential force is given by $2\pi\mu D_p v_\infty$. The first term is termed as the form drag and the latter as viscous drag or friction drag.

Thus the total drag force on the spherical particle is

$$F_{\mathrm{Drag}} = 3\pi\mu D_p v_\infty \tag{4.1.77}$$

This is the Stokes law. Based on the definition used to describe the Fanning friction factor for external flows (refer to Equation 4.1.75), the Fanning friction factor for creeping flow around a sphere can be determined as:

$$f_{\mathrm{F}} = \frac{24}{Re_D} \tag{4.1.78}$$

Experiments have shown that the Stokes law can be used to estimate the drag force with reasonable accuracy up to Re_{D_p} of 0.1. The law is useful for small particles moving in low viscosity gases and liquids as well as larger particles moving through viscous liquids.

Beyond the Stokes regime, it has not been possible to determine the drag force from theory alone; instead it needs to be estimated using dimensionless correlations developed using data obtained through experiments conducted by numerous researchers. The variation of Fanning friction factor, f_{F}, with the Reynolds number, Re_{D_p}, for spherical particles (sphericity $\phi = 1.0$, see Equation 4.1.53) is depicted in Figure 4.1.21. The figure gives the friction factor for some irregular particles too, where the particle size is defined based on the size of the sphere having equivalent volume (Equation 4.1.52).

Beyond the Stokes regime, the plot becomes nonlinear. Interestingly, the friction factor remains relatively constant at about 0.44 in the range of Reynolds numbers between 500 and 100,000; the drag force in this range is proportional to square of the velocity. This region is the Newton's regime. At Re_D greater than about 2×10^5, the flow all around the sphere becomes turbulent.

The variation in friction factor with Reynolds number can be correlated to some of the features observed in such flows. The region near the sphere where the velocity is significantly different from the undisturbed velocity in the free stream far away from the sphere is normally called the boundary layer. Any fluid packet flowing through the boundary layer undergoes accelerations and decelerations as it flows past the sphere. The packet approaching the sphere at a constant speed of v_∞ from far away decelerates as it comes close to the front of the sphere. It then accelerates as it flows past the sphere up to an angle of $\theta = 90°$, and then decelerates till it reaches the region near the rear. It again accelerates away downstream to reach the free stream value of v_∞. Bernoulli's equation
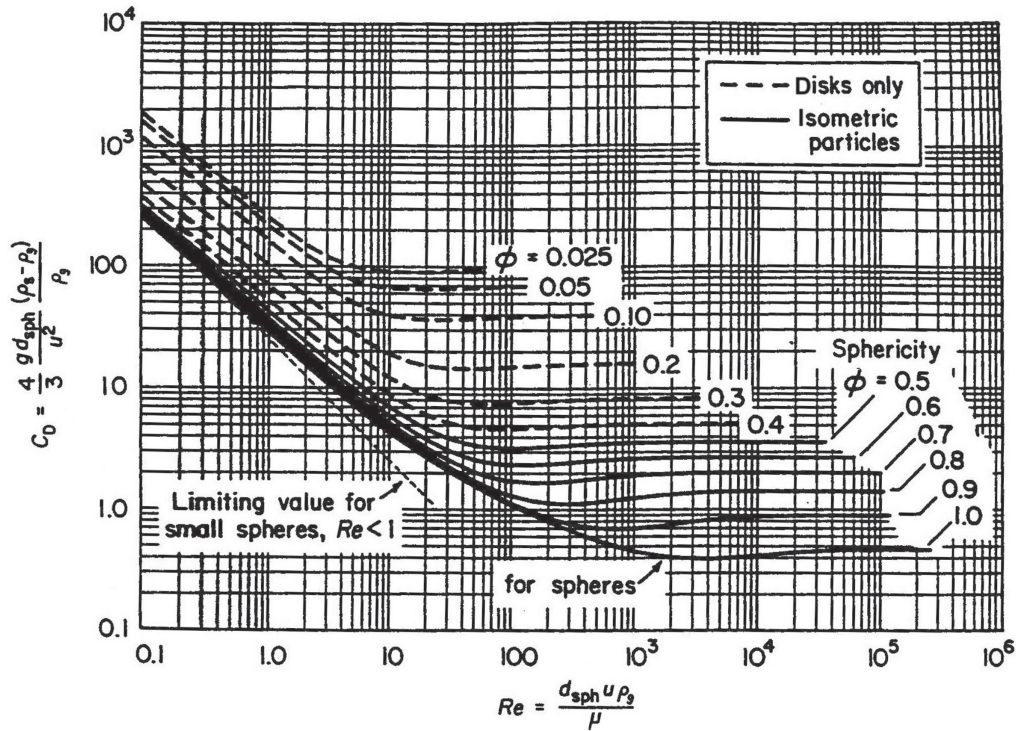
Figure 4.1.21 Fanning friction factor for flow across particles [1].

applied along a streamline helps understanding the pressure variations near the sphere. A fluid element reaching the surface of the sphere along the streamline normal to the sphere loses all its kinetic energy, which results in a corresponding increase in pressure. This high pressure point, called the front stagnation point, is shown as point S1 in Figure 4.1.20a. A second stagnation point, S2, is at the rear of the particle, diametrically opposite to S1. For an ideal fluid, the pressures at both S1 and S2 would be the same. Due to viscous dissipations in real fluids, however, the pressure at S2 is lower than that at S1. This asymmetry leads to a net force, called the form drag, along the flow direction. Additionally there is a viscous force, called the friction drag, due to transverse velocity gradients at the sphere surface. These two forces together form the total drag on the sphere (given by the Stokes law at low Reynolds numbers). Please note that the buoyancy force exists on the sphere irrespective of whether the fluid flows or not.

Due to the acceleration and deceleration in flow around the sphere, pressure decreases first (till $\theta = 90°$, Figure 4.1.20a) and then increases as the fluid flows toward the rear stagnation point. In the latter region, the flow is against a pressure gradient (uphill). The higher the velocity, the higher is the adverse pressure gradient. To avoid this uphill

pressure gradient, the flow *separates* at Re_D of about 20: the fluid moving towards the sphere moves away much earlier than the rear stagnation point. The fluid near the rear now remains attached to the sphere and recirculates in a toroidal fashion, as shown in Figure 4.1.20b. The point on the sphere that delineates the main flow from the recirculating region is called the separation point. The toroidal recirculating flow region is called the wake.

The size of the recirculating zone increases with increasing Reynolds number. It starts to oscillate at higher Reynolds numbers, and at Re_D of around 200, parts of it are *periodically* shed, i.e., they disengage from the sphere and move downstream as illustrated in Figure 4.1.20c. These recirculating flow formations traveling downstream are referred as vortices. A similar phenomenon of shedding of vortices is also observed in flows across long cylinders and other blunt shapes. In the case of cylinders, the shedding of vortices occurs alternately from each side of the cylinder. Interestingly, the frequency of vortex shedding in the case of cylinders correlates well with the free stream velocity and can be used as a measurement technique.

With further increase in Reynolds number, the flow in the wake region becomes more and more chaotic even as the flow before the separation point remains laminar. The separation point slowly moves upstream till the Reynolds number reaches a value of about 2×10^5 when it is positioned at an angle of approximately $85°$ (Figure 4.1.20d). Once this critical Reynolds number is exceeded, the boundary layer in the front of the particle itself turns turbulent. This delays separation (Figure 4.1.20e) and the separation point shifts to a point behind the sphere at an angle of approximately $140°$. This shift results in a sharp drop in friction factor. Experiments have shown that the transition occurs at lower Reynolds numbers for spheres having rough surfaces. Many phenomena are manifestations of the interesting flow dynamics in the wake region: the spiral paths that some bubbles take, the flutter of a flag behind the flag pole, swing of a cricket ball, singing of overhead wires, etc.

4.1.13. COMPRESSIBLE FLOW

Flow of gases with velocities less than that corresponding to a Mach number of 0.3 can be treated as incompressible flows as discussed in Section 4.1.3. For incompressible flows, the term $\int \frac{dP}{\rho}$ in the mechanical energy balance (Equation 4.1.8) simplifies to $\frac{1}{\rho} \int dP$. For compressible flows, however, the integral needs to be evaluated with density varying as the fluid flows through the system. This, in turn, is governed by local temperature and pressure. Thus for rigorous evaluations, one needs to solve the heat transfer equation along with the equations governing the motion. In undertaking simple analyses, the flow can be considered under two extreme conditions, namely, (1) adiabatic and (2)

isothermal. If the flow is through a short conduit or nozzle, it can be approximated as adiabatic. For long conduits, where the surface area available for heat transfer per unit volume of gas flowing through the system is large, the flow is expected to be closer to isothermal conditions. In reality, the system would be somewhere between these two extreme cases, depending on heat transfer.

4.1.13.1. Compressible Flow Through a Pipe of Constant Cross Section

First, let us look at an adiabatic steady-state flow of an ideal gas from a reservoir through a straight pipe of length L and diameter D, as shown in Figure 4.1.22.

In this system, it is expected that both the velocity as well as the density of the gas changes as it flows through the pipe. However, from mass conservation it can be easily inferred that the average mass flux of gas through the pipe remains constant along the length of the pipe. Let us denote this mass flux by G and let $\hat{V}$ denote the specific volume of the gas. Then

$$\hat{V} = \frac{1}{\rho} \quad \text{and} \quad v = \frac{G}{\rho} = G\hat{V}$$

The differential mechanical energy balance given by Equation (4.1.10) can then be written in terms of G as,

$$G^2 \hat{V} \, d\hat{V} + \hat{V} \, dP + \frac{2f_F}{D} G^2 \hat{V}^2 \, dL = 0 \qquad (4.1.79)$$

Dividing the above equation by V^2, we obtain

$$G^2 \frac{d\hat{V}}{\hat{V}} + \frac{dP}{\hat{V}} + \frac{2f_F}{D} G^2 \, dL = 0 \qquad (4.1.80)$$

The above equation can be integrated from location 1 near the entrance to the exit point 2, assuming adiabatic flow, i.e.,

$$P\hat{V}^\gamma = \text{constant} \quad \text{where} \quad \gamma = \frac{c_P}{c_{\hat{V}}} \qquad (4.1.81)$$

Since at large Reynolds numbers the friction factor for pipe flow remains relatively constant, it is reasonable to assume that f_F remains the same throughout the length of the pipe. If so, integration of Equation (4.1.80) and substitution of Equation (4.1.81) gives:
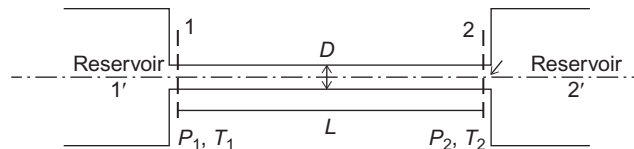

Figure 4.1.22 Schematic of a compressible flow through a straight pipe.

$$G^2 = \frac{\frac{\gamma}{\gamma+1} \frac{P_1}{V_1} \left[1 - \left(\frac{P_2}{P_1}\right)^{(\gamma+1/\gamma)}\right]}{\left[2 f_F \frac{L}{D} - \frac{1}{\gamma} \ln \frac{P_2}{P_1}\right]} \qquad (4.1.82)$$

The above equation shows a very interesting trend. If G^2 is plotted as a function of P_2 keeping P_1 constant, it can be easily observed that G^2 goes through a maximum. By differentiating Equation (4.1.82) with respect to P_2 and equating it to zero, the maximum value of the mass flux and the corresponding velocity, v_{max}, can be obtained. This velocity is:

$$v_{max} = \sqrt{\frac{\gamma R T_2}{M}} = \sqrt{\left(\frac{\partial P}{\partial \rho}\right)_S} = c \qquad (4.1.83)$$

where c corresponds to the sonic velocity under constant entropy (S).

Equation (4.1.82) suggests that beyond the maximum, decreasing the exit pressure P_2 (keeping P_1 constant) decreases the mass flux, which is nonphysical. This can only mean that this equation is not valid when P_2 is lowered below that corresponding to the maximum. In order to understand this, let us have a re-look at the experiment. Imagine initially the pressure at point 2 are equal to P_1. There will not be any flow of gas through the pipe. Now suppose the pressure at the reservoir at the exit end is decreased a little. The information of pressure decrease traverses at the speed of sound (speed of sound is the speed at which pressure disturbance travels through the medium) in the direction opposing the flow, a pressure profile develops in the tube and thus a steady flow is established. Once the velocity of the fluid reaches the sonic velocity, however, the information that the pressure has been decreased at reservoir 2 cannot reach the reservoir 1. In other words, the pressure at exit end (at point 2) of the pipe does not decrease beyond the critical value corresponding to the maximum mass flux. From the exit end of the pipe (point 2) to the reservoir 2 (point 2′), the pressure changes abruptly through a series of shock waves.

Once the maximum mass flux through the pipe is achieved, the mass flux cannot be altered by changing conditions at the exit end; the pipe is said to be choked. Further change in mass flux can be only achieved by changing the conditions at the upstream reservoir.

Similarly, the integration of Equation (4.1.80) can be undertaken under isothermal conditions for an ideal gas. The resulting expression for the mass flux, G, is:

$$G^2 = \frac{\frac{M}{2RT_1}\left(P_1^2 - P_2^2\right)}{2 f_F \frac{L}{D} - \ln \frac{P_2}{P_1}} \qquad (4.1.84)$$

Similar to the adiabatic flow, the velocity corresponding to the maximum mass flux (choked flow) is given by

$$\nu_{\max} = \sqrt{\frac{RT}{M}}$$

This corresponds to the speed of sound or sonic velocity under the isothermal assumption.

Example 4.1.7

Let us revisit the example problem 4.1.3 relaxing the assumption of flow being incompressible.

Solution

Let us use the same friction factor, f_F, of 0.0055.

Knowing the gas volumetric flow rate at STP, gas density at STP and the area of cross section of the pipe, the mass flux, G, can be determined and is equal to 1197 kg m^{-2}. As the pipe is very long, let us estimate the pressure drop assuming isothermal condition. If so, using the expression given in Equation (4.1.84), the value of P_1 can be calculated iteratively for a known value of P_2 (1.1×10^6 Pa) and T (300 K). The value of P_1 is equal to 1.92×10^6 Pa. The difference between this and the one calculated using incompressible flow is only 2%.

The pressure, P_1, can be estimated using adiabatic assumption as well using Equation (4.1.82) and its value is equal to 1.67×10^6 Pa. The difference between this value and the one calculated using incompressible flow assumption is 19%. This indicates that the assumption of isothermal conditions for this problem gives values close to that obtained for incompressible flow. For long tubes, the assumption of the isothermal flow may be more reasonable for the reasons mentioned earlier.

4.1.13.2. Compressible Flow Through Convergent–Divergent (de Laval) Nozzle

In the last section, we saw that for a compressible fluid, the exit velocity through a pipe of constant cross section cannot exceed the sonic velocity. To achieve velocities beyond sonic velocities, i.e., supersonic velocities, a convergent–divergent nozzle, otherwise called de Laval (named after a Swedish scientist who invented it in 1888) nozzle is used. In BOF, these nozzles are used to generate supersonic flow of oxygen that penetrates the liquid metal and slag and aids in achieving the rapid refining of steel.

A schematic of a convergent–divergent nozzle is shown in Figure 4.1.23. The diverging section is long compared to the converging section. The area of cross section changes slowly in the diverging section in order to suppress boundary layer separation. However, the converging section is short as the boundary layer separation does not occur in this section. The location where the cross-sectional area is the minimum is termed as the throat of the nozzle. As the total length of the nozzle is small, a simple analysis can be made by considering the flow to be adiabatic with negligible friction losses.
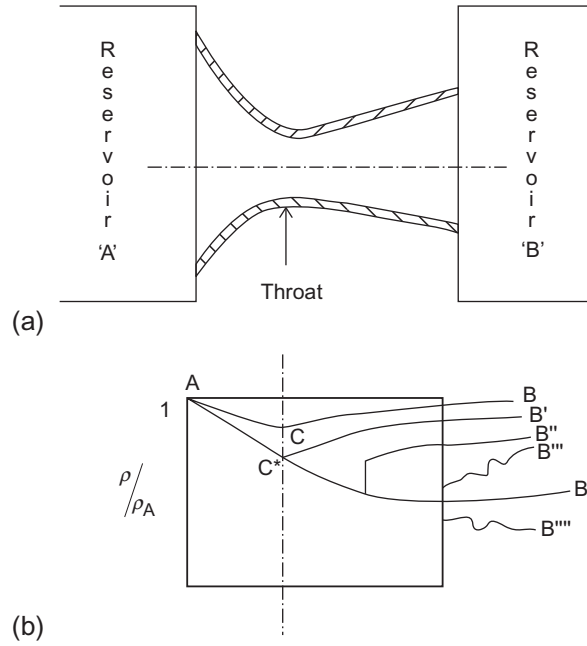
Figure 4.1.23 (a) Schematic of a convergent–divergent (de Laval) nozzle and (b) schematic of the pressure profiles under various flow regimes.

At steady state, the mass flow rate of gas through the nozzle remains constant along the length of the nozzle, i.e.,

$$A\rho v = \dot{m} = \text{constant}$$

$$\text{Thus } \frac{\mathrm{d}A}{A} + \frac{\mathrm{d}\rho}{\rho} + \frac{\mathrm{d}v}{v} = 0 \tag{4.1.85}$$

The mechanical energy balance equation (Equation 4.1.10), neglecting the friction loss term, reduces to

$$\frac{\mathrm{d}P}{\rho} + v\,\mathrm{d}v = 0 \tag{4.1.86}$$

Using the above equation and Equation (4.1.83) in Equation (4.1.85), we obtain

$$\frac{\mathrm{d}v}{v}\left(1 - \frac{v^2}{c^2}\right) + \frac{\mathrm{d}A}{A} = 0$$

$$\frac{\mathrm{d}v}{v}\left(1 - Ma^2\right) + \frac{\mathrm{d}A}{A} = 0 \tag{4.1.87}$$

From this equation, it can be inferred that through the converging section $\left(\frac{\mathrm{d}A}{A} < 0\right)$, for subsonic flows $(Ma < 1)$, the velocity of the flowing gas increases $\left(\frac{\mathrm{d}v}{v} > 0\right)$. Similarly, through a diverging nozzle $\left(\frac{\mathrm{d}A}{A} > 0\right)$, for subsonic flows $(Ma < 1)$, the velocity of the

flowing gas decreases along the direction of the flow. This trend is the same as that for flow of incompressible fluids through converging or diverging sections. For supersonic flows ($Ma > 1$), on the other hand, the trend reverses, i.e., the velocity decreases through a converging section and increases through a diverging section. This implies that supersonic flows can only be obtained if at the throat $\left(\frac{dA}{A} = 0\right)$ the velocity is sonic.

Before deriving the design equations for a supersonic nozzle, it is instructive to understand the flow regimes that are obtained when operating a convergent–divergent nozzle under different pressure differences. In Figure 4.1.23, a schematic of a converging–diverging nozzle connected across two gas reservoirs is shown. Keeping the pressure and temperature at reservoir A constant and by progressively reducing the pressure at reservoir B, various flow regimes are obtained. Figure 4.1.23b gives the profiles of pressure ratio, $\frac{P}{P_A}$ (P_A is the pressure at reservoir A or stagnation pressure) corresponding to each flow regime. The regimes are as follows:

Subsonic flow: Suppose the pressure at reservoir B (placed at the exit end of the nozzle) is decreased slowly starting from a value equal to P_A. In the beginning, the flow would be subsonic throughout the nozzle; the velocity increases and reaches a maximum at the throat and beyond the throat it decreases. The pressure would correspondingly decrease in the converging section reaching a minimum at the throat (point C) and increase in the diverging section. This is similar to a flow of incompressible fluid through a venturi. The pressure profile is shown in the figure 4.1.23b as ACB.

Flow is just choked: As the flow rate through the nozzle is increased, a situation arises when the velocity at the throat is sonic and the nozzle is choked. Two situations can take place: the flow can become subsonic in the diverging portion and the pressure can reach B′ along AC^*B'. The flow can instead become supersonic, in which case the pressure follows the path PC^*B^* and the exit pressure would be at B^*. This latter is the designed operation, the flow transitioning from subsonic to supersonic smoothly and reversibly.

Flow with a normal shock in the nozzle: Since flow cannot have a reversible transition from subsonic to supersonic state, or vice versa, in a diverging region, pressure between B′ and B^* is not reachable by reversible expansions. If an exit pressure is maintained at a value between B′ and B^*, the flow has to become irreversible somewhere in the diverging section. In the diverging section, the pressure suddenly jumps from a low value to a higher value through what is termed as a normal shock, as illustrated in the figure (see curve AC^*B''). Across the shock the flow changes suddenly from supersonic to subsonic. The shock wave moves toward the exit end of the nozzle decreasing in intensity as the pressure at B is progressively decreased and eventually, the shock wave would reach the exit end and disappear at the designed exit pressure of B^*.

Under expanded flow: Decreasing the pressure in reservoir B below B^* cannot change the flow inside the nozzle. Pressure at the exit remains at B^*, and decreases outside the nozzle to the reservoir pressure B″″ through a series of oblique shock waves. This jet is said to be under-expanded in the nozzle.

Irreversible phenomena such as shock waves dissipate mechanical energy into internal energy of the gas. A supersonic nozzle is designed for a given exit Mach number and pressure drop and should therefore be operated at design conditions.

Analytical expressions for pressure and velocity distribution along the length of the nozzle can easily be obtained for idealized conditions, wherein the gas flow through the de Laval nozzle can be approximated as adiabatic frictionless flow of an ideal gas (isentropic flow).

Equation (4.1.86) can be integrated using Equation (4.1.81). If the gas velocity in the supply tube is small compared to the sonic velocity, the contribution to kinetic energy can be neglected. Then we obtain at any section

$$v^2 = \frac{2}{(\gamma - 1)} \frac{\gamma P}{\rho} \left[\left(\frac{P_A}{P} \right)^{(\gamma - 1/\gamma)} - 1 \right] \tag{4.1.88}$$

In terms of Mach number, Ma (sonic velocity, $v_s = \sqrt{\frac{\gamma P}{\rho}}$):

$$Ma^2 = \frac{2}{(\gamma - 1)} \left[\left(\frac{P_A}{P} \right)^{(\gamma - 1/\gamma)} - 1 \right] \tag{4.1.89}$$

For a choked nozzle, the Mach number at the throat has to be 1, hence,

$$\frac{P_{C^*}}{P_A} = \left(\frac{2}{\gamma + 1} \right)^{(\gamma/\gamma - 1)} \tag{4.1.90}$$

Similarly for a given Mach number at the exit, $\frac{P_B}{P_A}$ can be determined as

$$Ma_B^2 = \frac{2}{(\gamma - 1)} \left[\left(\frac{P_A}{P_B} \right)^{\gamma - 1/\gamma} - 1 \right] \tag{4.1.91}$$

It should be noted that adiabatic flow results in continuous change in temperature of the gas and therefore the sonic velocity. The Mach number at any location is defined with respect to the sonic velocity at that point. Sonic velocities at A, B, and C are therefore different. From the pressures, the temperatures, the densities, and the velocities can be calculated at various locations throughout the length of the nozzle. Using these values, one can determine the dimensions of the nozzle.

4.1.14. MOMENTUM BALANCE AT DIFFERENTIAL SCALE

In Section 4.1.1.2, it was stated that the conservation equations can be applied at a macroscopic scale or at a differential scale depending on the objective. To this point in the discussion, the conservation principle has been applied at a macroscopic scale in most of the situations. For example, an overall energy balance pertaining to flow (see Section 4.1.4) is developed at a macroscopic scale to relate the net flow rate and the pressure drop, wherein the interest was not really to capture the detailed flow profiles in a system. For obtaining a

detailed flow profile in the fully developed flow region in a pipe, momentum balances were indeed made at a differential scale; this, however, was for a simple 1D steady-state flow. For 3D flows, this approach needs to be generalized.

In a generic case of a flowing fluid, it is desirable to know the spatial and temporal variation of velocities as well as the pressure in the system. Velocity being a vector needs to be described using three of its components according to the coordinate system. Thus, including pressure, the number variables add up to four; therefore four equations are required to obtain the flow profiles in any system. These four equations correspond to one of mass conservation and three momentum conservation equations corresponding to each component of velocity. The mass conservation equation (for an incompressible fluid this would lead to volume conservation) at the differential scale this is termed the equation of continuity. The momentum conservation at a differential scale for an incompressible Newtonian fluid having constant viscosity leads to one of the celebrated equations in fluid dynamics, the Navier–Stokes equation. In the following sections, the equation of continuity and the Navier–Stokes equation are described in detail. These equations are derived in Cartesian coordinates and these equations can also be transformed to other coordinate systems of interest such as cylindrical, spherical coordinates.

4.1.14.1. Equation of Continuity

Consider an infinitesimal control volume in a flowing fluid as shown in Figure 4.1.24. The control volume is located at (x,y,z) with respect to a chosen Cartesian coordinate system. The shape of the control volume corresponds with that of the coordinate system and its dimensions are Δx, Δy, and Δz.
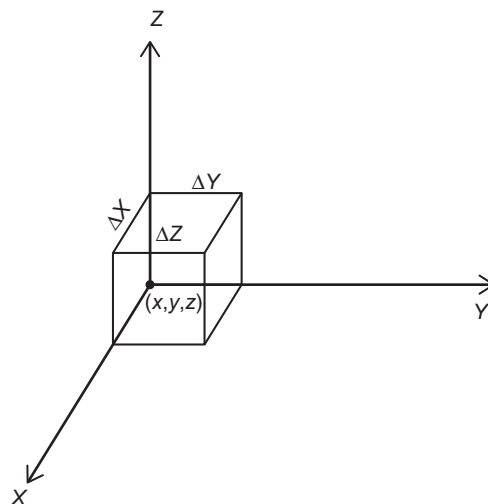

Figure 4.1.24 Infinitesimal control volume in Cartesian coordinates.

Let $v_x(x,y,z)$, $v_y(x,y,z)$, and $v_z(x,y,z)$ denote the x-, y-, and z-velocity components, respectively, and $\rho(x,y,z)$ denote density of the fluid at the location (x,y,z). Considering the conservation of mass in the control volume,

$$
\begin{aligned}
\frac{\partial \rho}{\partial t}\Big|_{(x+\frac{\Delta x}{2},y+\frac{\Delta y}{2},z+\frac{\Delta z}{2})}\Delta x \Delta y \Delta z = {}& (\rho v_x)\big|_{x,y+\frac{\Delta y}{2},z+\frac{\Delta z}{2}} - (\rho v_x)\big|_{(x+\Delta x,y+\frac{\Delta y}{2},z+\frac{\Delta z}{2})} \\
& (\rho v_y)\big|_{x+\frac{\Delta x}{2},y,z+\frac{\Delta z}{2}} - (\rho v_y)\big|_{(x+\frac{\Delta x}{2},y+\Delta y,z+\frac{\Delta z}{2})} \\
& (\rho v_z)\big|_{x+\frac{\Delta x}{2},y+\frac{\Delta y}{2},z} - (\rho v_y)\big|_{(x+\frac{\Delta x}{2},y+\frac{\Delta y}{2},z+\Delta z)}
\end{aligned}
\tag{4.1.92}
$$

Dividing the above equation by $\Delta x \Delta y \Delta z$ and taking the limit as the control volume is reduced to zero, the Equation (4.1.92) reduces to

$$
\frac{\partial \rho}{\partial t} + \nabla \cdot (\rho \vec{v}) = 0
\tag{4.1.93}
$$

This is the equation of continuity for any fluid. Here $\rho \vec{v}$ is the mass flux vector and $\nabla \cdot (\rho \vec{v})$ gives the net rate of mass flowing out of a unit volume fixed in space. Since $\nabla \cdot (\rho \vec{v}) = \rho(\nabla \cdot \vec{v}) + \vec{v} \cdot \nabla \rho$, it can be shown that

$$
\frac{\mathrm{D}\rho}{\mathrm{D}t} = \frac{\partial \rho}{\partial t} + \vec{v} \cdot \nabla \rho = -\rho(\nabla \cdot \vec{v})
$$

$\frac{\mathrm{D}\rho}{\mathrm{D}t}$ is the material or substantial derivative and gives the change in density of fluid packet as it travels (Lagrangian frame of reference). $\nabla \cdot \vec{v}$ is the rate of change of volume for the fluid packet.

If the flow is steady, then

$$
\nabla \cdot (\rho \vec{v}) = 0
\tag{4.1.94}
$$

If the flow is also incompressible, then

$$
\nabla \cdot (\vec{v}) = 0
\tag{4.1.95}
$$

4.1.14.2. Navier–Stokes Equation

In the control volume considered in Section 4.1.14.1, let us perform an x-momentum balance, i.e., balancing the x component of the momentum. For momentum conservation, the accumulation of momentum in the control volume, the rate at which the momentum enters and leaves the control volume, and the forces acting on the control volume need to be considered. As far as momentum being transported in and out of the control volume is concerned, there are basically two modes of transport, one by advection and another by momentum diffusion or viscous transport. Let us denote the diffusive momentum flux by τ_{ij}, where "i" denotes the direction in which the "j" component of momentum is transported. The reader may refer to Section 4.1.5 where the diffusive momentum flux has been elaborated.

It should be noted that the diffusive momentum flux, τ_{ii}, arises as the velocity component, v_i, changes in the "i" direction.

Let us look at each term in the x-momentum conservation one by one

Rate of accumulation:

$$\frac{\partial(\rho v_x)}{\partial t}\Big|_{(x+\frac{\Delta x}{2},y+\frac{\Delta y}{2},z+\frac{\Delta z}{2})}\cdot\Delta x\cdot\Delta y\cdot\Delta z$$

Advective momentum transfer:

Rate of advective x-momentum entering through surface $x=x$ in the control volume

$$(\rho v_x v_x)\Big|_{(x,y+\frac{\Delta y}{2},z+\frac{\Delta z}{2})}\cdot\Delta y\cdot\Delta z$$

and the rate leaving the control volume at $x=x+\Delta x$ is

$$(\rho v_x v_x)\Big|_{(x+\Delta x,y+\frac{\Delta y}{2},z+\frac{\Delta z}{2})}\cdot\Delta y\cdot\Delta z$$

Advective x-momentum entering through surface $y=y$ in the control volume

$$(\rho v_y v_x)\Big|_{(x+\frac{\Delta y}{2},y,z+\frac{\Delta z}{2})}\Delta x\Delta y$$

Please note that the net mass entering through the surface $y=y$ is

$$(\rho v_y)\Big|_{(x+\frac{\Delta y}{2},y,z+\frac{\Delta z}{2})}\Delta x\Delta y$$

and this fluid's x component of velocity is v_x

Similarly, advective momentum entering through surfaces $z=z$ as well as leaving through surfaces $y=y+\Delta y$ and $z=z+\Delta z$ can be written.

Viscous or diffusive momentum:

Rate of viscous momentum entering through face $x=x$ is

$$\tau_{xx}\Big|_{(x,y+\frac{\Delta y}{2},z+\frac{\Delta z}{2})}\Delta y\cdot\Delta z$$

and the viscous momentum entering through face $y=y$ is

$$\tau_{yx}\Big|_{(x+\frac{\Delta x}{2},y,z+\frac{\Delta z}{2})}\cdot\Delta y\cdot\Delta z$$

Similarly, viscous momentum entering through surfaces $z=z$ as well as leaving through surfaces $x=x+\Delta x$, $y=y+\Delta y$, and $z=z+\Delta z$ can be written.

Forces acting on the control volume along the x-direction

Due to pressure

$$\left(P|_{(x,y+\frac{\Delta y}{2},z+\frac{\Delta z}{2})} - P\Big|_{(x+\Delta x,y\frac{\Delta y}{2},z+\frac{\Delta z}{2})}\right)\Delta y\Delta z$$

Due to gravity

$$\rho\Delta x\Delta y\Delta z g_x$$

where g_x is a component of acceleration due to gravity (g), along the x-direction. It may be noted that if there are additional forces acting on the fluid, such as those arising from electromagnetic interaction, they can be appropriately incorporated as source terms in the conservation equation.

All these terms are put together using the conservation equation (Equation 4.1.1) and dividing by $\Delta x\Delta y\Delta z$ and taking the limit as the control volume is reduced to zero, the following expression is obtained

$$\begin{aligned}\frac{\partial\rho v_x}{\partial t} = &-\frac{\partial\rho v_x v_x}{\partial x} - \frac{\partial\rho v_y v_x}{\partial y} - \frac{\partial\rho v_z v_x}{\partial z}\\&-\frac{\partial\tau_{xx}}{\partial x} - \frac{\partial\tau_{yx}}{\partial y} - \frac{\partial\tau_{zx}}{\partial z}\\&-\frac{\partial P}{\partial x} + g_x\end{aligned}\tag{4.1.96}$$

Similar equations can be written for y- and z-momentum.

In deriving Equation (4.1.96), no assumptions have been made regarding the nature of the fluid (Newtonian or non-Newtonian) or the nature of the flow (laminar, transition, turbulent). In this form, these equations are therefore applicable for all types of fluids and flows, and are therefore termed generalized, differential momentum balance equations. These equations contain five unknowns: ρ, P, v_x, v_y, and v_z. These equations along with the continuity equations, Equation (4.1.93), and the equation of state for the fluid, which relates ρ to P and T, should be solved. If, in addition, temperatures are varying, the heat transfer equation should be solved simultaneously.

Before attempting to solve these equations, the constitutive equations for the fluid under consideration relating τ_{ij} with the velocity gradients should be written. For 1D flow of simple fluids it is the Newton's law of viscosity presented earlier in Equation (4.1.15). Even for these Newtonian fluids, the relationships in 3D flows are elaborate and are given by Stokes' relationships discussed below. For non-Newtonian fluids, such relationships can be even more elaborate.

Evidently, solutions of these equations are difficult. Analytical solutions do not exist, except for a few, very simple cases. For most systems of engineering interest, solutions need to be obtained numerically. Though several computational fluid dynamics (CFD) software codes are available, the effort involved in obtaining solutions is still very

large, even for laminar flows. Turbulent flows present further difficulties. Spatial variation of velocity is now at a very fine scale (inside eddies), and there is a certain stochasticity in the temporal variations. Direct numerical simulation (DNS) of these flows has to be at these fine scales of space and time, making computation intractable except for small regions. These turbulent flows are therefore "modeled" in terms of some new parameters that are smoother functions but still capture the effects of fine-scale variations. Turbulence models are briefly presented in Section 4.1.15. However, more elaborate description can be found in *Chapter 4, Treatise on Process Metallurgy, Volume 2: Process Phenomena.*

For a generalized flow of a Newtonian fluid, Stokes developed expressions for viscous momentum flux based on the primary assumption that the fluids are isotropic. Details regarding the development of Stokes relations can be found elsewhere [1]. The relationships valid for constant ρ and μ are:

$$\text{Normal components}: \tau_{ii} = -2\mu\frac{\partial v_i}{\partial i} \tag{4.1.97}$$

$$\text{Shear components}: \tau_{ij} = \tau_{ji} = -\mu\left(\frac{\partial v_i}{\partial j} + \frac{\partial v_j}{\partial i}\right)$$

Substituting these relationships into the momentum conservation equation, Equation (4.1.96), and using the equation of continuity, the following expression is obtained after rearrangement

$$\rho\left(\frac{\partial v_x}{\partial t} + v_x\frac{\partial v_x}{\partial x} + v_y\frac{\partial v_x}{\partial y} + v_z\frac{\partial v_x}{\partial z}\right) = \mu\left(\frac{\partial^2 v_x}{\partial x^2} + \frac{\partial^2 v_x}{\partial y^2} + \frac{\partial^2 v_x}{\partial z^2}\right) - \frac{\partial P}{\partial x} + \rho g_x \tag{4.1.98}$$

Similar equations can be written for the y- and z-momentum balances.

These are the Navier–Stokes equations valid for Newtonian fluids with constant ρ and μ. The expression on the left-hand side of Equation (4.1.98) denotes the x component of the acceleration of a particular fluid packet, i.e., in a Lagrangian frame of reference where the frame is moving with the fluid packet. In terms of the substantial or material derivative, the equation is:

$$\rho\frac{\mathrm{D}v_x}{\mathrm{D}t} = \mu\nabla^2 v_x - \frac{\partial P}{\partial x} + \rho g_x \tag{4.1.99}$$

Thus the Navier–Stokes equation can be interpreted as

$$\rho\frac{\mathrm{D}v_x}{\mathrm{D}t} = \rho a_x = \text{Viscous forces} + \text{Force due to pressure} + \text{Force due to gravity}$$

$$\tag{4.1.100}$$

which describes Newton's first law of motion for a unit volume fluid packet.

In vector form, the equation can be written as

$$\rho \frac{\mathrm{D}\vec{v}}{\mathrm{D}t} = \mu\left(\nabla\cdot\nabla\,\vec{v}\right) - \nabla P + \rho\vec{g} \tag{4.1.101}$$

The generalized equations are solved for particular systems by removing those terms that are either zero or insignificant and with appropriate boundary conditions, as the example below will demonstrate.

Example 4.1.8

Consider a Newtonian fluid such as water flowing steadily down an inclined plane as shown in Figure 4.1.25a. In the region of this plane away from entrance at the top, exit from the bottom, and the side plates, the flow may be considered to be fully developed: the velocity is unidirectional and varies only in the x-direction. We need to develop a relationship for the velocity profile.

Since $v_x = v_y = 0$, the equation of continuity (Equation 4.1.95) for an incompressible fluid gives

$$\frac{\partial v_z}{\partial z} = 0$$

which is to be expected in a fully developed region. The z-component Navier–Stokes equation is:

$$\rho\frac{\partial v_z}{\partial t} + v_x\frac{\partial v_z}{\partial x} + v_y\frac{\partial v_z}{\partial y} + v_z\frac{\partial v_z}{\partial z} = +\mu\left(\frac{\partial^2 v_z}{\partial x^2} + \frac{\partial^2 v_z}{\partial y^2} + \frac{\partial^2 v_z}{\partial z^2}\right) - \frac{\partial P}{\partial z} + \rho g_z$$

This equation can be simplified as follows:

LHS is zero, since $\frac{\partial v_z}{\partial t} = 0$ (steady state), $v_x = v_y = 0$ (fully developed), and $\frac{\partial v_z}{\partial z} = 0$ (continuity)

On the RHS, $\frac{\partial^2 v_z}{\partial z^2} = 0$ (continuity) and $\frac{\partial^2 v_z}{\partial y^2} = 0$ (far away from the side plates)

The equation is reduced to:

$$\mu\frac{\partial^2 v_z}{\partial x^2} = \frac{\partial P}{\partial z} = -\rho g_z \tag{4.1.102}$$
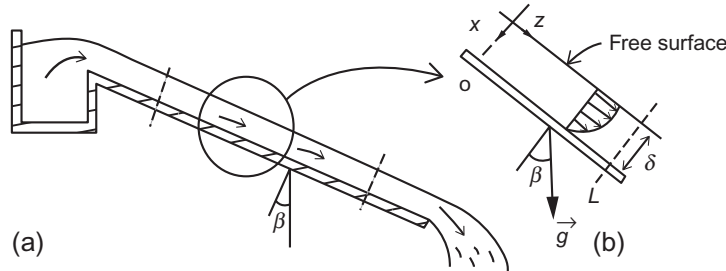

Figure 4.1.25 (a) Laminar flow over an inclined plane (b) Zoomed view of the circled section in (a).

An examination of the x- and y-component momentum equations will reveal (since $v_x = v_y = 0$)

$$\frac{\partial P}{\partial x} = \rho g_x \quad \text{and} \quad \frac{\partial P}{\partial y} = \rho g_y$$

Since $x = 0$ is a free surface, pressure is atmospheric and may be assumed as a constant for all z. Therefore for any x, the pressure $P = P_0 + \rho g_x x$ is independent of z. Therefore, $\frac{\partial P}{\partial z} = 0$.

Hence Equation (4.1.102) simplifies to

$$\mu \frac{\partial^2 v_z}{\partial x^2} = -\rho g_z = -\rho g \sin \beta \qquad (4.1.103)$$

Integrating the above equation,

$$v_z = -\frac{\rho g \sin \beta x^2}{2\mu} + C_1 x + C_2$$

where C_1 and C_2 are constants of integration to be evaluated with the boundary conditions.

Boundary condition 1: At the water–air interface ($x = 0$), air offers negligible resistance for the water flow. Therefore

$$\tau_{xz}|_{x=0} = -\mu \frac{\partial v_z}{\partial x}\Big|_{x=0} = 0 \Rightarrow C_1 = 0$$

Boundary condition 2: At $x = \delta$, $v_z = 0$ (no-slip boundary condition)

$$C_2 = \frac{\rho g \sin \beta \delta^2}{2\mu}$$

Hence the velocity profile is

$$v_z = \frac{\rho g \sin \beta \delta^2}{2\mu} \left[1 - \left(\frac{x}{\delta}\right)^2 \right]$$

The average velocity of the flowing film is:

$$\bar{v}_z = \frac{\rho g \sin \beta \delta^2}{3\mu}$$

4.1.15. MODELS OF TURBULENCE

In Section 4.1.4, the need to account for the friction losses was discussed. These friction losses result from work against frictional forces associated with velocity gradients. If the velocity field is fully known, these friction losses can be estimated, as shown for laminar flow through circular pipes in Section 4.1.6. Even fairly involved
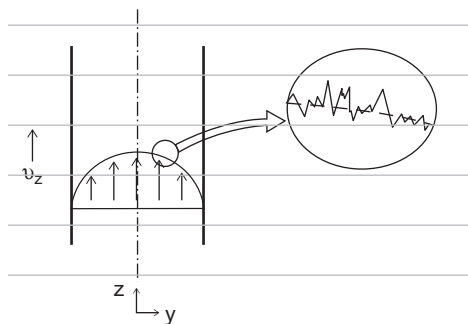
Figure 4.1.26 Schematic of the average velocity flow profile in a turbulent flow through a pipe.

2D and 3D laminar flow profiles can in principle be obtained from the continuity and the momentum balance equations within reasonable computational cost. Once the flow becomes turbulent, however, the velocity profiles develop a fine structure both spatially and temporally. Though a macroscopic representation of a velocity profile for turbulent flow may seem to be smooth, as for example, flow through a tube (Figure 4.1.26), at a much finer scale the velocity changes sharply over very small distances (inset in the figure). Further, these profiles change significantly in short time spans, even when the average flow shows the flow to be steady or changing slowly. Very fine space-wise grids and small time steps need to be employed (as in direct numerical simulation, DNS) to capture these phenomena, making it computationally unviable except for very simple flows over small regions.

Two approaches are employed to handle the turbulent flow in systems of interest in engineering. The expedient approach is to rely on empirical correlations to estimate the losses developed through dimensional analysis and experiments and perform conservation at the macroscopic scale as was done in the case of pipes earlier. In many systems, including those pertaining to process metallurgy, one may further be interested in investigating the flow characteristics in detail, i.e., the velocity variations within the system, and this can help in improving system performance and control through modification in design and operation. Experimental studies can be designed through similarity criteria, as has been done to understand flow in many process vessels such as ladles, BOF vessels, continuous casting tundish, and mold.

The second approach is to model the fine-scale turbulent characteristics in terms of a few parameters that are smooth functions over system dimensions and process time. These parameters, for example, the local rate of dissipation of mechanical energy, capture the effect of the fine-scale variations without performing calculations at the microscopic level. The parameters themselves are related to the microscopic flow characteristics that are being estimated through semi-empirical correlations. Such an approach is computationally more viable than the DNS, and at the same time gives more information

about the process than the purely empirical approach. Examples of these approaches are briefly discussed in the following section. Readers can find more detailed description of all these topics in *Chapter 4, Treatise on Process Metallurgy, Volume 2: Process Phenomena.*

4.1.15.1. Generic Flow Features in Turbulent Flows

Leonardo da Vinci (sixteenth century) was possibly the earliest to recognize and record the distinct features of turbulent flows, a copy of which can be found in Professor J. M. McDonough's lecture notes on turbulence [23]. In his lecture notes, Professor J. M. McDonough also gives the modern description of da Vinci's rendition, as is reproduced below

> ...*the smallest eddies are almost numberless, and large things are rotated only by large eddies and not by small ones, and small things are turned by small eddies and large.*

da Vinci termed the phenomena as "turbolenza," which corresponds to the modern word turbulence.

Reynolds' experiments on laminar and turbulent flows have already been presented in Section 4.1.3. With developments in flow visualization and measurement techniques, numerous investigations have been carried out to understand turbulent flows subsequent to Reynolds' experiments. Hinze, in his book on turbulence [24], summarizes turbulence based on these observations as "an irregular condition of the flow in which various quantities show a random variation with time and space coordinates, so that statistically distinct averages can be discerned."

With growing super computing power, it is widely accepted that the flow in the finest temporal and spatial scales can be deterministically predicted by equations such as the Navier–Stokes equation, and the randomness that is observed is due to high levels of sensitivity to initial conditions and boundary conditions at these finest scales. However, solutions by direct numerical simulations (DNS) at these fine time and length scales at present are restricted only to simple flows and are not amenable for large systems with the available computing resources.

Chapman and Tobak [25] summarized the evolution of the understanding of turbulence as three overlapping areas of (i) statistical (because of random variations with distinct averages), (ii) structural (because of eddies), and (iii) deterministic (in principle, turbulent flow can be obtained from Navier–Stokes equations). Turbulence models can also be classified along the same lines.

The models that are based on statistical methodologies applied to Navier–Stokes equations are addressed in a generic fashion, as Reynolds-averaged Navier–Stokes (RANS) equations. RANS models, especially, the κ–ϵ model, have been extensively used to understand flows in metallurgical systems (see *Chapter 4, Treatise on Process Metallurgy, Volume 2: Process Phenomena*). DNS techniques, on the other hand, are at present

largely restricted to understanding the nature of turbulence, due to high computational costs [23]. Large eddy simulations (LES), first proposed by Deardorff [26], lie somewhere between RANS and DNS and have been used to study some of the metallurgical flows in the recent past. In the following sections, a brief introduction to RANS and LES models are presented; details can be found elsewhere [23].

4.1.15.2. RANS Models

One of the important characteristic features of turbulent flow is mixing at the macroscopic level due to advective transport at the microscopic level from the random movements. This can be visualized macroscopically as enhanced diffusive transport. Many models simulate turbulent flow using an enhanced viscosity referred to as turbulent viscosity or eddy viscosity. Unlike molecular viscosity, turbulent viscosity is not just a fluid property, it is a property of the flow including geometry, and it is not constant in the flow domain.

RANS models of turbulence aim to determine this turbulent or eddy viscosity based on the statistical analysis of Navier–Stokes equations. The first step in such an analysis is to perform time smoothening of the Navier–Stokes equation; this is briefly described below.

Any instantaneous velocity in a turbulent flow can be split into a mean value, $\overline{v}$, and a fluctuating component, v'. This is referred to as Reynolds decomposition and can be written as

$$\mathbf{v} = \overline{\mathbf{v}} + \mathbf{v}'$$

The average here refers to an "ensemble average": averaged over several identical systems, measurements being made at a corresponding space point and time. Here, average of $\mathbf{v}'$, i.e., $\overline{\mathbf{v}}'$, is zero, since the fluctuations are truly random.

Substituting the above in Navier–Stokes equation and subsequently performing the smoothening (mean operation) result in the following equation (for x-momentum)

$$\rho\left(\frac{\partial \overline{v}_x}{\partial t} + \frac{\partial \overline{v}_x \overline{v}_x}{\partial x} + \frac{\partial \overline{v}_x \overline{v}_y}{\partial y} + \frac{\partial \overline{v}_x \overline{v}_z}{\partial z}\right) = -\frac{\partial \overline{\rho v'_x v'_x}}{\partial x} - \frac{\partial \overline{\rho v'_x v'_y}}{\partial y} - \frac{\partial \overline{\rho v'_x v'_z}}{\partial z}$$
$$+ \mu\left(\frac{\partial^2 \overline{v}_x}{\partial x^2} + \frac{\partial^2 \overline{v}_x}{\partial y^2} + \frac{\partial^2 \overline{v}_x}{\partial z^2}\right) - \frac{\partial \overline{P}}{\partial x} + \rho g_x \quad (4.1.104)$$

As the inertial terms or advective terms in the Navier–Stokes equations are nonlinear, smoothening of these terms gives rise to additional terms, namely, $\overline{\rho v'_x v'_x}$, $\overline{\rho v'_x v'_y}$, and $\overline{\rho v'_x v'_z}$. There will be also six more additional terms arising from y- and z-momentum equations. These terms together are called Reynolds stresses or turbulent momentum fluxes. Analogous to molecular viscosity, these turbulent momentum fluxes are modeled using "turbulent viscosity" and the gradient of averaged velocity field. This is expressed as

$$\overline{v'_x v'_z} = -v_T \left(\frac{\partial \overline{v}_x}{\partial z} + \frac{\partial \overline{v}_z}{\partial x} \right) \tag{4.1.105}$$

where v_T is turbulent kinematic viscosity. This concept was originally proposed by Boussinesq [27].

4.1.15.2.1 Mixing-Length Theory

This is one of the earliest turbulent models introduced by Prandtl [28]. Analogous to the kinetic theory of gases, Prandtl visualized fluid parcels (eddies) moving randomly with some characteristic velocity (v_{mix}) and a characteristic length (l_{mix}). The characteristic length can be interpreted as distance over which eddies retain their identities. Based on dimensional analysis, Prandtl proposed that

$$v_T = l_{mix}^2 \left| \frac{\mathrm{d}\overline{v}_x}{\mathrm{d}z} \right| \tag{4.1.106}$$

Further the mixing length l_{mix} has been experimentally correlated with the characteristic length of the system as $l_{mix} = C\delta(x)$. Here $\delta(x)$ is a characteristic length and C is a correlation constant. The correlation constant C needs to be determined for different flow geometries. Mixing-length theory has been applied fairly successfully to flows near the wall where there has been no flow separation. There have been many modifications to the basic mixing–length models. The success of the model has been limited in predicting engineering flows.

4.1.15.2.2 κ–ϵ Model [29]

The κ–ϵ model is one of the most widely used models in engineering for the investigation of fluid flows. This belongs to a family of two-equation models; κ denotes the turbulent kinetic energy and the ε denotes the dissipation rate of turbulent kinetic energy. The turbulent kinetic energy is expressed as

$$\kappa = \frac{1}{2} \left(\overline{v'_x v'_x} + \overline{v'_y v'_y} + \overline{v'_z v'_z} \right) \tag{4.1.107}$$

The turbulent kinetic energy does not distinguish between small and large eddies. The experimentally observed fact that the dissipation rate of smaller eddies is faster compared to the larger ones is accounted through a dissipation rate (ϵ) in the model, which is expressed in tensorial notation as

$$s'_{i,j} = \frac{1}{2} \left(\frac{\partial v'_i}{\partial j} + \frac{\partial v'_j}{\partial i} \right) \tag{4.1.108}$$

$$\epsilon = 2v\overline{s'_{i,j} s'_{i,j}} \tag{4.1.109}$$

where i and j stand for the coordinates x, y, and z.

The governing equations for the standard κ–ϵ model proposed by Launder and Spalding [29] in the vectorial form are

$$\nabla\cdot\overline{\mathbf{V}}=0 \tag{4.1.110}$$

$$\frac{\partial\overline{\mathbf{V}}}{\partial t}+\overline{\mathbf{V}}\cdot\nabla\overline{\mathbf{V}}=\nabla\overline{P}+\nabla\cdot((\nu+\nu_{\mathrm{T}})\nabla\overline{\mathbf{V}}) \tag{4.1.111}$$

$$\frac{\partial\kappa}{\partial t}+\overline{\mathbf{V}}\cdot\nabla\kappa=\mathcal{P}-\varepsilon+\nabla\cdot((\nu+\nu_{\mathrm{T}}/\sigma_\kappa)\nabla\kappa) \tag{4.1.112}$$

$$\frac{\partial\epsilon}{\partial t}+\overline{\mathbf{V}}\cdot\nabla\epsilon=C_{\epsilon1}\frac{\epsilon}{\kappa}\mathcal{P}-C_{\epsilon2}\frac{\epsilon^2}{\kappa}+\nabla\cdot((\nu+\nu_{\mathrm{T}}/\sigma_\epsilon)\nabla\epsilon) \tag{4.1.113}$$

where $\mathcal{P}$ is the rate of production of eddies (in Cartesian coordinate system) and is given by

$$\mathcal{P}=2\nu_{\mathrm{T}}\overline{s_{i,j}}\frac{\partial\overline{v}_i}{\partial j} \quad \text{(for incompressible flow)} \tag{4.1.114}$$

The turbulent viscosity, ν_{T}, is determined from κ and ϵ as

$$\nu_{\mathrm{T}}=C_\nu\frac{\kappa^2}{\epsilon} \tag{4.1.115}$$

The constants in the standard κ–ϵ model are

$$C_\nu=0.09, \quad C_{\epsilon1}=1.44, \quad C_{\epsilon2}=1.92, \quad \sigma_\kappa=1.0, \quad \text{and} \quad \sigma_\epsilon=1.3 \tag{4.1.116}$$

These are empirical model constants whose values were found through data fitting for a wide range of flows.

One of the drawbacks of these models is that they cannot be applied near the solid boundary; special formalisms are needed near the walls. It is generally hypothesized that the flow near the wall can be viewed as consisting of three layers, namely an innermost viscous layer, a middle buffer layer, and outer turbulent layer and the velocity profile near the wall can be reasonably represented by a logarithmic profile [30]. This wall function term has been extensively used to specify boundary conditions near the wall for turbulent flows. There are also more rigorous approaches wherein special low Re κ–ϵ formalisms have been applied at the vicinity of the wall, the details of which can be found elsewhere [31].

Other than the standard κ–ϵ model, there are other two-equation models, such as RNG κ–ϵ models [32], κ–ω models [31], and Reynolds stress models [29]. Many of these models are available for use in commercial CFD codes such as FLUENT, PHOENICS, and CFX.

4.1.15.3. LES Models

As mentioned in the beginning of this section, one of the important features of turbulence is continuous formation and dissipation of eddies in a large spectrum of both spatial and temporal scales. A schematic representation of the size of the eddies (represented as wave number, k, inverse of size) and their corresponding turbulent energy, $E(k)$, is shown in Figure 4.1.27.

According to Kolmogorov [33], most of the turbulent kinetic energy is carried by the larger eddies and they are not affected by the molecular viscosity. The larger eddies dissipate their energy to smaller eddies. He also postulated that in the intermediate scale, known as inertial scale, the eddies pass on the energy from larger eddies to the smaller ones at the same rate. The eddies at the lowest scales are the ones that actually dissipate the energy through molecular viscosity. Based on dimensional analysis, the size of the smallest eddy was estimated as $\eta = \frac{1}{4}(\frac{v^3}{\epsilon})$, known as the Kolmogorov scale. The spectrum widens with increasing Reynolds number. Thus, in principle, to obtain turbulent flow directly by solving the Navier–Stokes equations using numerical methods (DNS approach), the phenomena in the smallest of these scales need to be captured, which in turn are determine the grid spacing. For example, for channel flow the approximate number of nodes needed is $0.088 Re^{9/4}$ [31], which for a Re of 10^6 corresponds to 100 billion nodes. Thus, with the current computing power, DNS simulations at present cannot be used anything other than small and simple geometries. It has also been observed that there is a tendency toward more universal behavior as lower scales are approached; in other words, they are more amenable for modeling. Thus, in LES methodology, the lower scales of turbulence (part of inertial subrange and into the beginning of dissipation scales) are modeled. The principle idea behind LES methodology is presented here; readers are urged to refer elsewhere [31] for a much more detailed description.

As in Reynolds decomposition, any generic variable such as velocity can be represented as two parts, i.e.,
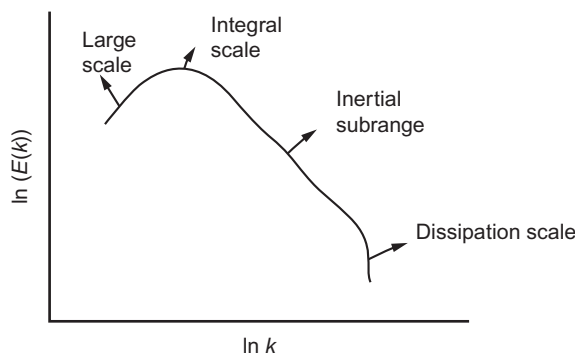

Figure 4.1.27 Schematic of the turbulence energy wave number spectrum.

$$\mathbf{v} = \widetilde{\mathbf{v}} + \mathbf{v}' \tag{4.1.117}$$

In this case, however, the decomposition is based on a low-pass spatial filter where $\widetilde{\mathbf{v}}$ is the filtered velocity and the $\mathbf{v}'$ is the residual part. A low-pass filter is a smoothening filter that attenuates the high frequencies (corresponding to sharp peaks) retaining the small frequencies unchanged. It should be noted that unlike Reynolds decomposition, the time average of $\mathbf{v}'$ need not be zero. The filtering can be performed by representing the variable in Fourier space and choosing a filter kernel, for example, a Gaussian filter.

The filtering of the continuity equation for an incompressible fluid is similar to that corresponding to Reynolds decomposition and can be written as

$$\nabla \cdot \widetilde{\mathbf{v}} = 0 \quad \text{and} \quad \nabla \cdot \mathbf{v}' = 0 \tag{4.1.118}$$

Filtering of the Navier–Stokes equation, i.e.,

$$\frac{\partial \mathbf{v}}{\partial t} + \nabla \cdot (\mathbf{v}\mathbf{v}) = -\nabla P + \nu \nabla^2 \mathbf{v} \tag{4.1.119}$$

gives the nonlinear term $\nabla \cdot \mathbf{v}\mathbf{v}$ that contains the residual part, $\mathbf{v}'$; the time average of which is not zero. Unlike Reynolds decomposition, therefore, the filtering gives rise to cross terms in addition to Reynolds' stress terms (4.1.105). That is

$$\left(\widetilde{v} + v'\right)\widetilde{\left(\widetilde{v} + v'\right)} = \left\{ \begin{array}{ccc} \widetilde{(\widetilde{v}_x + v'_x)(\widetilde{v}_x + v'_x)} & \widetilde{(\widetilde{v}_x + v'_x)(\widetilde{v}_y + v'_y)} & \widetilde{(\widetilde{v}_x + v'_x)(\widetilde{v}_z + v'_z)} \\ \widetilde{(\widetilde{v}_x + v'_x)(\widetilde{v}_y + v'_y)} & \widetilde{(\widetilde{v}_y + v'_y)(\widetilde{v}_y + v'_y)} & \widetilde{(\widetilde{v}_y + v'_y)(\widetilde{v}_z + v'_z)} \\ \widetilde{(\widetilde{v}_x + v'_x)(\widetilde{v}_z + v'_z)} & \widetilde{(\widetilde{v}_z + v'_z)(\widetilde{v}_y + v'_y)} & \widetilde{(\widetilde{v}_z + v'_z)(\widetilde{v}_z + v'_z)} \end{array} \right\} \tag{4.1.120}$$

Looking at one of the terms

$$\left(\widetilde{v}_x + v'_x\right)\widetilde{\left(\widetilde{v}_y + v'_y\right)} = \left(\widetilde{\widetilde{v}_x v_y}\right) + \left(\widetilde{\widetilde{v}_x v'_y}\right) + \left(\widetilde{\widetilde{v}_y v'_x}\right) + \left(\widetilde{v'_x v'_y}\right) \tag{4.1.121}$$

The last term $v'_x v'_y$ is also referred to as the Reynolds stress in the LES formalism.

To obtain the filtered momentum equation in a useful form, this can be written as

$$\widetilde{\mathbf{v}}\widetilde{\mathbf{v}} + \left(\left(\widetilde{\mathbf{v} + \mathbf{v}'})(\widetilde{\mathbf{v}} + \mathbf{v}'\right) - \widetilde{\mathbf{v}}\widetilde{\mathbf{v}}\right) = \widetilde{\mathbf{v}}\widetilde{\mathbf{v}} + \tau_{\text{SGS}} \tag{4.1.122}$$

where τ_{SGS} contains the lower scale part (higher frequency) of the LES equation. Thus, the momentum equation for solving the filtered part of the (large scale) of the velocity vectors can be written as

$$\frac{\partial \widetilde{\mathbf{v}}}{\partial t} + \nabla \cdot (\widetilde{\mathbf{v}}\widetilde{\mathbf{v}}) = -\nabla \widetilde{P} + \nu \nabla^2 \widetilde{\mathbf{v}} - \widetilde{\nabla} \cdot \tau_{\text{SGS}} \tag{4.1.123}$$

It is interesting to note that the numerical discretization of the Navier–Stokes equation can be interpreted as a filtering operation and the width of the filter is directly related to the discrete step size of the numerical approximation. Thus eddies whose sizes are of order of the scale corresponding to the step size and greater are captured by the filtered momentum equation. However, the scales below that of the step size need to be modeled and hence they are referred to as τ_{SGS}, where SGS stands for subgrid scale. In principle, as the step size becomes smaller and smaller, the LES scheme should converge to the DNS scheme and correspondingly the τ_{SGS} should go toward zero. In other words, the τ_{SGS} should depend on the grid size of the numerical scheme.

A number of models are proposed for τ_{SGS}. Among them, one of the oldest is by Smagorinsky [34] and is based on the Boussinesq hypothesis [27]. The equations for the Smagorinsky model are

$$\tau_{SGS} = -2v_{SGS}\widetilde{\mathbf{S}} \qquad (4.1.124)$$

$$v_{SGS} = (C_s\Delta)^2 |\widetilde{\mathbf{S}}| \quad \text{(Analogous to mixing length model, Equation 4.106)} \quad (4.1.125)$$

Here, $\mathbf{S}$ refers to the strain rate tensor (see Equation 4.1.108), Δ is the filter width, which is proportional to grid size, and C_s is the Smagorinsky constant. The typical values of C_s are of the order of 10^{-1}. In the recent past, many new methodologies have been constructed for LES wherein the constant C_s is determined by performing two or more filtering operations using different filter widths (multigrid). Detailed description of the formulation as well as implementation of LES can be found elsewhere [35].

4.1.16. INTRODUCTION TO HEAT TRANSFER

Heat transfer, in simple terms, is energy transfer arising from differences in temperature. In a static system, where there is a medium, the primary mode of heat transfer is by conduction. This mode of transfer is also termed as diffusive transfer and is caused by molecular interactions within the medium. Hence, the quantity of heat being transferred depends on the material of the medium. If there is a net flow in the medium, then, in addition to the conduction mode, there is also the advective transfer of heat that arises from the bulk motion and that occurs simultaneously with conduction. This is termed as convection. In a multiphase system, wherein there is a net relative motion between any two phases, there can be large gradients in velocity and temperature at the interface between the phases. Quantifying this heat transfer through the interface is essential in most engineering systems. Heat can be transferred even without a medium as electromagnetic waves or photons. This mode of heat transfer is termed as radiative heat transfer. Most condensed media absorb electromagnetic waves so heat transfer through such media cannot occur by this mechanism. Radiative heat transfer is, however, significant through gaseous media. The gas molecules can absorb, scatter as well as emit photons. The radiative exchange through gases depends on the characteristics of the gas molecules,

which constitute the gaseous media. The constitutive relations describing all these modes of heat transfer and their application in engineering problems through the conservation principle make up the subject of heat transfer and are described in the following sections.

4.1.17. CONSERVATION EQUATION AS APPLIED TO THERMAL SYSTEMS

The overall energy balance for a steady-state system has been discussed earlier in Section 4.1.4. This can be generalized for an unsteady state or a transient system as

$$\frac{dE^s}{dt} = -\dot{E}^{net\ out} - \dot{Q}^{net\ out} - \dot{W}^{net\ out} \tag{4.1.126}$$

Here, E^s denotes the energy in the system, $\dot{E}^{net\ out}$ is the net rate of energy advected out from the system with the flowing mass, $\dot{Q}^{net\ out}$ is the net rate of heat transfer out from the system by other mechanisms, and $\dot{W}^{net\ out}$ the net rate of work done by the system on the surroundings. Please note that the "net out" term for any conservative entity, say ϕ is defined by

$$\dot{\phi}^{net\ out} = \left(\dot{\phi}^{out} - \dot{\phi}^{in} \right)$$

The net energy that is advected out from the system with the flowing mass as well as that getting accumulated in the system, includes kinetic energy, potential energy arising from gravitation field, and the internal energy as explained in Section 4.1.4. In addition to this, there can be net flow of heat energy out from the system through the system boundaries by conduction and interface heat transfer by convection and radiation. The term 'work', in general, involves two important components, the flow work (as explained in Section 4.1.4) and the shaft work. Thus, the overall energy balance can be written in a more rigorous form as,

$$\frac{dE^s}{dt} = -\int_B \left(\hat{U} + \widehat{K.E.} + \widehat{P.E.} \right) d\dot{m} - \dot{Q}^{net\ out} - \int_B P\hat{V} d\dot{m} - \dot{W}^{net\ out}_{shaft} \tag{4.1.127}$$

Here, B refers to the system boundary, $\hat{U}$ the internal energy per unit mass, $\widehat{K.E.}$ the kinetic energy per unit mass, $\widehat{P.E.}$ the potential energy per unit mass, P the pressure, and $\hat{V}$ the specific volume. In thermodynamics, the term $\hat{U} + P\hat{V}$ is defined as enthalpy, $\hat{H}$. Thus, the above equation can be written as,

$$\frac{dE^s}{dt} = -\int_B \left(\hat{H} + \widehat{K.E.} + \widehat{P.E.} \right) d\dot{m} - \dot{Q}^{net\ out} - \dot{W}^{net\ out}_{shaft} \tag{4.1.128}$$

In general, most problems of interest to a process engineer can be considered as constant pressure processes. Besides, the potential and kinetic energies are generally much smaller than changes in enthalpy and are often neglected.

Hence, for constant pressure processes, the energy conservation equation can be written as

$$\frac{\mathrm{d}\left(m^s \hat{H}\right)}{\mathrm{d}t} = -\int_B \hat{H}\,\mathrm{d}\dot{m} - \dot{Q}^{\text{net out}} - \dot{W}_{\text{shaft}}^{\text{net out}} \tag{4.1.129}$$

Here, m^s refers to the mass in the system. Depending on the system, there can be other forms of energies such as magnetic, electric, chemical, interfacial, and nuclear, which may need to be included in the conservation equation. Detailed information on these aspects can be found in books on thermodynamics. In heat transfer, the focus is on the sensible part of the enthalpy, which results in a change in temperature. The other forms of energies such as those associated with phase changes, chemical reactions, electrical, magnetic, and nuclear phenomena are incorporated through generation terms. These conversions to sensible enthalpy are treated as volumetric phenomena. It is to be noted that the degradation of mechanical energy into internal energy also needs to be accounted for. This term, however, is often neglected as being small in comparison to changes in sensible enthalpy. Thus, the equation becomes

$$\frac{\mathrm{d}\left(m^s \hat{H}\right)}{\mathrm{d}t} = -\int_B \hat{H}\,\mathrm{d}\dot{m} - \dot{Q}^{\text{net out}} - \dot{W}_{\text{shaft}}^{\text{net out}} + \int_V \dot{Q}'''\,\mathrm{d}V \tag{4.1.130}$$

where $\dot{Q}'''$ denotes the rate of conversion of other forms of energies to thermal energy per unit volume.

The sensible enthalpy for a material is quantified using specific heat capacity at constant pressure, denoted by C_p

$$\hat{H} = \int_{T_{\text{ref}}}^{T} C_p\,\mathrm{d}T \tag{4.1.131}$$

where T_{ref} is an arbitrary reference temperature, usually taken as 298 K.

Using the above, the heat balance equation can be written as

$$m^s C_p \frac{\mathrm{d}T}{\mathrm{d}t} = -\int_B \hat{H}\,\mathrm{d}\dot{m} - \dot{Q}^{\text{net out}} - \dot{W}_{\text{shaft}}^{\text{net out}} + \int_V \dot{Q}'''\,\mathrm{d}V \tag{4.1.132}$$

Here onward, the symbol C will be used to denote C_p as most of the cases one deals with in process metallurgy are at constant pressure. Exceptions to this will be clearly spelt out.

4.1.18. CONDUCTION

Heat transfer resulting from atomic or molecular interactions in a medium is termed conduction. Consequently, conductive heat transfer is dependent on the constitution of the medium. Conductive transfer is characterized by the material property called thermal conductivity. The primary constitutive equation for conduction is named after Fourier, a great mathematician and a physicist. The law as stated is phenomenological and was based on experimental observations.

To demonstrate this form of heat transfer, consider a solid rod of cross section "A" and length "L" as shown in Figure 4.1.28. The curved side of the rod is insulated.
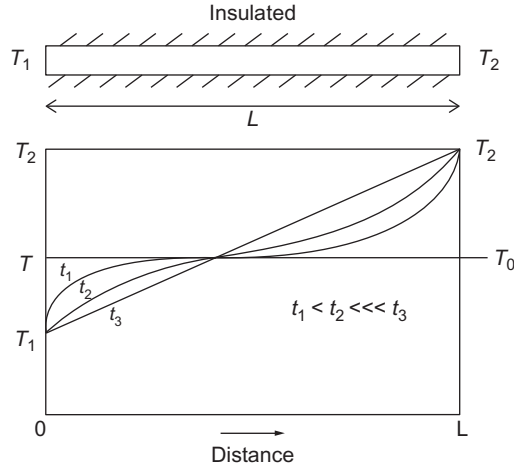
Figure 4.1.28 Schematic showing heat conduction through a rod of constant cross section.

The rod is initially at a uniform temperature, T_0. At time $t=0$, the two ends of the rod are brought to temperatures of T_1 and T_2, respectively, and are maintained at these values. The temperature profile along the length of the rod will change continuously over time as shown schematically in Figure 4.1.28. The system will attain steady state, after sufficiently long time; the profile would be nearly a straight line if temperature differences are small. Experimentally, the amount of heat transferred can be measured, for example, by keeping the cold side of the rod under an ice–water mixture and measuring the amount of ice melted. Fourier's law states that the heat transferred per unit time at steady state, ($\dot{q}$), is proportional to the difference in temperature of the two ends of the rod, $T_1 - T_2$ and the area of cross section "A" and is inversely proportional to the length of the rod, "L." That is

$$\dot{q} = \kappa \frac{(T_1 - T_2)A}{L}$$

The proportionality constant, κ, is the thermal conductivity of the material of the rod. In differential form in one dimension, the law is stated as:

$$\dot{q}''_x = -\kappa \frac{dT}{dx} \tag{4.1.133}$$

where $\dot{q}''_x$ is the heat flux, the rate of heat transfer per unit area [4]. The direction x is along the length of the rod.

----

[4] Fourier's law of heat conduction is analogous to Newton's law of viscosity when viewed as equation of momentum flux. Under the condition of constant ρ and C_p, Equations (4.1.133) and (4.1.15) can be written as:

$$\tau_{yx} = -\frac{\mu}{\rho}\frac{\partial \rho v_x}{\partial y} = -v\frac{\partial \rho v_x}{\partial y} \quad \text{and} \quad \dot{q}'' = -\frac{\kappa}{\rho C_p}\frac{\partial\left(\rho C_p(T - T_{ref})\right)}{\partial \infty} = -\alpha\frac{\partial\left(\rho C_p(T - T_{ref})\right)}{\partial \infty}$$

(ρv_x) and $\rho C_p(T - T_{ref})$ are conserved quantities, namely, momentum and enthalpy densities: (kg m^{-1} m^{-3}) and (J m^{-3}). The laws can be viewed as when there is a gradient in a conserved quantity, there is a flux of that quantity down the gradient. These two laws are further analogous to Fick's law of mass diffusion as discussed later in Section 4.1.21. The dimension of all the proportionality constants is m^2 s^{-1}.
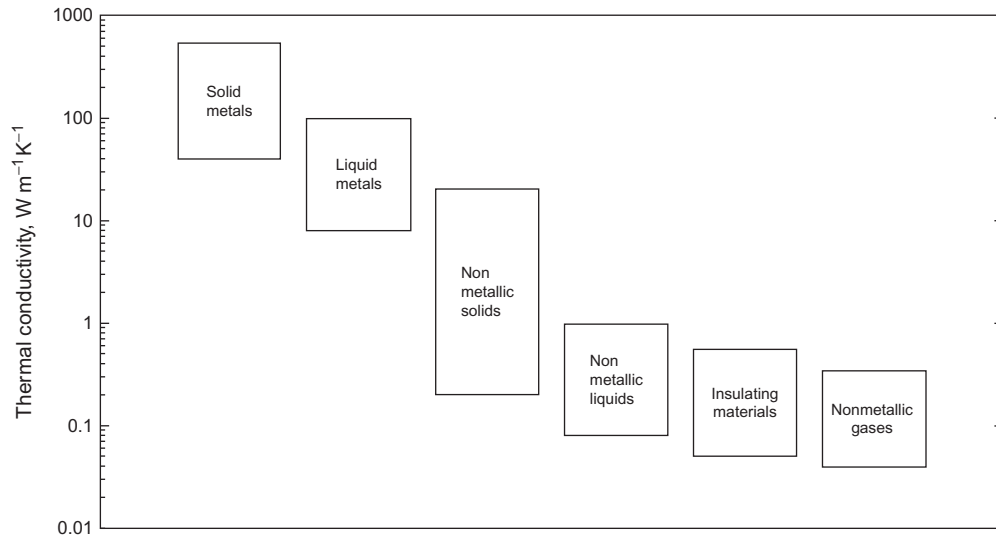
Figure 4.1.29 Ranges of thermal conductivities of different materials [36].

In a general 3D scenario, for an isotropic medium, Fourier's law of conduction can be written as

$$\dot{q}'' = -\kappa \nabla T \qquad (4.1.134)$$

It is to be noted that the heat flux vector, $\dot{q}''$, is orthogonal to an isothermal surface. In most engineering situations encountered in process metallurgy, the conductive medium can be considered to be isotropic. Readers may refer elsewhere for conductive heat transfer through anisotropic media [36].

Typical ranges of thermal conductivities of materials, are shown in Figure 4.1.29 adopted from Ref. [36]. Solid metals normally have high thermal conductivities, since both lattice vibrations and free electrons contribute to thermal conduction. With increasing temperature, the mean free path of electrons decreases resulting generally in a decrease in thermal conductivities with increasing temperature. In nonmetallic solids, on the other hand, only the lattice vibrations contribute to the thermal conductivity and their thermal conductivities generally increase with increasing temperature. Many insulating materials are made intentionally porous to serve as inhibitors for heat transfer. Hence their conductivities are closer to those of the gases.

As with viscosity, the thermal conductivities of gases and gas mixtures can be estimated with reasonable accuracy from the kinetic theory of gases [1]. For solids and liquids, these data must be obtained by experimental measurements, and data have been tabulated for a large number of materials [37,38].

4.1.18.1. Conduction Equation

The conservation equation given by Equation (4.1.132) is applied to a differential element in conjunction with Fourier's law (the constitutive relation for conduction) to deduce the generalized conductive heat transport equation. Consider a differential element in Cartesian coordinate system as shown in Figure 4.1.30.

The medium is static and hence there is only conductive heat transfer. There is no advective mass transport, and no radiative transfer through the medium. The conservation of heat in this control volume is written as

$$
\begin{aligned}
\rho C \frac{\partial T}{\partial t}(\Delta x \Delta y \Delta z) = & \Delta y \Delta z \left(-\kappa \frac{\partial T}{\partial x}\bigg|_{abcd} + \kappa \frac{\partial T}{\partial x}\bigg|_{efgh} \right) \\
& + \Delta x \Delta z \left(-\kappa \frac{\partial T}{\partial y}\bigg|_{adhe} + \kappa \frac{\partial T}{\partial y}\bigg|_{bcgf} \right) \\
& + \Delta x \Delta z \left(-\kappa \frac{\partial T}{\partial z}\bigg|_{adfe} + \kappa \frac{\partial T}{\partial z}\bigg|_{hgcd} \right) \\
& + \dot{Q}'''(\Delta x \Delta y \Delta z)
\end{aligned}
\tag{4.1.135}
$$

Taking the limit as Δx, Δy, and $\Delta z \longrightarrow 0$, then

$$
\rho C \frac{\partial T}{\partial t} = \frac{\partial}{\partial x}\left(\kappa \frac{\partial T}{\partial x} \right) + \frac{\partial}{\partial y}\left(\kappa \frac{\partial T}{\partial y} \right) + \frac{\partial}{\partial z}\left(\kappa \frac{\partial T}{\partial z} \right) + \dot{Q}'''
\tag{4.1.136}
$$

In vectorial form, this equation can be written as

$$
\rho C \frac{\partial T}{\partial t} = -\nabla \cdot (\kappa \nabla T) + \dot{Q}'''
\tag{4.1.137}
$$

If the thermophysical properties, namely ρ, C, and κ, are assumed to be constant within the temperature range of interest, the equation can be simplified to
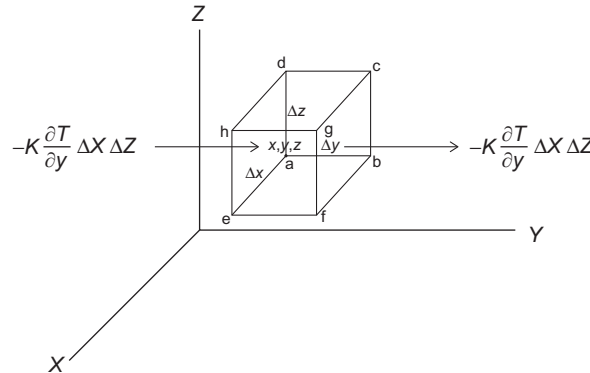

Figure 4.1.30 Differential element in Cartesian coordinates.

$$\frac{\partial T}{\partial t} = \alpha \nabla^2 T + \frac{1}{\rho C}\dot{Q}'''$$ (4.1.138)

The material property, α, termed thermal diffusivity, is given by $\frac{\kappa}{\rho C}$ the dimension of which is $\text{m}^2\,\text{s}^{-1}$, as also for kinematic viscosity, ν, and mass diffusion coefficient, $\mathbb{D}$.

Equation (4.1.137) is often termed as the heat equation or the diffusion equation belonging to the class of parabolic partial differential equations. Even though the heat equation was derived using the Cartesian coordinate system, the vectorial form can be easily expanded for any curvilinear coordinate system. The equation can be solved for any particular system, by specifying the temperature distribution in space at any given time (initial condition) and specifying conditions at the boundaries for the entire time duration of interest (boundary conditions). Some of the common boundary conditions encountered in conductive heat transfer are discussed below.

4.1.18.2. Boundary Conditions

4.1.18.2.1 Prescribed Surface Temperature

The temperature at the boundary is known for all times of interest (Figure 4.1.31):

$$\text{At } x = 0, \quad T = T_s(t).$$

This boundary condition is also known as the Dirichlet condition, after the famous mathematician. Such a condition can be imposed by keeping the boundary at a phase-transition temperature.
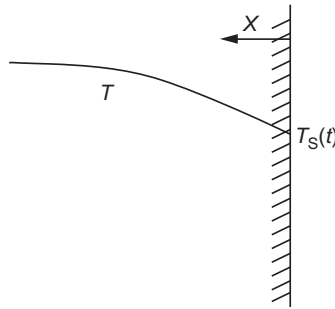

Figure 4.1.31 Illustration of the Dirichlet boundary condition.

4.1.18.2.2 Prescribed Heat Flux

The heat flux through the boundary is known as a function of time (Figure 4.1.32):

$$\text{At } x = 0, \quad -\kappa \frac{\partial T}{\partial x} = \dot{q}_s''(t).$$

This condition is named after the mathematician Neumann. Such a condition can be obtained, for example, by having an electric heater at the boundary, which is insulated perfectly on the other side.
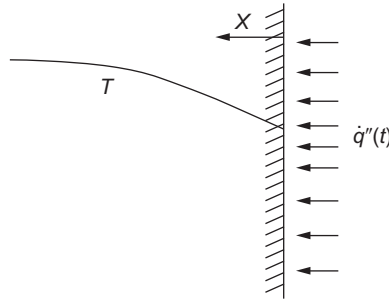
Figure 4.1.32 Illustration of the Neumann boundary condition.

A special case of the Neumann condition is an adiabatic surface, where the heat flux and, therefore, the temperature gradient at the surface are zero.

$$\text{At } x = 0, \quad \frac{\partial T}{\partial x} = 0.$$

A perfectly insulated boundary is adiabatic. Such a condition is obtained at symmetry planes, in perfectly symmetrical systems.
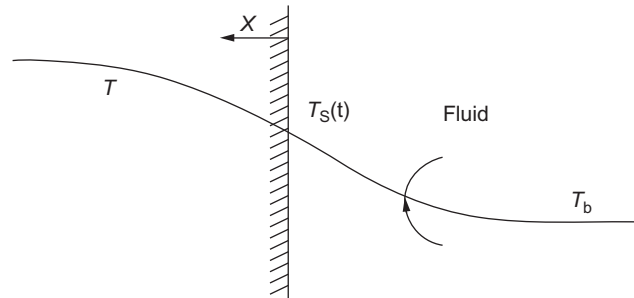
4.1.18.2.3 Convective Boundary Condition

The most common boundary condition specified is the one at a boundary between the stationary medium for which the conduction problem is being solved and a moving fluid. The stationary medium may be a solid, or a liquid that is relatively stagnant. Continuity of heat flux across the interface demands that the conductive heat flux on one side be equal to the convective heat flux on the other as shown in Figure 4.1.33.

Convective heat transfer at the interface is a function of fluid and flow properties, and is given by a phenomenological equation.

$$\dot{q}''_{x,\text{conv}} = h(T_{\text{b}} - T_{\text{s}}).$$

where T_{s} and T_{b} are the surface and bulk temperature in the moving fluid, respectively, and h is called the heat transfer coefficient, which is related to fluid and flow properties, often through empirical correlations (see Section 4.1.19). The boundary condition therefore becomes

Figure 4.1.33 Illustration of the Convective boundary condition.

$$\text{At } x = 0, \quad -\kappa \frac{\partial T}{\partial x} = h(T_b - T_s).$$

or

$$x = 0, \quad -\kappa \frac{\partial T}{\partial x} + h T_s = h T_b.$$

This condition neither specifies the surface temperature nor the temperature gradient at the surface; it specifies a linear combination of the two. It is therefore called the mixed condition; T_s adjusts itself to satisfy this condition.

Examination of the above equation tells us that, for any finite heat flux at the interface, $T_s \to T_b$ as $h \to \infty$. That is, the prescribed surface temperature condition is difficult to be practically achieved, except by having a high enough heat transfer coefficient for a given κ_s value. Phase changes, as when steam condenses on a surface, can provide such high heat-transfer coefficients.

4.1.18.2.4 A Boundary Between Two Conducting Media

If two conducting media are in perfect thermal contact, the heat flux as well as temperature at the interface should be continuous, since there can be no accumulation at a surface, $\kappa^I \frac{\partial T}{\partial x}\big|^- = \kappa^{II} \frac{\partial T}{\partial x}\big|^+$ (Figure 4.1.34).

If the two media are both solids, pressed together, the contact is never perfect and there is always a third medium in between, which is normally a gas such as air or a liquid. This thin layer, of indeterminate thickness, offers a further resistance to heat flow. Though the heat flux can still be assumed to be continuous (even in an unsteady heat flow situation), since the thermal capacity of these interface layers is very small, there can be a sharp temperature drop across this layer. The mechanisms of heat transport across the layer are conduction and radiation (if the medium in the layer is transparent); a theoretical treatment is, however, difficult, due to the uncertain geometry of the interface. An empirical approach is therefore adopted, and a heat transfer coefficient across this interface is defined (Figure 4.1.35).

$$\dot{q}'' = -\kappa^I \frac{\partial T}{\partial x}\bigg|^- = h(T_s^I - T_s^{II}) = \kappa^{II} \frac{\partial T}{\partial x}\bigg|^+$$

In a mixed condition, the heat flow away from the surface may have a radiative component superimposed on the convective: At $x = 0, -\kappa_s \frac{\partial T}{\partial x} = h(T_b - T_s) + \varepsilon \sigma (T_a^4 - T_s^4)$,
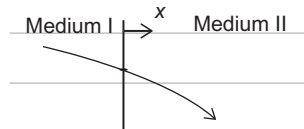
Figure 4.1.34 Illustration of the boundary condition between two conductive media in perfect thermal contact.
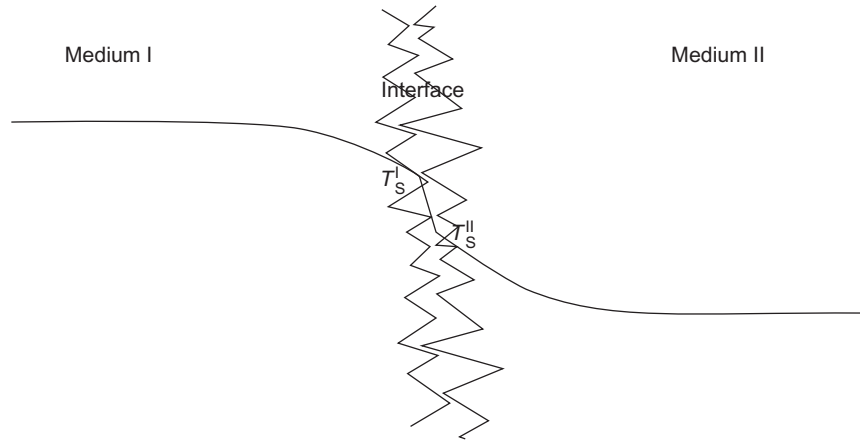
Figure 4.1.35 Illustration of the boundary condition between two conductive media in contact.

where T_a is the ambient temperature from which the radiation is received and σ is the Stefan–Boltzmann constant. This boundary condition is highly nonlinear in T_s and can give difficulties in computation. If the difference between T_a and T_s is small, a linearized form of the equation can be used,

$$\text{at } x = 0, \quad -\kappa_s \frac{\partial T}{\partial x} = h(T_b - T_s) + \varepsilon\sigma\left(T_a^4 - T_s^4\right) = h(T_b - T_s) + h_{rad}(T_a - T_s)$$
$$\text{where } h_{rad} = \varepsilon\sigma\left(T_s^2 + T_s^2\right)(T_s + T_a) \approx \varepsilon\sigma 4 T_{avg}^3 \quad \text{where } T_{avg} = (T_s + T_a)/2.$$

4.1.18.3. 1D Steady-State Conduction

The heat transfer process is at a steady state condition when temperature at any location remains constant over a long period of time. This can be achieved by maintaining a constant heat transfer condition at the boundary over a long period of time. For example, if a furnace or an oven is maintained at a constant temperature for a long time, then the walls of the furnace can attain a steady temperature profile. Similarly, when a hot fluid having a fixed inlet temperature flows at a constant rate through a pipe maintained in a steady environment, the walls of the pipe will attain a steady temperature profile. In many metallurgical processes, simple analyses can often be performed by approximating the heat transfer as a 1D steady-state heat transfer either in Cartesian or cylindrical coordinates. Quite often, in such simple systems, an electrical analogue can also be constructed to describe heat transfer, which can help in the analysis.

4.1.18.3.1 Conduction Through a Plane Wall

When the length and width of a wall are much larger than the thickness of a wall, steady-state heat transfer through the wall can often be approximated as 1D steady-state conduction in the Cartesian coordinate system. Heat transfer through plane walls of a large furnace is one such typical example.

The heat conduction equation (Equation 4.1.137) for steady-state conduction through a plane wall of thickness L with no generation of heat inside the wall reduces to

$$\frac{\partial}{\partial x}\left(\kappa\frac{\partial T}{\partial x}\right) = 0 \tag{4.1.139}$$

If the thermal conductivity of material of the wall is taken to be independent of temperature, the solution of the differential equation results in a linear temperature profile across the wall. In many engineering systems, it is reasonable to assume constant thermal conductivity (at the average temperature). The temperature profile and the heat flux through the wall can be written as

$$T(x) = T_0 - \frac{T_0 - T_L}{L}x$$

$$\dot{q}_x'' = \kappa\frac{T_0 - T_L}{L}$$

where T_0 and T_L refer to the temperature on the wall at location $x=0$ and $x=L$, respectively. These two temperatures when not specified can be deduced from the corresponding boundary conditions at $x=0$ and $x=L$.

Consider a case where convective boundary conditions are imposed with heat transfer coefficients h_0 and h_L and fluid temperatures of $T_{\infty,0}$ and $T_{\infty,L}$ at $x=0$ and $x=L$, respectively. Balancing the convective heat flux flowing from fluid at $x=0$, the conductive heat flux across the wall, and the convective flux flowing out to the fluid at $x=L$, the following equations can be written.

$$\dot{q} = A\dot{q}_x'' = Ah_0\left(T_{\infty,0} - T_0\right) = A\kappa\frac{T_0 - T_L}{L} = Ah_L\left(T_L - T_{\infty,L}\right) \tag{4.1.140}$$

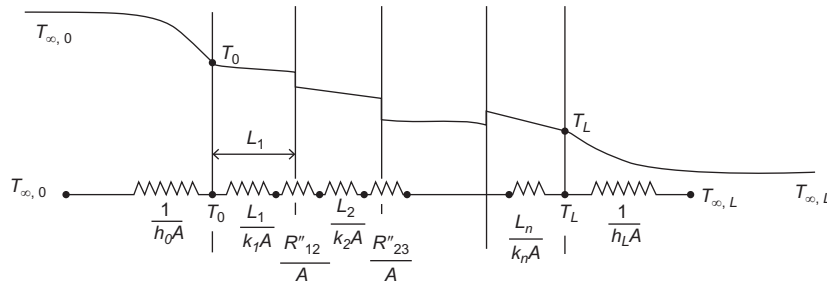A schematic temperature profile for the system is depicted in Figure 4.1.36a.

The temperature profile within the wall is linear. The convective heat transfer through the fluid on both sides of the wall is represented as a curved profile with a steep gradient near the fluid–solid interface. This is to depict the temperature profile resulting from the flow of liquid having a steep gradient in velocity at the solid–liquid interface. More discussions on this convective heat transfer can be found in later sections. The rate of heat transfer can be written after eliminating the unknown surface temperatures as:

$$\dot{q} = A\dot{q}_x''\frac{\left(T_{\infty,0} - T_{\infty,L}\right)}{\frac{1}{h_0 A} + \frac{L}{A\kappa} + \frac{1}{h_L A}} \tag{4.1.141}$$

The overall resistance to heat flow is the sum of the conductive and convective resistances (Fig 4.1.36b). The analogy can be extended to multiple conducting walls as shown in Figure 4.1.37.
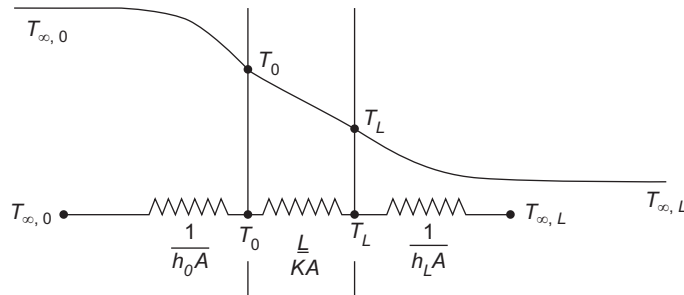
Figure 4.1.36 Steady-state conduction through a plane wall: schematic temperature profile and equivalent electrical analogue.

Figure 4.1.37 Steady-state conduction through a plane composite wall: schematic temperature profile and equivalent electrical analogue.

The heat transfer through the wall can be represented using an electrical analogue wherein the heat flowing through the system is equivalent to the current in the analogous electrical circuit, and the temperature difference is the driving force or the potential difference. The convective heat transfer on either side as well as the conductive heat transfer through the wall is represented using equivalent resistance terms as shown in Figures 4.1.36b and 4.1.37b. The intermediate temperatures at any intermediate point can also be determined as that corresponding to electric potential in the electrical analogue.

When designing walls for insulation of furnaces, many layers of different materials are laid to form a composite wall. Not only should the thermal conductivity of the insulation material be considered but its service temperature should also be taken into account. For example, refractory bricks can be used at the inner layers of the furnace where temperatures are high; for the outer layers, having lower temperatures, ceramic wools having relatively much lower thermal conductivities can be used.

In many systems, it is desirable to enhance the heat transfer so that the system can be maintained at lower temperatures. In such systems, the resistance offered by the interface between two different materials can significantly alter the heat transfer rates. These

interface resistances depend on the quality of the physical contact as well as the filling materials, if any, at the interface boundary. By selecting an interfacial medium with high thermal conductivity, the interface resistance can be decreased. A typical example of this application is the use of heat–conducting silver paste to bond heat sinks to the top of IC chips.

4.1.18.3.2 Conduction Through Radial Systems

Steady–state heat transfer through the walls of long cylindrical furnaces or pipes of circular cross section can be analyzed using the 1D heat transfer equation in the radial direction (refer to Equation 4.1.137).

$$\frac{1}{r}\frac{\partial}{\partial r}\left(r\kappa\frac{\partial T}{\partial r}\right)=0 \tag{4.1.142}$$

Integration, with temperatures specified at the inner and the outer wall, will give a situation similar to that obtained for the plane wall. The solution for the above equation can be expressed by an electrical equivalent as shown in Figure 4.1.38. The equation for the heat flow is

$$\dot{q}=\frac{T_0-T_1}{\frac{\ln(R_1/R_0)}{2\pi L\kappa}} \tag{4.1.143}$$

Here, L is length of the cylinder.

This approach can be extended with several concentric layers of different materials, and convective heat transfers at the inner and the outer surfaces.

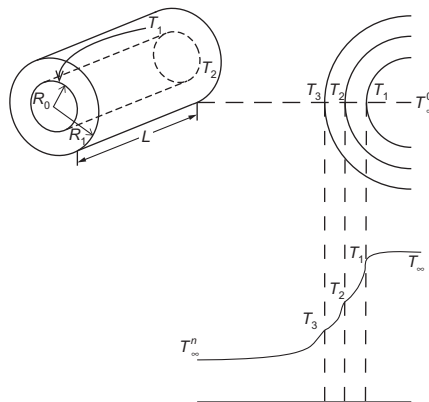$$\dot{q}=\frac{T_{\infty,0}-T_{\infty,n}}{R_{\text{total}}} \tag{4.1.144}$$

Figure 4.1.38 Illustration of Steady-state heat conduction through a cylindrical wall.

$$R_{\text{total}} = \frac{1}{2\pi R_0 L h_0} + \frac{\ln(R_1/R_0)}{2\pi L \kappa_1} + \frac{R''_{1,2}}{2\pi R_1 L} + \cdots$$
$$+ \frac{\ln(R_i/R_{i-1})}{2\pi L \kappa_i} + \frac{R''_{i,i+1}}{2\pi R_i L} + \cdots \qquad (4.1.145)$$
$$+ \frac{\ln(R_n/R_{n-1})}{2\pi L \kappa_n} + \frac{1}{2\pi R_n L h_n}$$

where $R''_{i,i+1}$ are interfacial resistances between layers i and $i+1$.

Heat transfer through a spherical shell can be similarly analyzed. The conduction resistance through a spherical wall is $\frac{1}{4\pi\kappa} \cdot \left(\frac{1}{R_i} - \frac{1}{R_o} \right)$, where R_i and R_o are inner and outer radii, respectively.

4.1.18.3.3 Heat Transfer Through Extended Surfaces

Extended surfaces are used in thermal systems to enhance the heat transfer rates. For example, electronic components, such as a processor chip in a computer, need to be maintained below a critical temperature. When the processor is on, the electric circuits generate thermal energy, which needs to be efficiently dissipated to avoid overheating of the chip. These extended surfaces, also known as fins, are also used in many electrical, electronic, and thermal systems, where thermal energy needs to be dissipated efficiently. In addition, extended surfaces are used in heat exchangers where one is interested in transferring heat efficiently from one medium to another. Heat transfer analysis through extended surfaces is also important when designing temperature-measuring probes using thermocouples. The thermocouple lead wires, or the tube in which the thermocouple is placed, can themselves act as heat dissipaters, giving rise to significant errors in measurements.

The basic purpose of using fins is to enhance the convective heat transfer at solid–fluid interface when the solid is a good conductor and the resistance due to conduction is minimal. The increase of surface area enables increase in heat dissipation to the surroundings. When designing these fins, care needs to be taken to ensure that the advantage of enhancing the heat transfer by increasing the convective surface area is not offset by the additional conductive resistance and, in cases where a separate heat sink is attached, an additional contact resistance.

Consider a simple pin fin of constant cross section of length L as shown in Figure 4.1.39.

The thickness of fins is generally small so that the convective heat transfer resistance can be considered dominant, and the temperature variation across the thickness is negligible. Along the length of the fin, on the other hand, conductive resistance is important. Performing a steady-state heat balance for an infinitesimal length of Δx of the fin as shown in the figure, one can write,
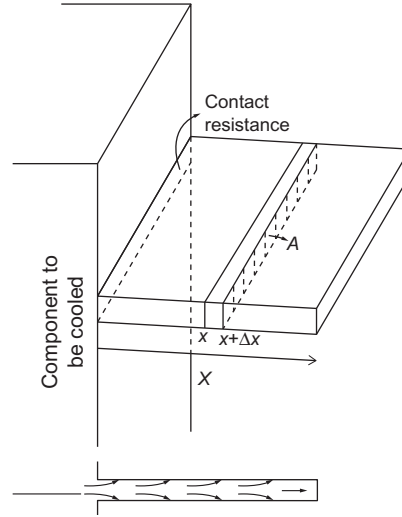
Figure 4.1.39 Schematic of a heat transfer fin having constant area and cross section.

$$\left(-A\kappa\frac{dT}{dx}\right)\bigg|_{x} - \left(-A\kappa\frac{dT}{dx}\right)\bigg|_{x+\Delta x} - h(P\Delta x)\left(T|_{x+\Delta x/2} - T_{\infty}\right) = 0$$

where, A is the area of cross section of the fin, P the perimeter of the fin, h the heat transfer coefficient, and T_{∞} the temperature of the surrounding fluid. One can then obtain the differential equation:

$$\frac{d}{dx}\left(\kappa A\frac{dT}{dx}\right) - hP(T - T_{\infty}) = 0 \qquad (4.1.146)$$

At the base of the fin $(x = 0)$, the boundary condition is

$$T|_{x=0} = T_{B}$$

The general boundary condition at the tip is

$$x = L, \quad -\kappa\frac{dT}{dx}\bigg|_{x=L} = h\left(T|_{x=L} - T_{\infty}\right)$$

Using these boundary conditions, the solution to Equation (4.1.146) is:

$$\frac{T - T_{\infty}}{T_{B} - T_{\infty}} = \frac{\cosh(m(L-x)) + \frac{h}{m\kappa}\sinh(m(L-x))}{\cosh(mL) + \frac{h}{m\kappa}\sinh(mL)} \qquad (4.1.147)$$

where

$$m = \sqrt{\frac{hP}{\kappa A}} \tag{4.1.148}$$

and the corresponding total heat transfer rate through the fin ($\dot{q}_f$) is given by

$$\dot{q}_f = \sqrt{hP\kappa A}(T_B - T_\infty)\frac{\sinh(mL) + \frac{h}{m\kappa}\cosh(mL)}{\cosh(mL) + \frac{h}{m\kappa}\sinh(mL)} \tag{4.1.149}$$

In most cases, the heat transfer surface would contain an array of fins, analysis for which can be easily obtained from the above. The expression for heat transfer would be different if the boundary condition at the tip of the film is different, as for example, an insulated tip.

The analysis described above is for fins of constant cross section (constant A). Fins can also have varying area cross sections along their length. Generally, all these fins are char-acterized by two parameters, namely (1) effectiveness and (2) efficiency. The effectiveness of a fin is defined as the ratio of heat transferred with the fin to that without the fin for a specified base temperature. Thus, for a fin of constant cross section, the effectiveness can be obtained from Equation (4.1.149) as

$$\varepsilon_f = \frac{\dot{q}_f}{\dot{q}_{\text{without fin}}} = \frac{\dot{q}_f}{hA(T_B - T_\infty)} = \sqrt{\frac{P\kappa}{Ah}}\frac{\sinh(mL) + \frac{h}{m\kappa}\cosh(mL)}{\cosh(mL) + \frac{h}{m\kappa}\sinh(mL)} \tag{4.1.150}$$

The efficiency of a fin is defined by comparing the heat transfer from the fin to that from an ideal one. An ideal fin is that which offers no conductive resistance. For an ideal fin, therefore, the entire fin would be at the base temperature T_B. The equation for the efficiency of a fin would be:

$$\eta_f = \frac{\dot{q}_f}{A_f h(T_B - T_\infty)} \tag{4.1.151}$$

where A_f is the total exposed surface area of the fin. For a given fin geometry, fin material and a convective heat transfer coefficient (h), one can obtain the efficiency, η_f, by solving the appropriate heat transfer equation similar to the one given in Equation (4.1.146). For commonly used fin geometries (radial, fins with varying cross sections, etc.), the effi-ciency of the fin is given in the form of charts, from which one can directly obtain q_f. If f is the fraction of the surfaces of the wall covered by fins, the heat transfer at the wall can be written as: $\dot{q}'' = \big((1-f) + A_{f,t}\eta_f\big)h(T_B - T_\infty)$, where $A_{f,t}$ is the total surface area of the array of fins on a wall of unit area. The net effect of the fins is therefore to enhance the effective heat transfer coefficient at a plane wall by a factor of $(1-f) + A_f\eta_f$. One

can solve multiwall problems using this enhanced heat transfer coefficient for the convective resistance.

### 4.1.18.4. 1D Transient Conduction

Transient systems where temperature varies with time are common in metallurgical processes starting from primary metal production from ore, followed by casting of liquid metal and finally to achieve microstructural control through thermomechanical treatments. In this section, analysis of transient heat transfer in bodies submerged in a fluid phase is presented.

The heat transfer process depends on one hand on the transfer within the solid and the size and the shape of the component, and material properties such as heat capacity and thermal conductivity. It also possible for the rate to depends principally on the flow and the fluid properties outside the component, i.e. the rate is determined convective transfer. At the one extreme, the conductive resistance can be much smaller than the convective resistance, as when the component is made of high conductivity materials and is of small size in relation to this conductivity. In this case it is expected that the temperature gradients within the body are small in comparison to gradients outside. These are called thermally thin bodies and can be approximated as having uniform temperatures within the body. If the gradients within the body are not insignificant, it is a thick body problem. If the heat transfer coefficient and the mass of the body to be heated are relatively large the difference between the surface temperature and the bulk fluid temperature is small; the temperature gradients are primarily within the body. It should be emphasized that the definitions of "thin" and "thick" are relative terms dependent not only on the component itself but also on the convective conditions.

Thermally thin and thick systems can be characterized using a simple analysis. Consider a slab of thickness $2L$ with other dimensions much larger than L as shown in Figure 4.1.40. This slab, starting with uniform initial temperature, T_0, is immersed in a fluid of temperature T_∞. The figure illustrates the two cases of thermally thin and thermally thick systems. The heat transfer is primarily in the direction of the slab thickness. The two resistances for the heat transfer are conduction resistance within the slab and the external convective heat transfer resistance from the slab surface to the fluid bulk.

For the slab, the conduction resistance can be written as $R_{\text{conduction}} \approx \frac{L}{A\kappa_S}$ and the external convective resistance on one side as $R_{\text{convection}} = \frac{1}{hA}$. Here, A denotes the area perpendicular to the slab thickness. The ratio of these two resistances is denoted as the Biot number

$$Bi = \frac{R_{\text{conduction}}}{R_{\text{convection}}} = \frac{L}{A\kappa_S} \bigg/ \frac{1}{hA} = \frac{hL}{\kappa_S} \qquad (4.1.152)$$
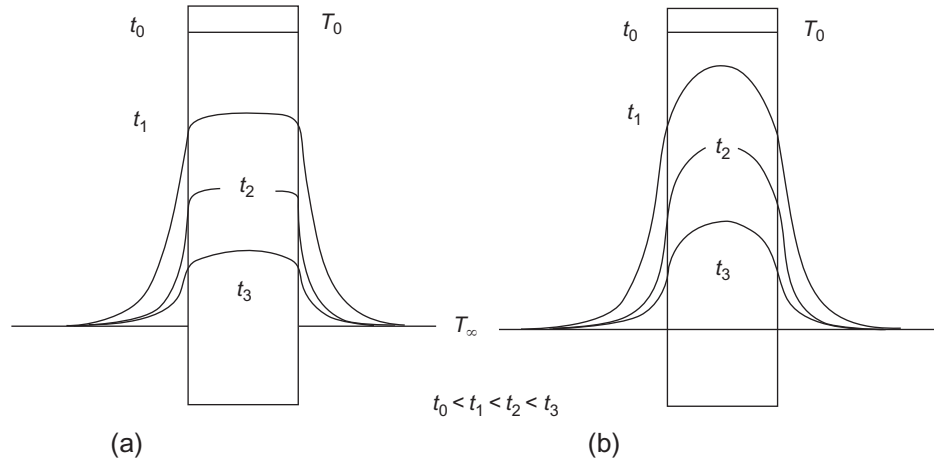
Figure 4.1.40 Schematic temperature profiles in (a) thermally thin and (b) thermally thick bodies.

In the above equation, L is the characteristic dimension for the slab, which can be generalized for irregular-shaped bodies as $\frac{V}{A_S}$, where V is volume of the component and A_S is the external surface area through which convection occurs. If the Biot number is very small, one can consider the component to be thermally thin, such that the temperature within the body is nearly uniform, spatially, at any instant of time. In general, a Biot number <0.1 can be considered to be a thermally thin system for common engineering heat transfer analysis. Such systems are also referred to as lumped parameter systems.

4.1.18.4.1 Thermally Thin Bodies

Transient heat transfer analysis in thin bodies is quite simple. Consider a solid body of volume V, surface area A_s, density ρ_s, and thermal conductivity κ_s initially at temperature T_0. It is immersed into a large volume of fluid at temperature T_∞, at time $t=0$. The amount of fluid is large enough for its bulk temperature to remain constant at T_∞. The convective heat transfer coefficient between the fluid and body is denoted by h. As discussed earlier, the Bi number, given by $\frac{hV}{A_s\kappa_s}$, is so small that the solid body can be considered to be at uniform temperature, T, at any instant of time. Thus, the heat balance gives:

$$V_s\rho_s C\frac{\mathrm{d}T}{\mathrm{d}t} = -A_s h(T - T_\infty) \tag{4.1.153}$$

The solution of the equation 4.1.153 with the initial condition of $t=0, T=T_0$ is

$$\frac{T(t) - T_\infty}{T_0 - T_\infty} = \exp\left(-\frac{A_s h}{V_s\rho_s C}t\right) = \exp\left(-\frac{t}{\tau}\right) \tag{4.1.154}$$

$\tau = \frac{V\rho_s C}{A_s h}$ has the dimension of time and can be termed as the characteristic response time for the system, which is quite useful in comparing transient responses of different systems. Since at large times the body will reach the temperature of the fluid, the LHS of the equation represents the unaccomplished temperature change. The equation can also be written as:

$$\theta^* = \frac{T(t) - T_\infty}{T_0 - T_\infty} = \exp\left(-\frac{hV/A_s}{\kappa_s} \cdot \frac{\kappa_s/\rho C}{(V/A_s)^2} t\right) = \exp(-Bi \cdot Fo) \qquad (4.1.155)$$

Fo, the Fourier number, is the dimensionless time and θ^* is the dimensionless temperature difference.

Example 4.1.9

A thermocouple junction, which may be approximated as a sphere, is to be used for temperature measurement in a gas stream. The convection coefficient between the junction surface and the gas is known to be $h = 400$ W m^{-2} K^{-1} and the junction thermophysical properties are $\kappa = 200$ W m^{-1} K^{-1}, $C = 400$ kg^{-1} K^{-1}, and $\rho = 8500$ kg m^{-3}. Determine the junction diameter needed for the thermocouple to have a time constant of 1 s. If the junction is initially at 298 K and is placed in a gas stream that is at 573 K, how long will it take for the junction to reach 572 K?

Solution

The time constant, as discussed earlier, is given by $\frac{V\rho_s C}{A_s h}$. For a sphere, this reduces to $\frac{D\rho_s C}{6h}$, where *D* is the diameter of the sphere. For the desired time constant of 1 s, *D* should be 0.7 mm.

The *Bi* number for the thermocouple tip-fluid system is given by

$$Bi = \frac{hV}{A_s \kappa} = \frac{hD}{6\kappa} = 0.0023$$

and is very small so that the thermally thin approximation is valid.

Using Equation (4.1.154), the time for the thermocouple junction to reach 572 K when immersed in a gas stream of 573 K can be calculated as

$$\frac{572 - 573}{298 - 573} = \exp(-t/1)$$

Thus, $t = 5.6$ s.

4.1.18.4.2 Thermally Thick Bodies

When the Biot number (*Bi*) is significantly large (>0.1), the difference between the center and surface temperature within the component is comparable to or larger than the difference between the surface temperature and the bulk temperature of the fluid. In such

cases, one needs to solve the transient heat conduction equation (Equation 4.1.137) with appropriate boundary conditions.

4.1.18.4.3 Conduction in 1D

For simple geometries such as a slab with finite thickness with the other two dimensions being larger, a long cylinder whose radius is much smaller in comparison to its length or a sphere, one can obtain approximate analytical solutions from a 1D analysis. Further, there are special cases wherein the system can be considered as a semi-infinite system as explained later in this section. These cases are primarily analyzed using the 1D transient heat conduction equation.

4.1.18.4.4 Slab

Consider a thermally thick slab shown in Figure 4.1.40. Here, a slab of thickness $2L$ initially at T_0 is being cooled for all $t>0$ by a fluid that is at T_∞. Because of symmetry, one needs to consider only one half of the slab (see Figure 4.1.40). The 1D heat equation in Cartesian coordinates, with thermal properties being independent of temperature, is:

$$\frac{\partial T}{\partial t} = \alpha_s \frac{\partial^2 T}{\partial x^2} \tag{4.1.156}$$

The initial and boundary conditions are:

$$t=0; \text{ and for } 0 \leq x \leq L : T = T_0 \quad \text{(Initial condition)} \tag{4.1.157}$$

$$t>0; \text{ and for } x=0 : \frac{\partial T}{\partial x} = 0 \quad \text{(Boundary condition : symmetry at the center)}$$

$$t>0; \text{ and for } x=L : -\kappa_s \frac{\partial T}{\partial x} = h(T|_{x=L} - T_\infty)$$
$$\text{(Boundary condition : surface heat balance)}$$

The governing equations can be nondimensionalized so that the number of parameters needed to express the solution can be reduced. The equation is nondimensionalized using the following:

$$x^* = \frac{x}{L} \quad \text{(Dimensionless space coordinate)}$$

$$Fo = \frac{\alpha_s t}{(L^2)} \quad \text{(Dimensionless time or Fourier number)}$$

$$\theta^* = \frac{T(x,t) - T_\infty}{T_0 - T_\infty} \quad \text{(Dimensionless temperature difference)}$$

to give,

$$\frac{\partial \theta^*}{\partial Fo} = \frac{\partial^2 \theta^*}{\partial x^{*2}} \qquad (4.1.158)$$

with the initial and boundary conditions,

$$
\begin{aligned}
Fo = 0; \ 0 \le x^* \le 1; &\quad \theta^* = 1 \\
Fo > 0; \ x^* = 0; &\quad \frac{\partial \theta^*}{\partial x^*} = 0 \\
Fo > 0; \ x^* = 1; &\quad \frac{\partial \theta^*}{\partial x^*} = -\mathrm{Bi}\theta^*\big|_{x^*=1}
\end{aligned} \qquad (4.1.159)
$$

Here Biot number (Bi) is $\frac{hL}{\kappa_s}$.

An analytical series solution is obtained for the above equation using variable separable method (see Ref. [39] for details) and is given as

$$\theta^* = \sum_{i=1}^{\infty} C_i \exp\left(-\lambda_i^2 Fo\right) \cos\left(\lambda_i x^*\right) \qquad (4.1.160)$$

$$\text{where } C_i = \frac{4\sin\left(\lambda_i\right)}{2\lambda_i + \sin\left(2\lambda_i\right)}$$

and

$$\lambda_i \tan\left(\lambda_i\right) = Bi$$

Please note that the parameter λ_i denotes the roots of the transcendental equation. In the above infinite series, the first term dominates over other terms, especially for $Fo > 0.2$. Therefore, in many engineering applications, the approximate solution containing only the first term is used, i.e.,

$$\theta^* = C_1 \exp\left(-\lambda_1^2 Fo\right) \cos\left(\lambda_1 x^*\right)$$

The parameter λ_1, which denotes the first root of the transcendental equation, and the corresponding C_1 are tabulated in Table 4.1.4 as given in Ref. [38]. It can also be computed using standard computing software such as MATLAB and OCTAVE; Equation (4.1.161) can be split into two as follows:

$$\theta^* = \theta_0^* \cos\left(\lambda_1 x^*\right) \quad \text{and} \quad \theta_0^* = C_1 \exp\left(\lambda_1^2 Fo\right)$$

Here θ_0^* represents the temperature at the center of the slab ($x^* = 0$). Thus the Equation (4.1.161) can be presented as a set of two charts: one showing the dimensionless center temperature (θ_0^*) as a function of Bi and Fo and the other giving θ^* (for $0 < x^* \le 1$) as a function of θ_0^* and Bi. These charts are named after Heisler, who drew them for the first time [40]. From the approximate solution, one can determine the amount of heat transferred from the beginning to any time t as

Table 4.1.4 Values of the Parameters in the Approximate Analytical Solution of 1D Transient Conduction in a Long Slab, Long Cylinder, and a Sphere [38]

Bi	Long Slab		Long Cylinder		Sphere	
	λ_1	C_1	λ_1	C_1	λ_1	C_1
0.01	0.0998	1.0017	0.1412	1.0025	0.1730	1.0030
0.02	0.1410	1.0033	0.1995	1.0050	0.2445	1.0060
0.04	0.1987	1.0066	0.2814	1.0099	0.3450	1.0120
0.06	0.2425	1.0098	0.3438	1.0148	0.4217	1.0179
0.08	0.2791	1.0130	0.3960	1.0197	0.4860	1.0239
0.1	0.3111	1.0161	0.4417	1.0246	0.5423	1.0298
0.2	0.4328	1.0311	0.6170	1.0483	0.7593	1.0592
0.3	0.5218	1.0450	0.7465	1.0712	0.9208	1.0880
0.4	0.5932	1.0580	0.8516	1.0931	1.0528	1.1164
0.5	0.6533	1.0701	0.9408	1.1143	1.1656	1.1441
0.6	0.7051	1.0814	1.0184	1.1345	1.2644	1.1713
0.7	0.7506	1.0918	1.0873	1.1539	1.3525	1.1978
0.8	0.7910	1.1016	1.1490	1.1724	1.4320	1.2236
0.9	0.8274	1.1107	1.2048	1.1902	1.5044	1.2488
1.0	0.8603	1.1191	1.2558	1.2071	1.5708	1.2732
2.0	1.0769	1.1785	1.5995	1.3384	2.0288	1.4793
3.0	1.1925	1.2102	1.7887	1.4191	2.2889	1.6227
4.0	1.2646	1.2287	1.9081	1.4698	2.4556	1.7202
5.0	1.3138	1.2403	1.9898	1.5029	2.5704	1.7870
6.0	1.3496	1.2479	2.0490	1.5253	2.6537	1.8338
7.0	1.3766	1.2532	2.0937	1.5411	2.7165	1.8673
8.0	1.3978	1.2570	2.1286	1.5526	2.7654	1.8920
9.0	1.4149	1.2598	2.1566	1.5611	2.8044	1.9106
10.0	1.4289	1.2620	2.1795	1.5677	2.8363	1.9249
20.0	1.4961	1.2699	2.2880	1.5919	2.9857	1.9781
30.0	1.5202	1.2717	2.3261	1.5973	3.0372	1.9898

Continued

Table 4.1.4 Values of the Parameters in the Approximate Analytical Solution of 1D Transient Conduction in a Long Slab, Long Cylinder, and a Sphere [38]—cont'd

Bi	Long Slab		Long Cylinder		Sphere	
	λ_1	C_1	λ_1	C_1	λ_1	C_1
40.0	1.5325	1.2723	2.3455	1.5993	3.0632	1.9942
50.0	1.5400	1.2727	2.3572	1.6002	3.0788	1.9962
100.0	1.5552	1.2731	2.3809	1.6015	3.1102	1.9990
∞	1.5708	1.2732	2.4048	1.6021	3.1416	2.0000

$$\frac{Q}{Q_0} = 1 - \frac{\sin \lambda_1}{\lambda_1} \theta_0^*,$$

where $Q_0 = \rho CV(T_i - T_\infty)$, the maximum heat transferred at $t \rightarrow \infty$.

4.1.18.4.5 Long Cylinder and Sphere

Using the same methodology, approximate solutions for long cylinders and spheres are also obtained [38]. For both cases, the characteristic dimension used for defining the dimensionless radius (r^*), Bi and Fo is the radius, R.

For a long cylinder of radius R,

$$\theta^* = C_1 \exp\left(-\lambda_1^2 Fo\right) J_0(\lambda_1 r^*) \tag{4.1.161}$$

where

$$C_1 = \frac{2}{\lambda_1} \frac{J_1(\lambda_1)}{J_0^2(\lambda_1) + J_1^2(\lambda_1)}$$

and

$$\lambda_1 \frac{J_1(\lambda_1)}{J_0(\lambda_1)} = Bi$$

$$\frac{Q}{Q_0} = 1 - \frac{2\theta_0^*}{\lambda_1} J_1(\lambda_1)$$

Here, J_0 and J_1 are the Bessel functions of the first kind.

For a sphere of radius R,

$$\theta^* = C_1 \exp\left(-\lambda_1^2 Fo\right) \frac{1}{\lambda_1 r^*} \sin\left(\lambda_1 r^*\right) \tag{4.1.162}$$

where

$$C_1 = \frac{4\left(\sin\left(\lambda_1\right) - \lambda_1\cos\left(\lambda_1\right)\right)}{2\lambda_1 - \sin\left(2\lambda_1\right)}$$

and

$$1 - \lambda_1 \cot\left(\lambda_1\right) = B_i$$

$$\frac{Q}{Q_0} = 1 - \frac{3\theta_0^*}{\lambda_1^3}\left(\sin\left(\lambda_1\right) - \lambda_1\cos\left(\lambda_1\right)\right)$$

The parameters λ_1 and C_1 for long cylinders as well as spheres are also tabulated in Table 4.1.4.

Analytical solutions given above are valid only for specific cases having an initial condition of spatially uniform temperature and a convective boundary condition with a constant heat transfer coefficient and a constant fluid temperature. For other cases, numerical methods have to be used. Readers may refer to books on numerical heat transfer [41] for further information.

Example 4.1.10

A 0.314 diameter stainless steel billet ($\rho_s = 7900$ kg m^{-3}, $k_s = 25$ W m^{-1} K^{-1}, $C = 600$ J kg^{-1} K^{-1}) is passing through a 6.1-m long heat-treating furnace. The initial billet temperature is 298 K. The temperature of the billet must be raised to a minimum of 1090 K before working. The heat transfer coefficient between the furnace gases and the billet surface is 85.2 W m^{-2} K^{-1}, and the furnace gases are at 1530 K. At what minimum velocity must the billet travel through the furnace to satisfy these conditions? What will be temperature difference between the center and the surface of the billet when it exits the furnace?

Solution

First verify whether the billet is a thermally thin or a thick system by computing the Biot number. When verifying this, the characteristic length for Bi should be $\frac{V}{A} = \frac{\pi R^2 L}{2\pi R L} = \frac{R}{2}$.

$$Bi = \frac{hR/2}{k_s} = \frac{85 \times 0.152/2}{25} = 0.258 > 0.1$$

The system needs to be treated as thermally thick.

As the minimum temperature that needs to be achieved is 1090 K, it is needed to make sure that the center temperature reaches this temperature as all other temperatures would be higher than this. Being a cylindrical body, the solution given in Equation (4.1.161) needs to be applied. The dimensionless time Fo has to be computed knowing $\theta^*(r^* = 0)$ and Bi. Here, Bi is calculated using characteristic length R.

$$\theta^*(r^*=0)=\frac{T(r=0)-T_\infty}{T(t=0)-T_\infty}=\frac{1090-1530}{298-1530}=0.357$$

$$\frac{hR}{k_s}=Bi=0.516$$

From Table 4.1.4, the values of λ_1 and C_1 are 0.941 and 1.115, respectively. From Equation (4.1.161), the dimensionless time Fo is 1.28. Therefore, the residence time for the billet in the furnace should be

$$Fo=1.28=\frac{\alpha_s t}{R^2}=\frac{\kappa_s t}{\rho_s C R^2}=\frac{25\times t}{7900\times 600\times 0.152^2}$$

$$\therefore t=5610\,\text{s}$$

Corresponding to this time, the velocity of the billet through 6-m long furnace would be 3.85 m h^{-1}. Using Equation (4.1.161) again, the dimensionless temperature at the surface of the billet is calculated as $\theta^*(r^*=1)=\theta^*(r^*=0)J_0(\lambda_1)=0.2822$ which gives the temperature at the surface of the billet as 1182 K, which is 92 K more than the billet center temperature.

4.1.18.4.6 Semi-infinite System

Semi-infinite systems are those that span from $x=0$ to $x=\infty$, the primary boundary condition being applied at the surface at $x=0$. Practically, a slab can be treated as a semi-infinite solid if it has a thickness large enough such that changes applied on one surface ($x=0$) do not, in the time period of interest, result in any noticeable change at the centre line of the material.

Consider a slab that is initially at temperature T_0 stretching from $x=0$ to $x\rightarrow\infty$ (Figure 4.1.41). At $t=0$, the temperature at the surface at $x=0$ is raised to T_s and maintained thereafter. A schematic of the evolution of the temperature profile with time ($t_3>t_2>t_1>0$) is shown in the figure. The governing heat equation and the initial and boundary conditions are:

$$\frac{\partial T}{\partial t}=\alpha_s\frac{\partial^2 T}{\partial x^2};\quad t>0;\ 0<x<\infty;\qquad\qquad (4.1.163)$$

$$\text{Initial condition at}\,(t=0,\,0<=x<=\infty)\,T=T_0$$

$$\text{Boundary condition 1 at}\,(t>0,\,x=0)\,T=T_s$$

$$\text{Boundary condition 2 at}\,(t>0,\,x\rightarrow\infty)\,T=T_0$$

The solution to the equation is obtained by making use of the fact that the temperature profiles at different times have the same shape, i.e., one would get the profile at, say, $t=t_3$ from the profile at $t=t_2$ by appropriately stretching the time axis. In that case, it should be possible to transform the above partial differential equation with the initial
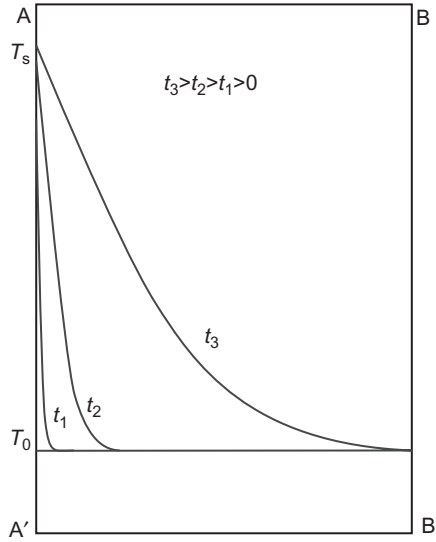
Figure 4.1.41 Schematic of heat conduction in a semi-infinite system.

and the boundary conditions to an ordinary differential equation by appropriately scaling the distance, x, using the time t. This is accomplished by introducing a new variable, called the similarity variable, $\eta = \frac{x}{2\sqrt{(\alpha_s t)}}$:

$$\frac{d^2 T}{d\eta^2} = -2\eta \frac{dT}{d\eta}; \quad 0 < \eta < \infty; \tag{4.1.164}$$

Boundary condition 1 $T(\eta = 0) = T_s$

Boundary condition 2 $T(\eta \to \infty) = T_0$

One may note that the initial condition and boundary condition 2 merge into a single boundary condition. The solution of the above equation is

$$\frac{T(x,t) - T_s}{T_0 - T_s} = \mathrm{erf}\left(\frac{x}{2\sqrt{\alpha_s t}}\right) \tag{4.1.165}$$

and the flux at $x = 0$ (surface AA')

$$\dot{q}''(x = 0) = \frac{\kappa_s (T_s - T_0)}{\sqrt{\pi \alpha_s t}} \tag{4.1.166}$$

Similar analytical solutions for the semi-infinite system with other boundary conditions, either convective heat transfer or a constant heat flux at the surface, have also been obtained [38].

Example 4.1.11

Rate of solidification of a liquid metal poured into a mold depends on the rate of heat that can be extracted through the mold. Hence, understanding the heat transfer through the mold and the metal is of great importance in casting designs. One of the most widely used and simple rule to estimate the solidification time for castings is Chvorinov's rule, named after Nicolas Chvorinov [42]. This rule states that

$$t_{\text{solidification}} = C\left(\frac{V}{A_s}\right)^n$$

Here V and A_s denote the volume and surface area of the casting, respectively. C and n are constants, the value of n being close to 2. The parameter C depends on the properties of metal as well as the mold. Using a 1D heat transfer analysis through a sand mold, the scientific rationale behind this rule can be appreciated (Figure 4.1.42).

Consider a long slab casting of thickness $2L$ being cast in a sand mold as illustrated in the figure. Initially the mold is at room temperature. Consider the hypothetical case where liquid metal is poured just at its melting point T_M. Let us assume that the time for filling the mold is very small compared to the solidification time. Initially the solid–ification rate will be very high as the mold starts out being cold. As regions in the mold closer to the hot metal are heated, the rate of heat transfer and correspondingly the rate of solidification decrease. If the casting is small and the mold is comparatively thick and is made of low conducting materials such as porous sand, the outer side of the mold can remain at room temperature till the solidification is complete. If the resistance for heat
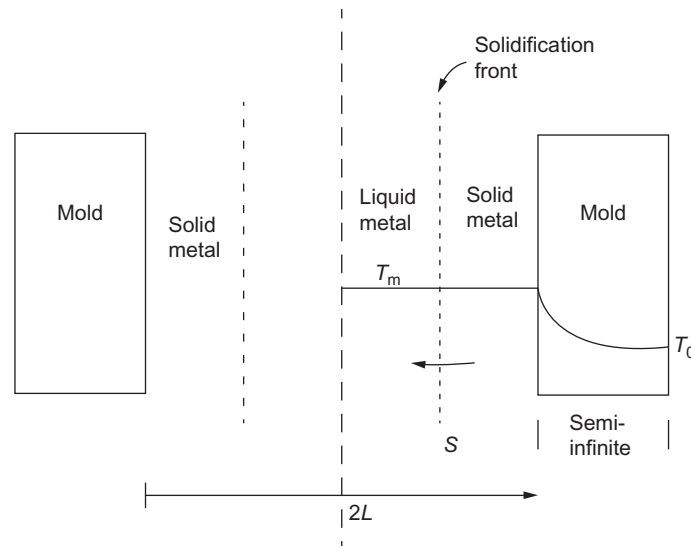
Figure 4.1.42 Solidification of a slab in sand mold.

transfer through the solidified metal is much lower than that through the sand mold, one may further assume that the solidified metal remains close to T_M till the end of solidification. The time–temperature profiles through the mold can then be considered to be those corresponding to a semi-infinite system. Equating the heat flux given by equation for a semi-infinite system to rate at which heat of fusion is released by the solidifying metal gives:

$$\dot{q}'' = \frac{\kappa_{\text{mold}}(T_M - T_0)}{\sqrt{\pi \alpha_{\text{mold}} t}} = \rho_{\text{metal}} \frac{dS}{dt} \Delta H_M \qquad (4.1.167)$$

where $\frac{dS}{dt}$ is velocity of the solidification front or the rate of solidification. Integration of the above equation from $x=0$ corresponding to the mold–metal interface to $x=L$ corresponding to the center of the casting gives

$$t_{\text{solidification}} = \left(\frac{\rho_{\text{metal}} \Delta H_M \sqrt{\pi \alpha_{\text{mold}}} L}{2\kappa_{\text{mold}}(T_M - T_0)} \right)^2 \qquad (4.1.168)$$

That is, the time for solidification is proportional to the square of the slab thickness, L, which agrees with the Chvorinov's law. One needs to note that many assumptions are made in the above analysis.

For the analysis of solidification of castings of shapes other than long slabs, ideally, heat transfer analysis in 2D or 3D needs to be performed. However, as a first approximation, for such cases, the ratio of volume of the casting to its external surface area, $\frac{V}{A_s}$ can be used in place of L in the above equation. Further, the exponent, n and C in the Chvorinov rule can be empirically estimated for castings of specific shape cast in a specific mold. For molds having higher thermal conductivities, such as metallic molds, the heat transfer analysis becomes more elaborate with both the conductive heat transfer resistance through the mold and the external convective and radiative heat transfer resistances becoming significant.

More often than not, numerical methods are needed for solving such problems in two and three dimensions. More details on these methodologies can be found elsewhere [41].

4.1.19. CONVECTION

Convective heat transfer refers to the transfer phenomena in the presence of flow of a fluid. In addition to transfer of heat by conduction discussed above, sensible energy can also be transferred when a fluid particle itself moves from one place to another (advection). The sum of these two processes is the total energy transferred and is termed convective transfer.

There are two kinds of engineering situations where convective transfers are important:

– Temperature variations within a flowing fluid. Examples of this type of problem are temperature profiles in liquid metal bath in a stirred ladle, tundish used in continuous casting, liquid in the mold that is electromagnetically stirred, or variation of temperature within a gas–fired furnace (here radiation is also important since the gas is not transparent). Temperature redistribution takes place when packets of fluids are carried from one place to another dissipating heat along the way by conduction. The flow equations for predicting the flow (continuity and momentum balance equations) in addition to the convective–diffusive heat transport equations must be solved. The generalized heat transport equation is derived by performing a differential heat balance on an infinitesimal volume element, as was done in the case of momentum. In this, both advective and conduction fluxes in and out of the control volume need to be considered. A simplified approach would be to apply the conduction equation developed in an Eulerian frame of reference (fixed with respect to the laboratory frame of reference) in a Lagrangian frame: a fluid particle advecting with the fluid. The partial derivative $\partial/\partial t$ in Equation (4.1.137) is replaced by the substantial derivative D/Dt. The same equation is obtained in both approaches for the cases of constant density, and specific heat, C, i.e.,

$$\rho C \frac{DT}{Dt} = \nabla \cdot (\kappa \nabla T) + \dot{Q}''' \qquad (4.1.169)$$

Here, the term $\dot{Q}'''$ should also include viscous dissipation of mechanical energy into thermal energy; however, in most problems, this term is small enough to be neglected. The heat generation, however, from other sources, such as electromagnetic interactions and chemical reactions, needs to be accounted through the term $\dot{Q}'''$. For most realistic systems of importance, one needs to spend considerable computational effort to obtain solutions to these equations.

– The second situation, which is quite frequently encountered, is where interest is in determining the rate of heat transferred to/from an interface between two media, one which is flowing past the interface. The medium on the other side of the interface can either be a solid or a liquid. Heat transferred from the surface of a piece made of steel when quenched in water during heat treatment is one example. Heat getting lost to air from the liquid metal surface in an open ladle is another.

In the case of a fluid flowing past the surface of solid (or a stagnant liquid), the fluid at the surface is at rest with respect to the solid. The heat transfer mechanism at the surface is by conduction and is proportional to the temperature gradient at the surface. In the liquid away from the surface, the heat transfer and thereby the surface temperature gradient are influenced by fluid flow. To estimate this temperature gradient, a knowledge of the flow is required and estimating this from first principles would involve solving flow and heat transfer equations simultaneously.

Interface heat transfer fluxes are normally represented phenomenologically using the Newton's law of cooling through a quantity called the "heat transfer coefficient," h:

$$\dot{q}'' = h(T_s - T_\infty) = -\kappa_f \frac{\partial T}{\partial s}\Big|_{s=0} \tag{4.1.170}$$

where T_s and T_∞ are temperatures at the interface and the bulk of the flowing fluid, respectively; κ_f is the fluid conductivity, and the temperature gradient is that in the fluid at the interface.

Over a finite surface, the heat transfer condition may be different at different locations; one can define a local heat transfer coefficient, h_{loc} as:

$$\mathrm{d}\dot{q} = h_{loc}(T_s - T_\infty)\mathrm{d}A \tag{4.1.171}$$

where $\mathrm{d}\dot{q}$ is the infinitesimal heat transferred over a differential area $\mathrm{d}A$.

In many engineering systems, the average heat transfer across the interface is of more interest than the detailed spatial distribution of it. In such cases, a mean heat transfer coefficient is defined to characterize the net heat across the interface. Mathematically this can be expressed as

$$\overline{h} = \frac{1}{A}\int_A h(\mathrm{d}A_{interface}) \tag{4.1.172}$$

For most problems dealt with in this section only the average heat transfer coefficient $\overline{h}$ is required. For brevity, the symbol h has been used to denote average heat transfer coefficient. Exceptions from this notation have been specifically mentioned for those special cases.

Convective transport is generally classified into two categories: forced convection and free convection. In the case of forced convection, the flow is generated by external means, such as blowing a fan around a solid object or making a hot fluid flow through a cold tube. On the other hand, in the absence of any external force, gradients in density assisted by gravity can give rise to flow within the system, which ultimately results in heat transfer. A hot object kept in a still fluid is a typical example. These are free convection or natural convection situations. Additionally, systems operate at high enough temperatures where one of the phases undergoes a phase change at the interface. Cooling water jets falling on hot rolled steel sheets at a temperature of approximately 1200 K in a run-out table is one such example. Readers may refer books on heat transfer [38] for these additional topics.

Heat transfer coefficients have been obtained for various situations of engineering importance, either by solving the generalized equations for flow and heat transfer or more commonly through empirical methods. When presenting these correlations, for both forced and natural convection situations, the flow is classified into external and internal flows.

In internal flows, the flowing fluid is confined with an external boundary through which heat transfer is taking place. The amount of fluid is limited and heat transfer leads

to accumulation/depletion of the total energy contained in the fluid. Heat transfer from/ to the walls of a pipe to water flowing through it, wall heat transfer in a gas–fired furnace, and heat loss through the walls of a ladle are some examples.

In external flows, a large body of fluid flows relative to the body on the surface of which heat transfer takes place. When the body of the fluid is large enough, temperature of the fluid far away from the body remains unaffected by the heat transfer. Flow over a cylinder or a sphere and flow over a plate such as a wing of an aeroplane are some examples. Flow around a bubble or an inclusion rising in a large ladle, flow around a rising aluminum droplet shot as a bullet into liquid steel bath for deoxidation, and flow around a temperature probe dipped into the stream of pig iron flowing in the blast furnace runner can be viewed as external flows.

Since in external flows, properties such as velocity and temperature are disturbed only near the boundary of the submerged object, only this boundary region, called the boundary layer, needs to be analyzed. Transfer process in a boundary layer is treated as a separate section called the boundary layer phenomena, and the book by Schlichting and Gersten [30] is a classic reference. Though extensive treatment of this subject is beyond the scope of this chapter, a simple analysis is illuminating since most of the correlations are built around this idea.

4.1.19.1. Boundary Layer Theory

At the beginning of the twentieth century, Prandtl proposed [43] the boundary layer concept. It is considered to be one of the revolutionary concepts in fluid dynamics worth the Nobel Prize [44]. He conceptualized a thin layer of fluid flowing around a body, which ultimately governs the resistance and other consequent heat and mass transfer characteristics.

Consider a flat stationary solid plate and a fluid that moves parallel to this plate as shown in Figure 4.1.43. The fluid approaching the plate has a uniform flow parallel to the length of the plate with a velocity V_∞ (approach velocity). As soon as the fluid layer reaches the plate, the fluid layer adjacent to the plate would come to rest because of the no-slip condition. Subsequently, due to viscous transport, the adjacent fluid layers also start decelerating. As the fluid moves farther along the length of the plate in direction x, more and more fluid layers are decelerated. Thus a velocity profile develops in the neighborhood of the plate as shown in Figure 4.1.43. Moving away from the plate in the y direction, the velocity asymptotically approaches the bulk fluid velocity, v_∞. The large gradients in velocity are restricted to the neighborhood of the plate. By convention, the locus of the points where the velocity is 99% of the approach velocity, v_∞ (also called free stream velocity) is defined as the velocity boundary layer. The thickness of the boundary layer at any cross section increases as x increases. The boundary layer thickness is smaller at higher fluid flow velocities.
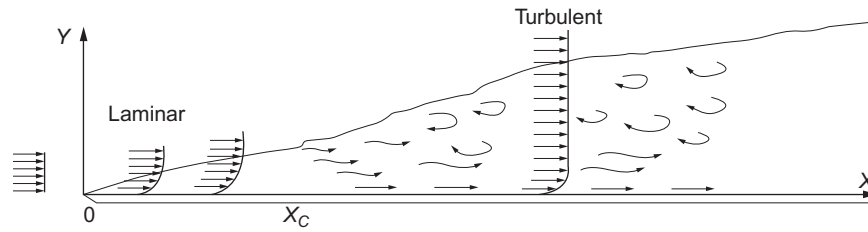
Figure 4.1.43 Schematic of a velocity boundary layer for a parallel flow over a flat plate.
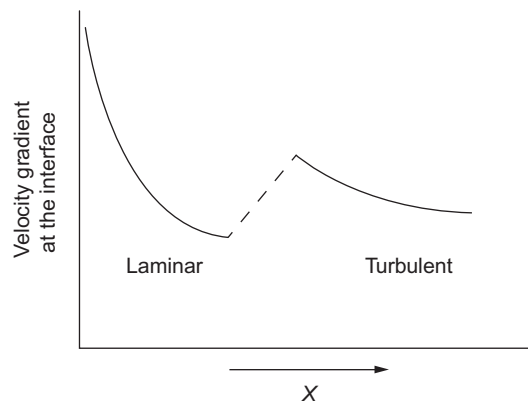
Figure 4.1.44 Illustration of variation of the velocity gradient at the interface in the boundary layer for flow parallel to a flat plate.

The transition from laminar to turbulent flow also occurs for boundary layer flows. For a flat plate, at $Re_x = \frac{\rho V_\infty x}{\mu}$ of about 5×10^5, the flow changes from laminar to turbulent with a transition layer in between. Here x is distance from the leading edge as shown in Figure 4.1.44. Observations have shown that the boundary layer thickness increases significantly during transition from laminar to turbulent flow. The flow structure is stream-lined in the laminar region. The turbulent region predominantly consists of eddies; however, close to the plate, eddy strengths become so low that they almost die down and researchers identify a thin fluid layer close to the surface in which the flow is nearly laminar; this is referred to as the laminar sublayer.

Figure 4.1.44 illustrates the variation of velocity gradient for the fluid layer adjacent to the plate along the length of the plate. Ideally for a plate with sharp leading edge, the velocity gradient should approach infinity at $x = 0$ (singularity). Further along the length of the plate the gradient drops. During transition from laminar to turbulent, the velocity gradient shows a sharp increase. In the turbulent regime, the velocity gradient again starts decreasing along the length of the plate.

Since the flow variations are primarily restricted to the boundary layer, it is necessary to solve the flow equations only in this layer. These equations, called the boundary layer equations, are deduced from the Navier–Stokes equations using the order of magnitude approximation [43], which makes the problem considerably simpler. The main basis for this approximation is the observation that for high Reynolds number flows, the boundary layer thickness δ_x at any x is much smaller than x ($\delta_x \ll x$), making gradients in y direction predominant compared to those in the x-direction. The details of these approximations are not presented here; readers can find them in Schlichting's book [30]. The boundary layer equations for flow of an incompressible fluid over a flat plate at zero incidence (plate is parallel to the approach velocity) are:

$$\frac{\partial v_x}{\partial x} + \frac{\partial v_y}{\partial y} = 0 \qquad (4.1.173)$$

$$v_x \frac{\partial v_x}{\partial x} + v_y \frac{\partial v_x}{\partial y} = v \frac{\partial^2 v_x}{\partial x^2} \qquad (4.1.174)$$

For a uniform flow, the gradient in pressure is zero and this is impressed on the boundary layer too.

These equations can be nondimensionalized using a characteristic length L (length of the plate) and the characteristic velocity v_∞ (approach velocity), which yields

$$\frac{\partial v_x^*}{\partial x^*} + \frac{\partial v_y^*}{\partial y^*} = 0 \qquad (4.1.175)$$

$$v_x^* \frac{\partial v_x^*}{\partial x^*} + v_y^* \frac{\partial v_x^*}{\partial y^*} = \frac{1}{Re_L} \frac{\partial^2 v_x^*}{\partial x^{*2}} \qquad (4.1.176)$$

From the above equation, the dimensionless velocity parallel to the plate can be written as

$$v_x^* = f(x^*, y^*, Re_L) \qquad (4.1.177)$$

The expression for a friction factor (also termed as drag coefficient), f, from the friction factor definition for external flows (see Equation 4.1.75) can be written as

$$f = \frac{\tau_{yx}|_{y=0}}{\frac{1}{2}\rho V_\infty^2} = \frac{-\mu \frac{\partial v_x}{\partial y}|_{y=0}}{\frac{1}{2}\rho V_\infty^2} = \frac{-2}{Re_L} \frac{\partial v_x^*}{\partial y^*}\bigg|_{y^*=0} \qquad (4.1.178)$$

From the above equation, the friction factor can be interpreted as the dimensionless velocity gradient at the fluid–solid interface. From Equation (4.1.177), it is evident that the friction factor at any location x^* is given by

$$f_{loc} = f(x^*, Re_L)$$

and mean friction factor, f,

$$\bar{f} = f(Re_L)$$

A dimensional analysis (see Section 4.1.9) produces the same results, and therefore the above dimensionless relations are valid for turbulent flows as well.

The above example can be extended to heat transfer by considering the plate being maintained at a constant temperature T_s and the approaching fluid at a uniform temperature of T_∞. The temperature of the fluid adjacent to the plate should be the same as that of the plate, T_s, which is different from the free stream fluid temperature. Note the similarity of this condition to the flow situation arising out of the no-slip condition. Very far away from the plate, along the y direction, the temperature asymptotically approaches the free stream temperature of T_∞. Analogous to the velocity boundary layer, a thermal boundary layer then can be defined as the locus of points where the temperature difference $(T_s - T)$ is 99% of the maximum temperature difference $(T_s - T_\infty)$. The thermal boundary layer depends on both flow and thermal characteristics and can have thickness different from the velocity boundary layer. From Equation (4.1.169), the heat transport equation for the boundary layer can be deduced using the order of magnitude analysis:

$$v_x \frac{\partial T}{\partial x} + v_y \frac{\partial T}{\partial y} = \alpha \frac{\partial^2 T}{\partial x^2} \tag{4.1.179}$$

A dimensionless temperature difference $\theta^* = \frac{T_s - T}{T_s - T_\infty}$ can be defined and the heat transport equation can also be made dimensionless:

$$v_x^* \frac{\partial \theta^*}{\partial x^*} + v_y^* \frac{\partial \theta^*}{\partial y^*} = \frac{1}{Re_L Pr} \frac{\partial^2 \theta^*}{\partial x^{*2}} \tag{4.1.180}$$

Here, Pr is the dimensionless number in honor of Prandtl and is defined as $\frac{v}{\alpha} = \frac{\mu C}{\kappa}$.

The dimensionless temperature profile can be obtained from Equation (4.1.180) using velocities deduced through the velocity boundary layer equation (Equation 4.1.176). The dimensionless temperature difference would be

$$\theta^* = f(x^*, y^*, Re_L, Pr) \tag{4.1.181}$$

The heat transfer at the solid–fluid interface is related to the definition of heat transfer coefficient as

$$-\kappa_f \frac{\partial T}{\partial y}\bigg|_{y=0} = h(T_s - T_\infty) \tag{4.1.182}$$

Here, κ_f is thermal conductivity of the fluid; the subscript f is used to distinguish that from the solid. The above equation is made dimensionless as

$$\left.\frac{\partial \theta^*}{\partial y^*}\right|_{y^*=0} = \frac{hL}{\kappa_f} = Nu_L \tag{4.1.183}$$

The LHS of the above equation denotes the dimensionless temperature gradient at the interface similar to the friction factor denoting the dimensionless velocity gradient at the interface. Thus, this dimensionless temperature gradient, termed as Nusselt Number, Nu, can be used to characterize the heat transfer at the interface for different flow and thermal conditions for a given system.

In fact, when $Pr=1$, boundary layer equations for velocity, heat transfer, and mass transfer become identical. If so, Equations (4.1.178) and (4.1.183) yield,

$$f\frac{Re_L}{2} = Nu \quad \text{or} \quad \frac{f}{2} = \frac{Nu}{Re_L} \tag{4.1.184}$$

The above equation demonstrates the equivalence of friction factor and a corresponding dimensionless number for heat transfer. In other words, knowing the friction factor, the heat transfer coefficient can be estimated from the above equation. This is known as the Reynolds analogy. For Prandtl numbers other than 1, this analogy is further modified as,

$$\frac{f}{2} = St\,Pr^{2/3} = \frac{Nu}{Re\,Pr^{1/3}} \tag{4.1.185}$$

where St is the Stanton number given by $\frac{Nu}{Re \cdot Pr}$. This is known as modified Reynolds analogy or Chilton–Colburn analogy [38].

From the expression for the dimensionless temperature difference given by Equation (4.1.181), the expression for a local Nu_{loc} can be written as

$$Nu_{\text{loc}} = \left.\frac{\partial \theta^*}{\partial y^*}\right|_{y^*=0} = f_{\text{loc}}(x^*, Re_L, Pr) \tag{4.1.186}$$

A mean Nusselt number $(\overline{Nu})$ using mean heat transfer coefficient $(\overline{h})$, hence, can be written as

$$\overline{Nu} = f(Re_L, Pr) \tag{4.1.187}$$

which is obtained by integrating over the entire surface.

For laminar flow, the boundary layer equations can be solved using similarity principles [30] to obtain the velocity boundary layer thickness as well as the friction factor. Flow remains laminar up to a distance from the leading edge where local Reynolds number, defined as $Re_x = \frac{\rho V_\infty x}{\mu}$, remains less than 5×10^5.

$$\delta(x) = \frac{5x}{\sqrt{Re_x}} \tag{4.1.188}$$

$$f_{loc} = \frac{0.664}{\sqrt{Re_x}} \tag{4.1.189}$$

$$\overline{f} = \frac{1.328}{\sqrt{Re_x}} \tag{4.1.190}$$

At distances where Re_x is greater than 5×10^5, transitions to turbulent flow take place. For turbulent flows, the following correlations have been obtained empirically

$$\delta(x) = 0.37xRe_x^{-(1/5)} \tag{4.1.191}$$

$$f_{loc} = 0.0592(Re_x)^{-(1/5)} \tag{4.1.192}$$

$$\overline{f} = 0.074(Re_x)^{-(1/5)} - \frac{1742}{Re_x} \tag{4.1.193}$$

Please note that in case of turbulent flows, the mean friction factor, $\overline{f}$, includes the initial laminar flow region as well.

In general for laminar flows, the thickness of the thermal boundary layer (δ_t) and the velocity boundary layer (δ) are related as

$$\frac{\delta}{\delta_t} \approx Pr^{1/3} \tag{4.1.194}$$

For gases, the Prandtl number is of the order of 1 and consequently the thickness of velocity boundary layer and thermal boundary layers is comparable. For oils, whose viscosities are high and thermal conductivities are low, the Prandtl number is high. Hence, their velocity boundary layers are relatively thicker compared to thermal boundary layer. The converse is true for the liquid metals.

Similar to the friction factor, the correlations for Nu for a flow parallel to an isothermal flat plate are developed either analytically (for laminar flows) or empirically (for turbulent flows) and these are [38]:

For laminar flows

$$Nu_{loc} = 0.332Re_x^{1/2}Pr^{1/3} \quad Re < 5 \times 10^5 \; \overline{Nu}_L = 2Nu_{loc} \quad Pr \gtrsim 0.6 \tag{4.1.195}$$

Liquid metals have relatively low viscosities compared to their thermal diffusivities, i.e., Pr is small

$$Nu_{\text{loc}} = 0.564 Re_x^{1/2} Pr^{1/2} \quad Pr \leq 0.05, \ Re_x \cdot Pr \lesssim 100 \qquad (4.1.196)$$

$$\overline{N}u_x = 2Nu_{\text{loc}} \qquad (4.1.197)$$

For turbulent flows (obtained using Chilton–Colburn analogy)

$$Nu_{\text{loc}} = 0.0296 Re_x^{4/5} Pr^{1/3} \quad 0.6 \lesssim Pr \lesssim 60 \qquad (4.1.198)$$

$$\overline{N}u_x = \left(0.037 Re_x^{4/5} - 871 \right) Pr^{1/3} \quad 0.6 \lesssim Pr \lesssim 60 \qquad (4.1.199)$$

4.1.19.2. Forced Convection: Heat Transfer Coefficient Correlations

For geometrically similar systems, numerous experimental data on heat transfer coefficient with forced convection are correlated using the generic relation $Nu = f(Re, Pr)$. In the following sections, some important correlations relevant for a metallurgical process engineer are presented. Even though these correlations are suitable for engineering calculations, caution needs to be exercised as far as accuracy of these correlations are concerned. Depending on the uncertainties associated with heat transfer experiments, errors as large as 25% are expected. It should be noted that these correlations can be highly sensitive to changes in geometry.

Often correlations are built on some theoretical framework; depending on these, a number of correlations are possible for identical geometric systems. With more sophistication in experimental techniques, existing correlations are often modified with greater accuracy. In the following sections, some popular correlations for selected systems are presented. It is always recommended, however, to refer to recent literature specific to the system under consideration for improved correlations.

Since heat transfer essentially results from temperature variations and materials properties depend on temperature, there is a degree of uncertainty about which representative temperature should be chosen for estimating the properties used in the nondimensionless numbers. Since the correlations are empirical, the procedure followed during the development of the correlation should be adopted. Correlations should therefore prescribe the temperatures at which the material properties need to be evaluated.

4.1.19.3. External Flow

Complex flow patterns such as the boundary layer, its separation, and wake region are developed in external flows, as was discussed earlier. Correspondingly, the local heat transfer also shows complex variations along the surface of an object. These variations in detail can be quite challenging to determine either through experiments or CFD

techniques. Detailed investigations have been carried out especially for simple shapes such as flat plates, long cylinders, and spheres. However, one can make a relatively simpler analysis of these systems by estimating the average heat transfer coefficient using empirical correlations developed specifically for these purposes. These are prescribed below:

4.1.19.3.1 Flow over a Flat Plate
The correlations for laminar flow obtained from the boundary layer analysis were presented earlier in Section 4.1.19.1.

4.1.19.3.2 Flow Across Cylinder
Empirical correlation recommended by Hilpert [45] is one of the most widely used correlations to estimate average heat transfer coefficient for flow around sphere and is given by

$$\overline{Nu}_D = \frac{\overline{h}D}{\kappa_f} = CRe_D^m Pr^{1/3} \quad \text{for } Pr \gtrsim 0.7 \tag{4.1.200}$$

The empirical constants C and m have been tabulated in Table 4.1.5. The fluid properties need to be evaluated at the film temperature, which is the average of the temperature of the approaching fluid, T_∞, and the temperature at the surface of the cylinder, T_s, i.e., $T_f = (T_\infty + T_s)/2$. This correlation has also been extended to cross flow across noncircular cylinders by modifying the values of empirical constants C and m; details can be found elsewhere [38].

Churchill and Bernstien [46] have proposed a single comprehensive correlation for Nusselt number that can be used for the entire range of Re_D as

$$\overline{Nu}_D = 0.3 + \frac{0.62 Re_D^{1/2} Pr^{1/3}}{\left[1 + (0.4/Pr)^{2/3}\right]^{1/4}} \left(1 + \left\{\frac{Re_d}{282,000}\right\}^{5/8}\right)^{4/5} \quad \text{for } Re_D Pr \gtrsim 0.2. \tag{4.1.201}$$

Table 4.1.5 Constants of Equation (4.1.200) to estimate average, $\overline{h}$ for flow across circular cylinder [45]

Re_D	C	m
0.4–4	0.989	0.330
4–40	0.911	0.385
40–4000	0.683	0.466
4000–40,000	0.193	0.618
40,000–400,000	0.027	0.805

The properties are evaluated at the film temperature $T_f = (T_\infty + T_s)/2$.

4.1.19.3.3 Flow Around Sphere

Whitaker recommends the following expression to estimate the average heat transfer coefficient for flow around spheres [47]

$$\overline{Nu_D} = 2 + \left(0.4Re_D^{1/2} + 0.06Re_D^{2/3}\right)Pr^{0.4}\left(\frac{\mu}{\mu_s}\right)^{1/4} \qquad (4.1.202)$$

$$\text{for} \quad 0.71 \leq Pr \lesssim 380;$$
$$3.5 \lesssim Re_D \lesssim 7.6 \times 10^4;$$
$$1.0 \lesssim \frac{\mu}{\mu_s} \leq 3.2$$

Here, all properties are evaluated at the temperature of the approaching fluid, T_∞, except μ_s which is evaluated at T_s.

Ranz and Marshall's [48] correlation for freely falling liquid drops is relatively a simple expression to evaluate heat transfer around particles

$$\overline{Nu_D} = 2 + 0.6Re_D^{1/2}Pr^{1/3} \qquad (4.1.203)$$

It may be noted that in both of these expressions, when $Re_D \to 0$,

$$Nu_D = 2 \qquad (4.1.204)$$

This corresponds to heat transfer by pure conduction from spherical surface to a stationary, infinite medium around the surface.

4.1.19.4. Internal Flow: Flow Through Conduits

In many metallurgical plants, hot flue gases from furnaces flowing through ducts, heat exchangers, and gas–cleaning systems are finally dispersed in the atmosphere through a stack. In order to attain high thermal efficiencies, process gases, blast air, etc., are preheated using heat exchangers such as Cooper stoves and recuperators before feeding them into reactors or furnaces. Large amounts of water are made to flow through channels to achieve cooling in continuous casting, walls of blast furnace and EAF, supersonic nozzle tip in BOF, etc. The extent of heat transfer achieved through such internal flow systems affects the productivity, product quality, and component life. Therefore, heat transfer to/from flowing fluids through conduits is of prime importance.

The definition of a bulk fluid temperature away from the surface is nonobvious in the case of internal flows, since the heat transfer process keeps changing the total heat content as the fluid flows downstream. The definition of the heat transfer coefficient, h, for flow through conduits is therefore modified as follows

$$\dot{q}''(z) = h(T_s(z) - T_m(z)) \qquad (4.1.205)$$

where $\dot{q}''$ is the heat flux from the inner surface of the conduit to the fluid flowing through it, T_s is the inner surface temperature of the conduit, and T_m is the mean temperature of the fluid. Here z stands for the location along the length of the conduit. The expression for the mean temperature T_m is given by

$$T_m(z) = \frac{\int_{A_c} \rho v_z C_p T dA_c}{\dot{m} C_p} \qquad (4.1.206)$$

The mean temperature $T_m(z)$ at an axial location, z, can be physically interpreted as the mean temperature of the fluid collected at the cross section at z. $T_m(z)$ is also referred to as the end mixing temperature.

Consider a simple case of cold fluid flowing through a tube (Figure 4.1.45). By some external means, the wall of the tube is maintained at a constant temperature. Let us consider the case where the temperature at the wall of the pipe is more than that of the mean temperature of the fluid. A schematic of the temperature profile of the fluid as it traverses through the pipe is shown in Figure 4.1.45. If the length of the pipe is much larger than its diameter, the velocity attains a constant profile along the axial direction (fully developed velocity profile, as discussed in Section 4.1.6). The temperature profile, however, changes both along with the radial and axial directions of the pipe. The analogy with the velocity profile is the fact that after some entrance length, the shapes of the profiles become self-similar, and can be scaled to make a constant profile. A dimensionless temperature difference can be defined as follows

$$\theta^* = \frac{T(r,z) - T_s}{T_m(z) - T_s} \qquad (4.1.207)$$
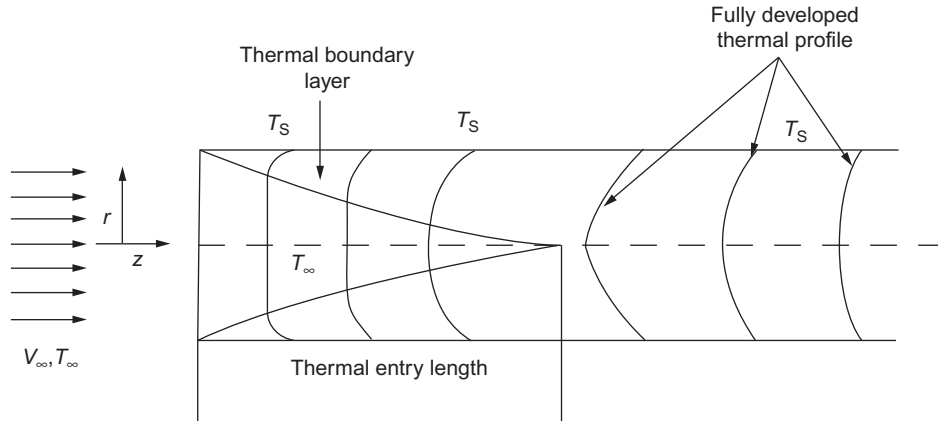
Figure 4.1.45 Schematic temperature profile of a cold fluid flowing through a tube maintained at constant temperature.

where, $T(r, z)$ denotes the temperature of fluid at any location in the pipe, T_s is the temperature at the surface of the pipe, and T_m is the mean temperature of the fluid.

The fluid attains a fully developed temperature profile if the dimensionless temperature, θ^*, becomes independent of z ($\frac{\partial \theta^*}{\partial z} = 0$). It can be proven theoretically that fully developed temperature profiles can be attained for two cases: (1) when the surface temperature of pipe is maintained constant and (2) when a constant heat flux is maintained at the pipe surface. The former case is more common and needs detailed analysis. The latter case is simpler, since rate of heat transfer is constant and specified.

Figure 4.1.46 illustrates the variation of the heat transfer coefficient, h, along the length of a pipe. The local heat transfer coefficient near the entrance decreases with increasing z and attains a constant value once the temperature profile is fully developed. The distance from the entrance to the location where the temperature profile becomes fully developed is termed as the thermal entry length. For laminar flows, the thermal entrance effects would prevail up to a distance z, such that $\frac{z/D}{Re_D Pr} = \frac{1}{Gz_D} \approx 0.05$. Gz_D is the Graetz number [38].

The heat transfer correlation for laminar flow through conduits of circular cross section [49,50] is given by

$$\overline{Nu_D} = \frac{hD}{\kappa_f} = 3.66 + \frac{0.0668 Gz_D}{1 + 0.04 Gz_D^{2/3}} \text{ Laminar flow, } T_s = \text{constant} \qquad (4.1.208)$$

For long pipes $\left(\frac{1}{Gz_D} \gg 0.05\right)$, the second term on the RHS becomes negligible. For laminar flows through conduits other than circular cross sections, readers may refer to the monograph by Shah and London [51].
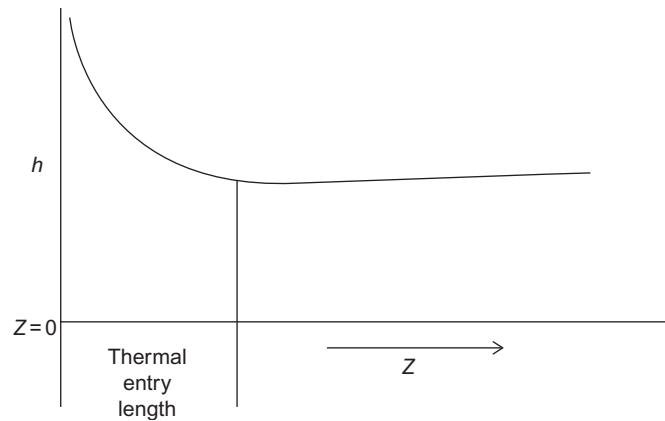
Figure 4.1.46 Schematic temperature profile of a cold fluid flowing through a tube maintained at constant temperature.

Most engineering flows through conduits are turbulent. For fully developed turbulent flow through smooth tubes, the heat transfer coefficient can be estimated using the Dittus–Boelter equation [52]

$$\overline{Nu_D} = \frac{hD}{\kappa_f} = 0.023 Re_D^{4/5} Pr^n \qquad (4.1.209)$$

with $n = 0.4$ for heating $(T_s > T_m)$ and $n = 0.3$ for cooling $(T_s < T_m)$

$$Re_D \gtrsim 10{,}000; \quad 0.6 \lesssim Pr \lesssim 160; \quad \frac{L}{D} \gtrsim 10$$

In the above equation, all the properties need to be evaluated at T_m.

For flows where T_s is significantly different from T_m, the following equation due to Sieder and Tate [53] is recommended

$$\overline{Nu_D} = \frac{hD}{\kappa_f} = 0.023 Re_D^{4/5} Pr^{1/3} \left(\frac{\mu}{\mu_s} \right) \qquad (4.1.210)$$

$$Re_D \gtrsim 10{,}000; \quad 0.7 \lesssim Pr \lesssim 16{,}700; \quad \frac{L}{D} \gtrsim 10$$

In the above equation, all properties except μ_s are evaluated at T_m. μ_s denotes the viscosity at T_s.

Entry lengths for turbulent flow are typically small, $10 \lesssim \frac{z}{D} \lesssim 60$. For long tubes, it is reasonable to assume the average Nusselt number for the entire length. For short tubes, the following equation is recommended

$$\frac{\overline{Nu_{D,\text{short}}}}{\overline{Nu_D}} = 1 + \frac{C}{(z/D)^m} \qquad (4.1.211)$$

The values of C and m depend on the nature of the inlet such as sharp-edged and nozzle. More details on these can be found in Refs. [54,55].

Liquid metals have small Prandtl numbers. Seban and Shimazaki [56] recommend the following correlation

$$Nu_D = 5.0 + 0.025 Pe_D^{0.8} \quad T_s = \text{constant} \quad Pe_D = Re_D Pr \gtrsim 100 \qquad (4.1.212)$$

For turbulent flow through noncircular conduits, the above correlations can be used applying the concept of equivalent diameter or hydraulic radius (see Section 4.1.9.2) with reasonable accuracy.

Knowing the heat transfer coefficient, h, the variation of the mean temperature of a fluid flowing through a conduit with the inner walls of the conduit maintained at a constant temperature, T_s, can be developed performing an overall heat balance. Consider a fluid at $T_{m,\text{in}}$ entering a conduit at a mass flow rate of $\dot{m}$. Considering an infinitesimal length, Δz, and performing a heat balance (as shown in Figure 4.1.47a)
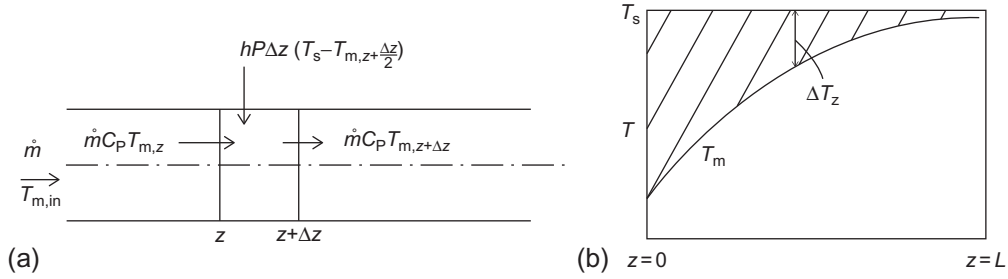
Figure 4.1.47 Heat balance for a fluid flowing through a pipe at constant surface temperature: (a) control volume and (b) schematic temperature profile of the fluid.

$$\dot{m}C_\mathrm{p}\left(T_{\mathrm{m},z} - T_{\mathrm{m},z+\Delta z}\right) + hP\Delta z\left(T_\mathrm{s} - T_{\mathrm{m},z+\Delta z/2}\right) = 0 \qquad (4.1.213)$$

Here, P is the perimeter of the conduit. From the above, the following differential equation can be deduced

$$\dot{m}C_\mathrm{p}\frac{\mathrm{d}T_m}{\mathrm{d}z} = hP\left(T_\mathrm{s} - T_\mathrm{m}\right) \qquad (4.1.214)$$

For a constant h, C_p, and T_s this equation can be integrated for a length of pipe, L of the conduit as

$$\ln\left(\frac{T_\mathrm{s} - T_\mathrm{m}(L)}{T_\mathrm{s} - T_{\mathrm{m,in}}}\right) = -\frac{hP}{\dot{m}C_\mathrm{p}}L \qquad (4.1.215)$$

A schematic of the evolution of the mean temperature is shown in Figure 4.1.47b. Here $\Delta T_z = T_\mathrm{s} - T_{\mathrm{m},z}$ is the temperature difference at location z and is the driving force for the convective heat transfer. As the temperature profile is logarithmic, it is possible to define a logarithmic mean temperature difference (LMTD) given by the shaded area divided by the axial length z. The expression for the LMTD is

$$\Delta T_\mathrm{LM} = \frac{\Delta T_L - \Delta T_{\mathrm{in}}}{\ln(\Delta T_L/\Delta T_{\mathrm{in}})} \qquad (4.1.216)$$

Thus, the heat balance equation can also be written as

$$\dot{m}C_\mathrm{p}\left(T_{\mathrm{m},L} - T_{\mathrm{m,in}}\right) = h(PL)\Delta T_\mathrm{LM} \qquad (4.1.217)$$

Under conditions of varying rates of heat transfer along the axis, it is difficult to maintain a constant surface temperature. In many practical applications, the temperature of the external fluid, which surrounds the pipe, is constant rather than the inner surface temperature of the conduit as illustrated in Figure 4.1.48. Convective heat transfer takes place both externally and internally. In cases where the length of the pipe is much larger than its diameter, the conductive heat transfer through the pipe is predominantly in the direction
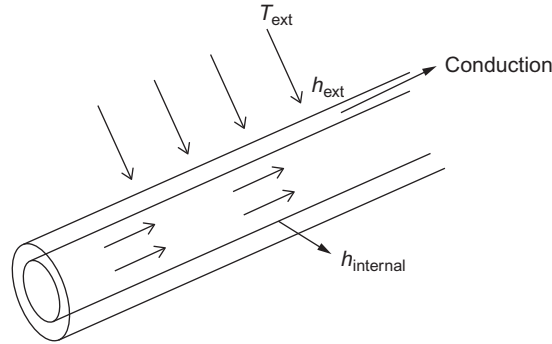
Figure 4.1.48 Schematic showing the heat transfer from a hot/cold fluid flowing through a thick pipe.

normal to the axis of the conduit. The problem therefore becomes that of radial conduction with convective boundary conditions discussed in Section 4.1.18.3. It is possible to define an overall heat transfer coefficient, $h_{overall}$ by considering the internal convective heat transfer, the conduction through the pipe, and the external convective (also radiation if significant) heat transfer. The expression for $h_{overall}$ can be deduced by considering all the heat transfer resistances in series and is given by

$$\frac{1}{A_{external}h_{overall,ext}} = \frac{1}{A_{internal}h_{overall,int}}$$
$$= \frac{1}{A_{internal}h_{internal}} + \text{Conduction resistance} + \frac{1}{A_{external}h_{external}} \quad (4.1.218)$$

The heat transfer rate is given by

$$\dot{Q} = A_{external}h_{overall,ext}\Delta T_{LM} = A_{internal}h_{overall,int}\Delta T_{LM} \quad (4.1.219)$$

where ΔT_{LM} is given by Equation (4.1.217).

Example 4.1.12
In a continuous slab caster, the wide face mold consists of a copper plate of 20 mm thickness and 1.25 m wide (exposed surface), backed by a steel plate, with slots for the water to flow as shown in Figure 4.1.49a. The typical heat flux profile in the mold for different casting speeds is given in Figure 4.1.49b [57]. Design engineers need to determine the minimum velocity needed to maintain a rate of heat transfer such that the cooling water that is in contact with the copper mold (cold face) does not boil, which otherwise can come in the way of heat transfer that could result in mold damage. Consider a casting speed of 1.2 m min^{-1}. The heat transfer coefficients for the slots may be approximated by the use of correlation for tube heat transfers, with appropriate equivalent diameters (hydraulic radius concept). Calculate the minimum velocity of water flow in the mold,
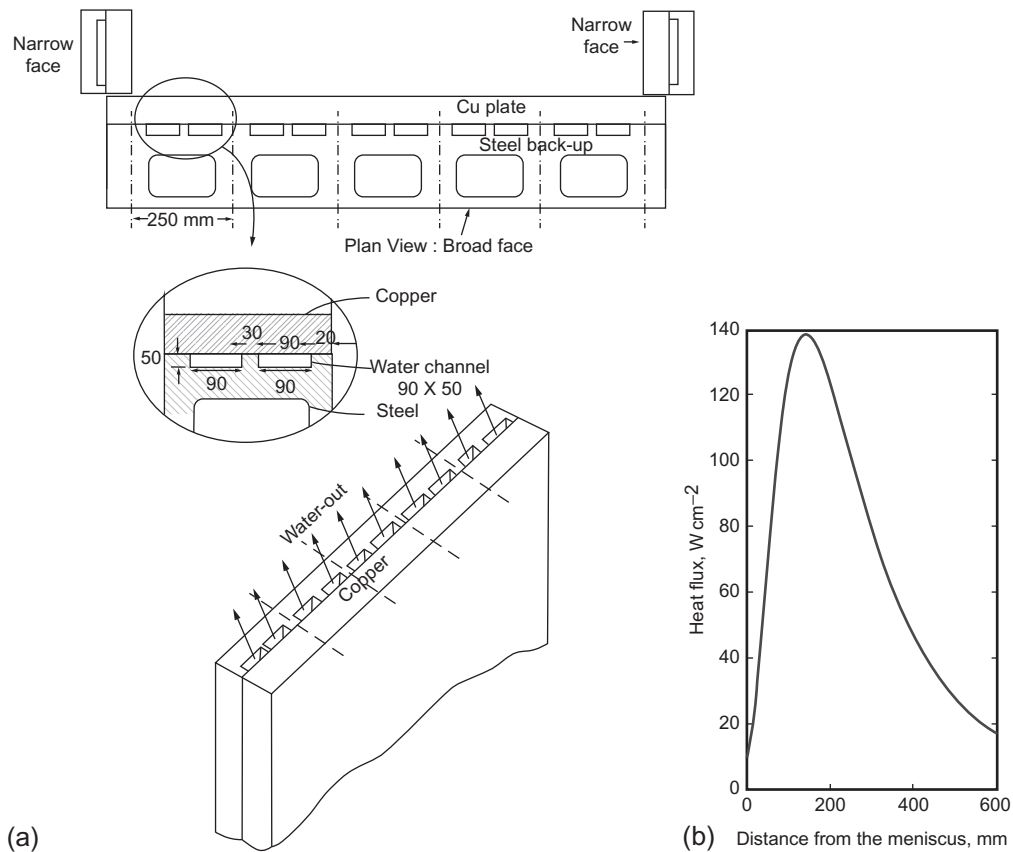
Figure 4.1.49 (a) Schematic of a continuous casting mold with cooling channel and (b) heat flux through a continuous casting mold. (For color version of this figure, the reader is referred to the online version of this chapter.)

so that at no place in the cold surface of copper plate the temperature exceeds $100\ ^{\circ}$C, if the bulk water temperature is $20\ ^{\circ}$C.

Data: water: density $= 950\ \mathrm{kg\ m^{-3}}$, viscosity $= 0.37 \times 10^{-3}\ \mathrm{Pa\ s}$, $C_\mathrm{p} = 4195\ \mathrm{J\ kg^{-1}}$, $\kappa = 0.67\ \mathrm{Wm^{-1}\ K^{-1}}$, and $Pr = 2.29$.

Solution

The heat transfer through the cooling channel needs to be high enough so that the temperature at the hot face (mold face in contact with the liquid/solid steel) is kept well below the melting point of copper. This is maintained through high heat transfer coefficients in the cooling channels. It is to be noted that the slots are in the steel plate and this is in contact with the cold surface of the copper mold. Only some part of the cold face of the copper mold is in contact with the cooling water. The conductive resistance of the steel plate is significantly larger than that of the copper mold; heat flux through the steel plate is neglected.

From the measured heat flux profile given in Figure 4.1.49b,

- Maximum heat flux at the hot face $= 1.40 \times 10^6 \, \mathrm{W m^{-2}}$
- Maximum heat flux in cooling channels $= 1.40 \times 10^6 \times 250/(2 \times 90) = 1.94 \times 10^6 \, \mathrm{W m^{-2}}$ (only part of cold face of the copper mold is in contact with the cooling water)

The minimum heat transfer coefficient, $h_{\min}$, needed for the cooling channel $= 1.94 \times 10^6 \, \mathrm{W m^{-2}} = h_{\min}(100 - 20)$. Here, 100 °C is the boiling of water at a pressure 1 atm.; the cold face of the copper mold needs to be below the boiling point of water to avoid any formation of steam bubbles. The boiling point of water increases with increasing pressure; the static pressure in the channel is kept at a pressure much higher than the atmospheric pressure to keep the surface temperature well below the boiling point.

$h_{\min} = 2.43 \times 10^4 \, \mathrm{W m^{-2} \, K^{-1}}$. Flow rate needed to maintain $h_{\min}$ of $2.43 \times 10^4 \, \mathrm{W m^{-2} \, K^{-1}}$ can be back calculated using correlation for internal flow (Equation 4.1.210)

$$Nu = 0.023 Re_D^{4/5} Pr^{0.4}$$

Equivalent diameter for the cooling channel (see Section 4.1.9.2)

$$D_{\text{equivalent}} = \frac{4A}{P} = \frac{4 \times 90 \times 50}{2 \times (90 + 50)} = 64.3 \, \mathrm{mm}$$

$$Nu = \frac{h_{\min} D_{\text{equivalent}}}{\kappa_f} = \frac{3.038 \times 10^4 \times 64.3 \times 10^{-3}}{0.67} = 2332 = 0.023 Re_D^{4/5} Pr^{0.4}$$

From the above, $Re = \rho v D_{\text{equivalent}} / \mu = 1.19 \times 10^6$, which yields a minimum velocity of $\bar{v} = 7.24 \, \mathrm{m s^{-1}}$.

4.1.19.5. Heat Transfer in Packed Beds

Incropera and Dewitt [38] recommend the following correlation developed based on the modified Reynolds or Chilton–Colburn analogy (see Section 4.1.19.1), for estimating heat transfer coefficients in packed beds

$$\varepsilon \bar{j}_H = St Pr^{2/3} = 2.06 Re_D^{-0.575} \psi \quad \text{for } Pr \approx 0.7 \text{ and } 90 \lesssim Re_D \lesssim 4000 \qquad (4.1.220)$$

where

$$Re_D = \frac{\rho v_0 D_p}{\mu}$$

$$St \, (\text{Stanton number}) = \frac{Nu}{Re_D Pr}$$

$$\psi = \text{Correction factor for particle shape}$$

Here D_p is the particle diameter and V_0 is the superficial velocity. ψ is 0.79 for cylin-drical particles with aspect ratio 1 and 0.71 for cubes. The properties should be evaluated at the arithmetic mean of the fluid inlet and outlet temperatures.

4.1.19.6. Natural Convection or Free Convection

Natural or free convection is one of the common modes of heat transfer that is encoun-tered in many engineering processes. A pipe carrying a hot fluid and a furnace kept in a common plant environment are some typical examples. The surface at the exterior of the pipe or the furnace wall is cooled by the still air in the plant environment. Adjacent to the exterior surface where temperature is different from the surroundings, results in density gradient which due to gravity results in fluid to flow close to the surface. Free convective velocity boundary layer close to vertical hot flat plate is illustrated in the Figure 4.1.50.

As can be readily seen from Figure 4.1.50, the flow characteristic depends on the ori-entation of the surface with respect to the gravitational direction and therefore the heat transfer characteristics also would change depending on the orientation. Unlike forced con-vection, a Reynolds number for free convection cannot be defined as there is no charac-teristic velocity that is known *a priori*. The velocity profile in the boundary layer depends on the variation of density with respect to temperature, decided by a property called volumet-ric thermal expansion coefficient $\beta = -\frac{1}{\rho}\left(\frac{\partial \rho}{\partial T}\right)_P$. For relatively small differences in temper-atures in the boundary layer and in the surrounding fluid, a linear relation can be assumed
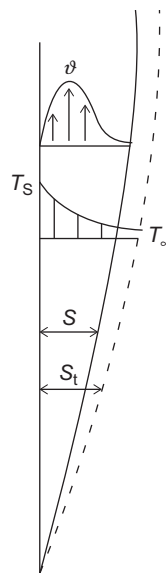
Figure 4.1.50 Schematic of free convective velocity and thermal boundary layer from hot vertical plate.

$$\beta \approx -\frac{1}{\rho}\left(\frac{\Delta\rho}{\Delta T}\right) = -\frac{1}{\rho}\left(\frac{\rho - \rho_\infty}{T - T_\infty}\right) \tag{4.1.221}$$

to yield

$$\rho - \rho_\infty \approx \rho\beta(T - T_\infty) \tag{4.1.222}$$

This simplification is known as the Boussinesq approximation [58]. The driving force for the natural convection is evident in the above equation. The boundary layer analysis presented earlier can be extended for natural convection using the Boussinesq approximation. In this analysis, the Reynolds number is defined using a characteristic velocity v_0. Buoyant force being origin of flow, v_0 is chosen such that $v_0^2 = g\beta(T_s - T_\infty)L$. Then, the Reynolds number becomes $\sqrt{g\beta(T_s - T_\infty)L^3/v^2}$. In place of this Reynolds number, another number called Grashof number, Gr, is defined as the square of the Reynolds number given by

$$Gr_L = \frac{g\beta(T_s - T_\infty)L^3}{v^2} \tag{4.1.223}$$

For free convective flows without any forced convection, the Nusselt number, Nu, will be a function of Gr and Pr, $Nu = f(Gr, Pr)$. Since in most correlations Gr and Pr occur as a product, another number called Rayleigh number, $Ra = GrPr$, is also used in many free convection correlations. In principle, most forced convection flows will have associated free convective flows as well, hence $Nu = f(Re, Gr, Pr)$. However, the forced convection encountered in engineering is generally where $Re_{forcedconvection}$ is much larger than $\sqrt{Gr}$ and contribution due to free convection is often neglected.

4.1.19.6.1 Flat Plates

As mentioned earlier, the correlations for free convective flows around flat plates depend on the orientation of the plate with respect to the gravitational direction.

For vertical plates, Churchill and Chu [59] recommend the correlation,

$$\overline{Nu}_L = \left[0.825 + \frac{0.387 Ra_L^{1/6}}{\left[1 + (0.492/Pr)^{9/16}\right]^{8/27}}\right]^2 \tag{4.1.224}$$

Here L is the length of the plate in the vertical direction. All the properties need to be evaluated at the film temperature, $T_f = (T_s + T_\infty)/2$. This correlation can also be used for vertical cylinders as long as the diameter of the cylinder is much higher than the boundary layer thickness, i.e., $\frac{D}{L} \gtrsim \frac{35}{Gr^{1/4}}$.

For horizontal plates, the characteristic length L is defined as the ratio of surface area to the perimeter, $\frac{A_s}{P}$. The correlations are

Upper surface of hot plate or lower surface of cold plate [60]

$$\overline{Nu}_L = 0.54 Ra_L^{1/4} \quad \text{for} \left(10^4 \lesssim Ra_L \lesssim 10^7, Pr \gtrsim 0.7\right)$$

$$\overline{Nu}_L = 0.15 Ra_L^{1/3} \quad \text{for} \left(10^7 \lesssim Ra_L \lesssim 10^{11}, \text{ for all } Pr\right)$$

Lower surface of hot plate or upper surface of cold plate [61]

$$\overline{Nu}_L = 0.52 Ra_L^{1/5} \quad \text{for} \left(10^4 \lesssim Ra_L \lesssim 10^9, Pr \gtrsim 0.7\right)$$

For inclined surfaces with top and bottom surfaces cold and hot, respectively, the correlation for the vertical surface can be used, except that in calculating Gr, g should be replaced by $g \cos \theta$. Here, θ is the angle the surfaces makes with the vertical. Unfortunately, for an inclined surface with top and bottom surfaces being hot and cold, respectively, the flow has three-dimensionality and no generalized correlation can be recommended [38].

4.1.19.6.2 Cylinders

For horizontal cylinders, Churchill and Chu [62] recommend the correlation

$$\overline{Nu}_D = \left[0.6 + \frac{0.387 Ra_D^{1/6}}{\left[1 + (0.559/Pr)^{9/16}\right]^{8/27}}\right]^2 \quad \text{for } Ra_D \lesssim 10^{12} \qquad (4.1.225)$$

4.1.19.6.3 Spheres

For free convection around spheres, Churchill [63] recommends the following correlation

$$\overline{Nu}_D = 2.0 + \frac{0.589 Ra_D^{1/4}}{\left[1 + (0.469/Pr)^{9/16}\right]^{4/9}} \quad \text{for } Ra_D \lesssim 10^{11}, \; Pr \gtrsim 0.7 \qquad (4.1.226)$$

For other specific systems, readers may refer other sources [38].

4.1.20. RADIATION

Unlike momentum and mass transport, heat can be transported without the presence of a medium as electromagnetic waves or photons; this is termed radiative transport. All materials emit and absorb radiation. For gases and semitransparent materials, this is a volumetric phenomenon. In most solids and liquids, radiation emitted by interior molecules is absorbed by the neighboring molecules; surface emission originates from volume within a distance of approximately 1 μm. Hence, such emission and absorption of radiation can be viewed as surface phenomena. Radiative heat exchange between such opaque surfaces is often encountered in engineering. Additionally, the gaseous medium present between these opaque surfaces may participate in the radiative exchange. In this section, methodologies to estimate the heat exchange between opaque surfaces are discussed in detail. At the end of the section, a brief description of a methodology to estimate radiative exchange in the presence of participating gaseous medium is presented.

4.1.20.1. Definitions

Before, describing these methodologies, some of the important terminologies used to describe radiative exchange need to be defined.
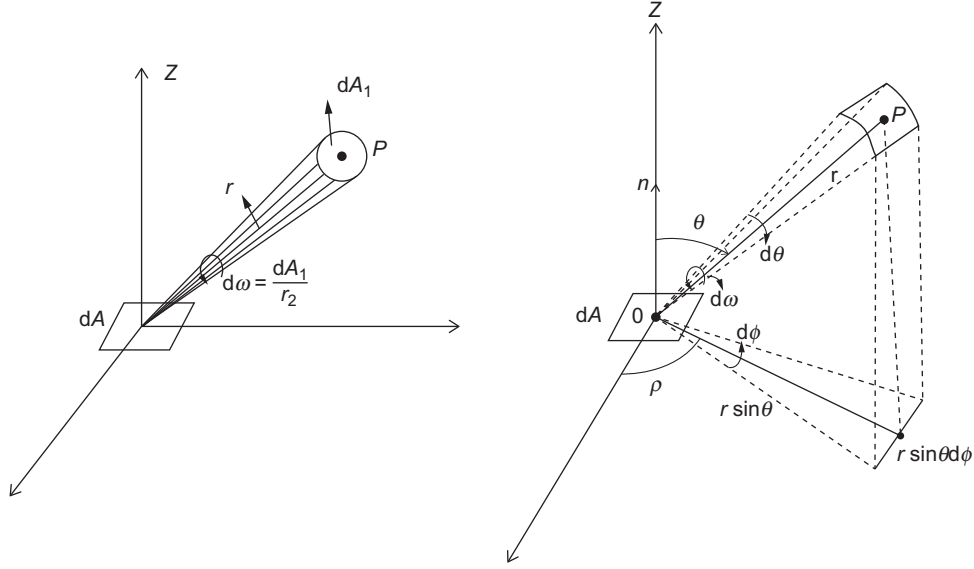
4.1.20.1.1 Radiation Intensity

Radiation originating from a point source travels at the speed of light in all directions. Hence, by its very nature, spherical coordinates are needed to describe radiation. Consider a surface with an infinitesimal area, dA, emitting radiation in a direction θ with respect to the normal, as shown in Figure 4.1.51. In the spherical coordinate system with its origin, O, located at the surface dA and z-coordinate aligned with the normal to the surface, (r,θ,ϕ) denotes the coordinates of a point P. The intensity of radiation at point P, $I_{\lambda,e}$, for the radiation emanating from surface dA at a wavelength, λ, is defined based on the energy that reaches the point P. This is written as

$$d\dot{q}_{\lambda,e} = I_{\lambda,e}(\lambda,\theta,\phi)dA\cos(\theta)\cdot d\omega\cdot d\lambda \qquad (4.1.227)$$

$d\dot{q}_{\lambda,e}$ is the rate of radiative energy that reaches an area dA_1 around point P subtending solid angle $d\omega$ along the direction OP from surface dA having wavelength between λ and $\lambda + d\lambda$. It may be noted that the term $dA\cos\theta$ denotes the component of area dA along the direction OP.

In a nonparticipating medium, the intensity of radiation does not change along its direction of travel; this can be easily comprehended from the concept of solid angle and the fact that radiation travels along straight lines. Further, using spherical coordinates,

Figure 4.1.51 Radiation intensity definition illustrated in spherical coordinate system.

it can be easily shown that $d\omega = \sin(\theta)d\theta\,d\phi$. Thus, the spectral (with respect to wavelength), directional (with respect to θ and ϕ) intensity for emission is defined as

$$I_{\lambda,e}(\lambda,\theta,\phi) = \frac{d\dot{q}_{\lambda,e}}{dA\cos(\theta)\cdot d\omega \cdot d\lambda} \tag{4.1.228}$$

Equation (4.1.228) can be integrated for all the wavelengths from 0 to ∞ to obtain directional intensity, I_e given by

$$I_e(\theta,\phi) = \int_0^\infty I_{\lambda,e}(\lambda,\theta,\phi)d\lambda \tag{4.1.229}$$

If the intensity of radiation emitted is same in all directions, then such a surface is termed as a diffuse emitter, i.e., for a diffuse emitter, $I_e(\theta,\phi)$ is a constant.

4.1.20.1.2 Emissive Power

If all the radiations per unit time per unit area of the emitted by the surface dA in all directions at all wavelengths are accounted for, this yields the emissive power, E of the surface.

$$E = \int_0^{2\pi} \int_0^{\frac{\pi}{2}} \int_0^\infty I_{\lambda,e}(\lambda,\theta,\phi)\cos(\theta)\sin(\theta)d\lambda\,d\theta\,d\phi \tag{4.1.230}$$
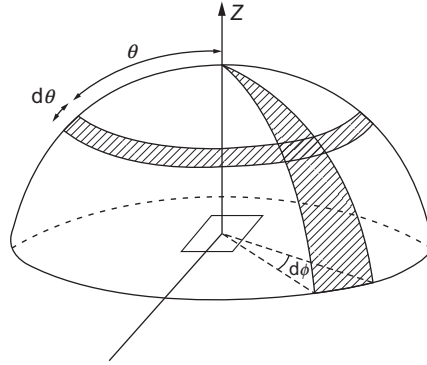
Figure 4.1.52 Illustration of the emissive power of radiant heat source as a function of geometry.

This is illustrated in Figure 4.1.52. Please note that from an opaque surface, the emissions are only in one half of sphere and hence in Equation (4.1.230) the θ varies from 0 to $\frac{\pi}{2}$ (see Figure 4.1.52). For a diffuse emitter, the Equation (4.1.230) yields

$$E = \int_0^{2\pi} \int_0^{\frac{\pi}{2}} I_e \cos(\theta) \sin(\theta) \mathrm{d}\theta \, \mathrm{d}\phi = \pi I_e \tag{4.1.231}$$

4.1.20.1.3 Black Body

A black body is characterized by the following

- It absorbs all the incident radiations at all wavelengths coming from all directions.
- For a given temperature, no surface can emit more energy than a black body at all wavelengths.
- The intensity of radiation from a black body is the same in all directions; in other words a black body is a diffuse emitter.

Planck [64] derived the expression for intensity of emission from a black body as

$$I_{\lambda,T} = \frac{2hc_o^2}{\lambda^5 \left(\exp(hc_o/\lambda k_B T) - 1 \right)} \tag{4.1.232}$$

Integrating the above expression for all wavelengths for all directions, the emissive power, E_b, for black body is given by

$$E_b = \sigma T^4 \tag{4.1.233}$$

where σ is the Stefan–Boltzmann constant, a universal constant whose value is given by 5.67×10^{-8} W m^{-2} K^{-4}. Being a diffuse emitter, the direction intensity, I_b for a black surface would be E_b/π.

It can be proven that radiation inside a closed isothermal cavity or enclosure is that corresponding to a black surface even if the emitting surface is not black owing to infinite multiple reflections. This argument can be extended to show that the radiation from isothermal surroundings falling on a surface can be approximated to that from a black surface at the temperature of the surrounding.

4.1.20.1.4 Irradiation
Definitions described earlier for emission can be extended for incident radiation or irradiation, namely, for spectral, directional intensity of irradiation, $I_{\lambda,i}(\lambda,\theta,\phi)$, directional intensity of irradiation, $I_i(\theta,\phi)$, and total irradiation, G.

If the incident radiation is diffuse, then the intensity of irradiation is the same from all directions and hence $I_i = G/\pi$. A black body would absorb all the incident radiation. When a real surface is irradiated, the radiation may be neglected, absorbed, or transmitted. For opaque bodies, transmission would be zero.

4.1.20.1.5 Emission from Real Surfaces
Radiation emanating from real opaque surfaces consists of two parts: (a) that emitted by the surface by virtue of its temperature (emission) and (b) that from incident radiation reflected by the surface. Similar to E and G, radiosity J is defined as the rate of energy emanating (emitted + reflected) from a unit area of surface. It is to be noted that for a black surface, $J_b = E_b$, as all incident radiations are absorbed by the surface.

Figure 4.1.53 shows a schematic of intensity of radiation, $I_{\lambda,e}$ for a real surface. The intensity of emission from a real surface is always less than that from a black surface. The deviation in intensity of emission for real surfaces from that of black surfaces can vary with wavelength and direction of emission, as illustrated in Figure 4.1.53. In order to characterize the radiations emitted by real surfaces, a term called emissivity, ϵ, is used by comparing its intensity of emission with that from a black surface and is given by

$$\epsilon(\lambda,\theta,\phi,T) = \frac{I_{\lambda,e}(\lambda,\theta,\phi,T)}{I_{\lambda,b}(T)} \qquad (4.1.234)$$
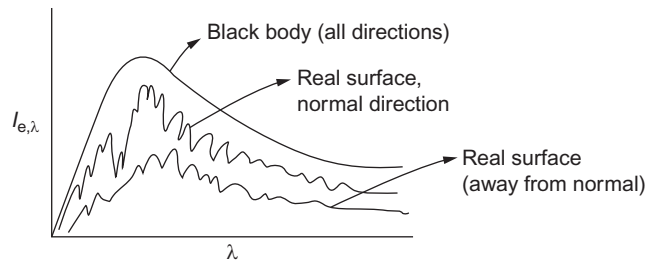

Figure 4.1.53 Illustration of intensity of emission from real surfaces.

By integrating the denominator and numerator for all directions and wavelengths, the total emissivity ϵ is defined as

$$\epsilon(T) = \frac{\int_0^{\frac{\pi}{2}} \int_0^{2\pi} \int_0^{\infty} I_{\lambda,\mathrm{e}}(\lambda,\theta,\phi,T)\sin\theta\cos\theta\,\mathrm{d}\lambda\,\mathrm{d}\phi\,\mathrm{d}\theta}{\pi I_{\lambda,\mathrm{b}}(T)} = \frac{E(T)}{E_{\mathrm{b}}(T)} \tag{4.1.235}$$

Metallic surfaces have low emissivity; highly polished surfaces can reach ϵ as low as 0.02 and in presence of oxide layer emissivity can go beyond 0.6. Emissivities of non-conductors generally exceed 0.6. The emissivity also varies with direction (θ) for both metals and nonconductors. Starting from the normal direction, the emissivity remains almost constant with increasing θ and significant variations occur only when θ reaches close to $\pi/2$ (tangential direction). Hence, for engineering calculations, the total emissivity of real surfaces is approximated as emissivity in the normal direction. Further, as the emissivity remains almost constant with θ, real surfaces can be approximated as diffused emitters for engineering calculations. Real surfaces for which emissivity is independent of both directions and wavelengths are termed as gray surfaces.

4.1.20.1.6 Absorptivity and Reflectivity for Opaque Surfaces

For incident radiations on an opaque surface, a part of the radiation is absorbed and the rest is reflected. The fraction of the incident radiation that is absorbed by the surface is defined as the absorptivity, α, of a surface. Like, emissivity, the absorptivity can be defined for wavelength and direction of the incident radiation and is given by,

$$\alpha_\lambda(\alpha,\theta,\phi) = \frac{I_{\lambda,\mathrm{i,abs}}(\lambda,\theta,\phi)}{I_{\lambda,\mathrm{i}}(\lambda,\theta,\phi)} \tag{4.1.236}$$

Similarly, total absorptivity α is defined as

$$\alpha = \frac{G_{\mathrm{abs}}}{G} \tag{4.1.237}$$

It is to be noted that unlike emissivity, which depends only on the surface and its temperature, absorptivity depends also on the spectral, directional characteristics of incident radiation. Absorptivity of a black surface is 1.

For an opaque surface, the reflectivity $\rho = 1 - \alpha$. Ideally for a smooth surface the reflections are specular (which obeys Snell's law of the angle of incidence being equal to the angle of reflection). Rough surfaces encountered in practical applications reflect diffusely.

4.1.20.1.7 Kirchoff's Law

Emission occurs from a material when transitions of electrons from excited states to ground states occur and are quantized. The reverse transition of electrons from ground

states to excited states occurs during absorption. In others words, emission and absorption are complementary phenomena. The consequence of this is that the spectral directional emissivity and spectral directional absorptivity are equal to each other, i.e.,

$$\epsilon(\lambda,\theta,\phi,T) = \alpha(\lambda,\theta,\phi,T) \qquad (4.1.238)$$

This is not so, however, for the directional absorptivity, $\alpha(\theta,\phi,T)$, and the total absorptivity, α, whose values depend on the spectral directional intensity distribution of the incident radiation. Kirchoff's law states that only under special circumstances is the total emissivity, ϵ, equal to the total absorptivity, α, i.e., $\epsilon = \alpha$. These special conditions are:

- the surface kept in an isothermal enclosure whose temperature is the same as that of the enclosure. This corresponds to irradiation from black body at the same temperature as the surface.
- the surface is diffuse and gray.

For practical applications of estimating the radiation exchange between opaque surfaces, the surfaces are normally approximated as diffuse, gray surfaces, as this allows relatively simple formulation and computation of radiative heat exchange. Caution needs to be exercised as this approximation is reasonable only when the spectral distribution of irradiation and emission are close. In the following section, radiative exchange between diffuse–gray surfaces is presented. For more advanced formulations, the reader may refer elsewhere [65].

## 4.1.20.2. Radiation Exchange Between Opaque–Diffuse–Gray Surfaces

Radiative exchange between any two surfaces depends on the proportion of radiation emanating from one surface that is intercepted by the second one. This depends on the geometrical configuration of the surfaces. For determining the radiation exchange between opaque–diffuse–gray surfaces, it is necessary to define a view factor or a configuration factor.

4.1.20.2.1 View Factor or Configuration Factor

Consider two gray surfaces "i" and "j" having surface areas A_i and A_j, respectively, as shown in Figure 4.1.54. Let $I_{e+r,i}$ be the intensity of emission and radiation from surface "i."

Based on the definition of intensity, the amount of this radiation from surface "i" intercepting surface "j" can be written as

$$\dot{q}_{i \to j} = \int d\dot{q}_{i \to j} = \iint I_{e+r,i} dA_i \cos(\theta_i) d\omega_{j \to i} = \int_{A_j} \int_{A_i} I_{e+r,i} dA_i \cos\theta_i \frac{dA_j \cos\theta_j}{(r_{ij})^2} \qquad (4.1.239)$$
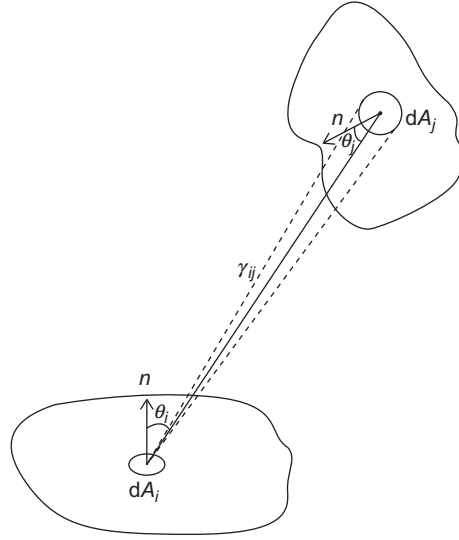
Figure 4.1.54 Illustration for the definition of view factor.

If the radiosity, J_i is uniform throughout the surface "i," then,

$$\dot{q}_{i \to j} = \int_{A_j} \int_{A_i} \frac{J_i}{\pi} dA_i \cos(\theta_i) \frac{dA_j \cos\theta_j}{\left(r_{ij}\right)^2} \tag{4.1.240}$$

Let F_{ij} be the view factor, that is, the fraction of radiations from "i" being intercepted by "j," then,

$$\dot{q}_{i \to j} = A_i J_i F_{ij} = \int_{A_j} \int_{A_i} \frac{J_i}{\pi} dA_i \cos\theta_i \frac{dA_j \cos\theta_j}{r_{ij}^2} \tag{4.1.241}$$

Therefore,

$$F_{ij} = \frac{1}{A_i} \int_{A_j} \int_{A_i} \frac{dA_i \cos\theta_i dA_j \cos\theta_j}{\pi r_{ij}^2} \tag{4.1.242}$$

Conversely, the view factor from $j \to i$, i.e., the fraction of radiation from surface "j" being intercepted by surface "i" is given by

$$F_{ji} = \frac{1}{A_j} \int_{A_j} \int_{A_i} \frac{dA_i \cos\theta_i dA_j \cos\theta_j}{\pi r_{ij}^2} \tag{4.1.243}$$

Therefore,

$$A_i F_{ij} = A_j F_{ji} \tag{4.1.244}$$

This relation is known as the reciprocity relation. From the expression for the view factor, it can be clearly seen that it is a geometrical factor that depends only the configuration of the surfaces. For some of the common configurations encountered engineering, for example, circular discs separated by a distance, two rectangular walls facing each other or at $90°$ angle, two parallel cylinders, cylinder and a flat plate, etc., the view factor has been computed analytically and is available in the form of charts or expressions. A few of these expressions are presented in Table 4.1.6. Readers can find these charts or expressions in books on heat transfer and radiation [38,65]. Radiation from a concave surface will be intercepted by the surface itself, but not for flat or convex surface. Hence for a flat or convex surface, "i," the self view factor $F_{ii} = 0$ and for a concave surface $F_{ii} > 0$. For n number of surfaces, there would be n^2 view factors including the self view factors (F_{ii}). If those n surfaces form an enclosure, then the radiation from a surface "i" will be intercepted completely by all surfaces together. Therefore,

$$\sum_{j=1}^{n} F_{ij} = 1 \qquad\qquad (4.1.245)$$

These relations for each surface will make n relations. The reciprocity relation between any two surfaces will form nC_2 relations. Therefore, $n^2 - n - nC_2 = n(n-1)/2$ view factors need to be calculated directly using the expressions for configuration factors.

Example 4.1.13
Find the view factors corresponding to an annular enclosure formed by two long pipes as illustrated in Figure 4.1.55. The radii of inner and outer cylinders are R_1 and R_2, respectively.
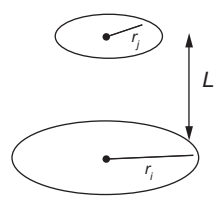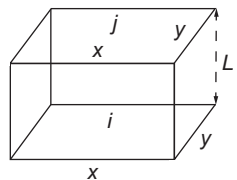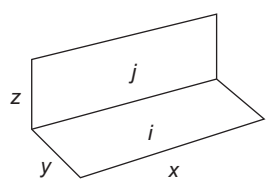
Solution
The exchange is between the outer surface of inner pipe and the inner surface of the outer pipe. As the outer surface of the inner pipe is convex, its self view factor (fraction radiation from the surface being intercepted by the same surface) $F_{11} = 0$. In other words, all the radiation from 1 is intercepted by surface 2, $F_{12} = 1$. Using the reciprocity relation $F_{21} = A_1 F_{12}/A_2 = R_1 F_{12}/R_2 = R_1/R_2$. Therefore, $F_{22} = 1 - F_{21} = R_1/R_2$.

4.1.20.2.2 Heat Balance at an Opaque–Diffuse–Gray Surface
Consider an opaque–diffuse–gray surface, "i" kept at a temperature T_i. This surface exchanges heat with other surfaces through radiation. Thus, in order to maintain the surface "i" at a constant temperature other means such as a heat source (if the surface loses energy by net radiative exchange) or a heat sink (if the surface gains energy by net radiative exchange) need to be adopted. This is schematically shown in Figure 4.1.56.

Table 4.1.6 View Factors for Selected Geometrical Configurations

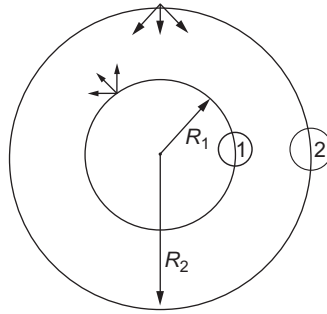| Configuration	View Factor
	$R_i = r_i/L, \quad R_j = r_j/L$ $S = 1 + \dfrac{1 + R_j^2}{R_i^2}$ $F_{ij} = \dfrac{1}{2}\left(S - \left[S^2 - 4\left(r_i/r_j\right)^2\right]^{\frac{1}{2}}\right)$
	$\overline{X} = X/L, \quad \overline{Y} = Y/L$ $F_{ij} = \dfrac{2}{\pi\overline{X}\,\overline{Y}}\left\{ \ln\left[\dfrac{\left(1+\overline{X}^2\right)\left(1+\overline{Y}^2\right)}{1+\overline{X}^2+\overline{Y}^2}\right]^{1/2}\right.$ $+\overline{X}\left(1+\overline{Y}^2\right)^{1/2}\tan^{-1}\dfrac{\overline{X}}{\left(1+\overline{Y}^2\right)^{1/2}}$ $+\overline{Y}\left(1+\overline{X}^2\right)^{1/2}\tan^{-1}\dfrac{\overline{Y}}{\left(1+\overline{X}^2\right)^{1/2}}$ $\left. -\overline{X}\tan^{-1}\overline{X} - \overline{Y}\tan^{-1}\overline{Y}\right\}$
	$H = Z/X, \quad W = Y/X$ $F_{ij} = \dfrac{1}{\pi W}\left\{ W\tan^{-1}\dfrac{1}{W} + H\tan^{-1}\dfrac{1}{H}\right.$ $-\left(H^2+W^2\right)^{1/2}\tan^{-1}\dfrac{1}{\left(H^2+W^2\right)^{1/2}}$ $\dfrac{1}{4}\ln\left[\dfrac{(1+W^2)(1+H^2)}{1+W^2+H^2}\right.$ $\left(\dfrac{W^2(1+W^2+H^2)}{(1+W^2)(W^2+H^2)}\right)^{W^2}$ $\left.\left. \times\left(\dfrac{H^2(1+W^2+H^2)}{(1+H^2)(W^2+H^2)}\right)^{H^2}\right]\right\}$

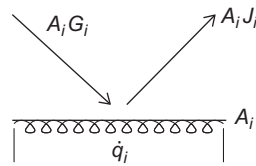**Figure 4.1.55** View factor for an annular enclosure.

Figure 4.1.56 Heat balance at an opaque surface for radiative exchange.

If G_i denotes the uniform irradiation the surface "i" receives and J_i the uniform radiosity, then balancing the net energy yields

$$\dot{q}_i + A_i G_i = A_i J_i \qquad (4.1.246)$$

Radiosity being the sum of emission and reflection and for an opaque–diffuse–gray surface, $\epsilon = \alpha$, it can be written

$$J_i = (1 - \alpha) G_i + E_i = (1 - \epsilon_i) G_i + \varepsilon_i E_{b,i} \qquad (4.1.247)$$

Here, $E_{b,i}$ is emissive power of a black surface at the temperature corresponding to surface "i" (T_i). Substituting this in Equation (4.1.246) yields

$$\dot{q}_i = \frac{E_{b,i} - J_i}{(1 - \epsilon_i)/\epsilon_i A_i} \qquad (4.1.248)$$

If the surface is black, $\varepsilon_i = 1$. Since, $\dot{q}_i$ is not zero, $E_{b,i} = J_i$. This is as expected, since a black surface does not reflect any incident radiation. Equation (4.1.248) can be interpreted as an electrical analogue, where there is a resistance R_s at a gray surface: $R_s = (1 - \varepsilon_i)/(\varepsilon_i A_i)$.

4.1.20.2.3 Radiation Exchange at a Surface in an Enclosure Consisting of Opaque–Diffuse–Gray Surfaces

Consider an enclosure formed by opaque–diffuse–gray surfaces as illustrated in Figure 4.1.57. Each of these surfaces is isothermal having a distinct temperature. Consider one such opaque–diffuse–gray surface, "i" at temperature T_i. Let us determine the total
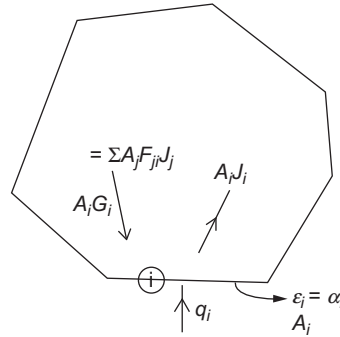
Figure 4.1.57 Illustration of heat balance in an enclosure formed by opaque–diffuse–gray surfaces.

irradiation reaching the surface "i"; this consists of the summation of the emitted and reflected radiations from all the surfaces forming the enclosure. This can be written as

$$A_i G_i = \sum_{j=1}^{n} A_j F_{ji} J_j = \sum_{j=1}^{n} A_i F_{ij} J_j \quad \text{(Reciprocity relation)} \tag{4.1.249}$$

Combining Equations (4.1.246) and (4.1.249), the radiation exchange at an opaque–diffuse–gray surface, "i" for the enclosure shown in Figure 4.1.57 can be written as

$$\dot{q}_i = A_i J_i - A_i G_i = A_i J_i - \sum_{j=1}^{n} A_i F_{ij} J_j = \sum_{j=1}^{n} A_i F_{ij} \left(J_i - J_j \right) \tag{4.1.250}$$

Equations (4.1.248) and (4.1.250) can be written for each surface resulting in $2n$ equations for an enclosure formed by n opaque–diffuse–gray surfaces. These equations can be represented using the electrical analogue as follows

$$\dot{q}_i = \frac{E_{b,i} - J_i}{(1 - \varepsilon_i)/\varepsilon_i A_i} = \frac{E_{b,i} - J_i}{R_{s,i}}$$

$$\dot{q}_i = \sum_{j=1}^{n} \frac{J_i - J_j}{\left(A_i F_{ij} \right)^{-1}} = \sum_{j=1}^{n} \frac{J_i - J_j}{R_{ij}}$$

Here $\dot{q}_i$ is equivalent to the current and E_b and J represent the potentials. $R_{s,i}$ can be denoted as surface resistance and R_{ij} as view factor resistance. A pictorial representation of the electrical analogue for any surface "i" is shown in Figure 4.1.58.

If a surface is adiabatic or completely insulated from the other side (no heat sink or heat source), then $\dot{q}$ for the surface is zero. All the irradiations on to this surface are radiated back to the enclosure through emission and reflection. Such surfaces are referred to as re-radiating surfaces.

Example 4.1.14

250-tonnes ladle has inner diameter of 3.4 m and depth of 4.0 m. It is filled with 250 tonnes of liquid steel at 1800 K. The thickness of the slag layer over the liquid
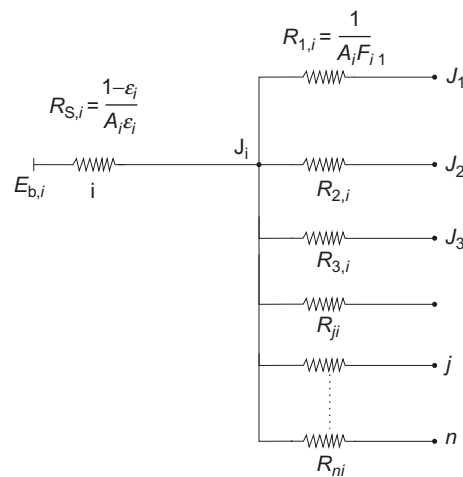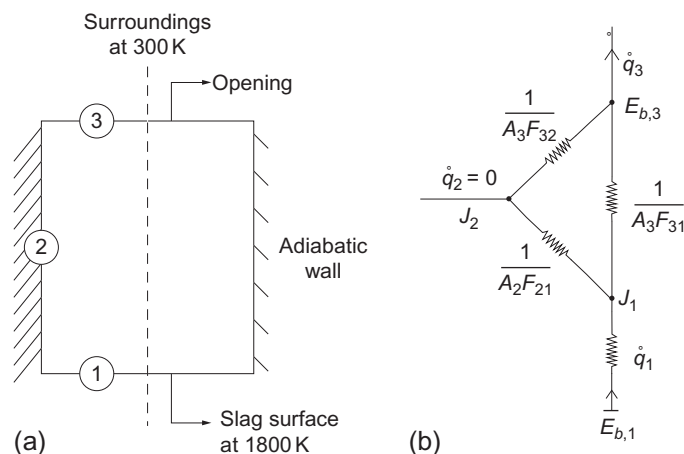
Figure 4.1.58 Electrical analogue for radiation exchange.

steel can be neglected. The free board at the top of the ladle is 0.5 m in height. The emissivity of the slag layer is 0.8. Assuming the walls to be adiabatic, estimate the radiative heat loss from the open ladle. The temperature of the surroundings is 300 K.

Solution

The radiative heat transfer from the top of the slag surface is illustrated in Figure 4.1.59a. The slag layer is denoted by 1 (diffuse–gray surface), the side walls by 2 (re-radiating surface), and the opening by surface 3 (black surface).

The electrical analogue depicting the radiative heat transfer is shown in Figure 4.1.59b. Net heat flow from surface 2, $\dot{q}_2$, is zero as it is a re-radiating surface.

Figure 4.1.59 Radiation loss from a ladle: (a) illustration of the radiation enclosure and (b) electrical analogue.

The net heat flow can be written as

$$\dot{q}_1 = -\dot{q}_3 = \frac{E_{b,1} - E_{b,3}}{(1-\epsilon_1)/(A_1\epsilon) + ([1/A_1F_{12} + 1/A_3F_{32}]||1/A_1F_{13})}$$

The view factor, F_{13}, is 0.764 (using the expression for view factor for two coaxial circular discs facing each other in Table 4.1.6). Hence, $F_{12} = 1 - F_{13} = 0.236$. Therefore,

$$\dot{q}_1 = -\dot{q}_3 = \frac{\sigma 1800^4 - \sigma 300^4}{0.0275 + ([0.4667 + 0.4667]||0.1442)} = \frac{\sigma 1800^4 - \sigma 300^4}{0.1524} = 3.903\,\text{MW}$$

This corresponds to a drop in temperature at a rate of $1.13\ \text{K}\ \text{min}^{-1}$. In addition to this, there would be conduction losses through the walls of the ladle.

In the above treatment of enclosures, each surface was considered to be isothermal. In large furnaces, the surface temperatures can vary along the surface of a wall or a component. In such cases, both the wall surfaces and component surfaces can be divided into a number of subsurfaces having distinct temperatures. This would result in a large number of simultaneous equations to be solved to determine the radiative heat transfer. For such cases, J_is can be eliminated from Equations (4.1.246) and (4.1.249) to obtain equations in terms of qs and E_bs alone. In all these problems, either the q or E_b would be unknown for each surface and hence the following equation can be accordingly rearranged for the unknowns to compute the radiative exchange and temperatures.

$$\frac{\dot{q}_i}{A_i\epsilon_i} - \sum_{j=1}^{n}\frac{1-\epsilon_j}{\epsilon_j}F_{ij}\frac{\dot{q}_j}{A_j} = \sum_{j=1}^{n}F_{ij}\left(E_{b,i} - E_{b,j}\right) \quad \text{for } i = 1\ldots n \qquad (4.1.251)$$

Conductive losses through the walls can also be incorporated as current sinks, and heat inputs as current sources.

4.1.20.3. Gas Radiation

Nonpolar gases such as N_2 and O_2 do not emit thermal radiations and are transparent to thermal radiations. However, polar molecules especially CO_2 and H_2O present in combustion products on the other hand can emit and absorb radiation. Unlike condensed phases wherein the radiation spectra are continuous, for gases the spectra are banded; the emission and absorption take place over specific wavelength intervals. Additionally, gaseous radiation is a volumetric phenomenon.

The absorption and radiation for a gaseous medium is defined through a linear absorption coefficient, k_g, as

$$dI_\lambda = -k_g I_\lambda\, ds \qquad (4.1.252)$$

where dI_λ is the change in intensity of radiation as it travels a distance of ds through a gas medium. Thus, integrating this expression along the direction $\vec{s}$,

$$I_\lambda(s) = I_{\lambda,s=0} \exp\left(-k_g s\right) \tag{4.1.253}$$

The spectral directional absorptivity of a gas is defined as

$$\alpha_{\lambda,g} = \frac{\text{Radiation absorbed}}{\text{Incident radiation}} = \frac{\left(I_{\lambda,s=0} - I_{\lambda,s=0} \exp\left(-k_g s\right)\right)}{I_{\lambda,s=0}} = 1 - \exp\left(-k_g s\right) \tag{4.1.254}$$

The directional, spectral emissivity, $\epsilon_{\lambda,g}$, of a gas is defined by comparing the emission to that from a black surface. For the reasons mentioned earlier (Kirchoff's law), the spectral direction absorptivity, $\alpha_{\lambda,g}$ of a gas is equal to the spectral directional emissivity, $\epsilon_{\lambda,g}$. Please note that both these definitions are for a radiation traveling along a direction, $\vec{s}$, for a distance traveled $\left|\vec{s}\right|$.

In order to determine the radiation exchange in a system where volume of gas and opaque surfaces are involved, a radiation energy balance needs to be performed for all the directions. This would result in complex integro-differential equations [65] that need sophisticated numerical techniques to solve and are also computationally very expensive. Instead, relatively easier but approximate methodologies have been developed. In this section, the simplest approach proposed by Hottel and Sarofim [66], which can be used for engineering calculation with reasonable accuracy, is presented. For more sophisticated methods, readers may refer other sources [65].

Analogous to the total emissivity for a surface, Hottel and Sarofim [66] defined emissivity from a gas temperature T_g contained in a hemisphere of radius L to a surface element located at the center of hemispherical base (see Figure 4.1.60).

$$\epsilon_g(L) = \frac{\int_{\text{hemisphere}} \int_0^\infty \epsilon_{\lambda,g}(L) I_{\lambda,b}\left(T_g\right) d\lambda \, dA \cos(\theta) d\omega}{\int_{\text{hemisphere}} \int_0^\infty I_{\lambda,b}\left(T_g\right) d\lambda \, dA \cos(\theta) d\omega} \tag{4.1.255}$$

$$\epsilon_g(L) = \frac{\int_{\text{hemisphere}} \int_0^\infty \epsilon_{\lambda,g}(L) I_{\lambda,b}\left(T_g\right) d\lambda \cos(\theta) d\omega}{\sigma T^4}$$
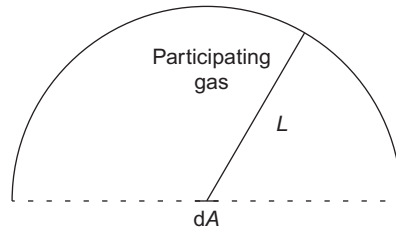

Figure 4.1.60 Illustration for defining total emissivity/absorptivity for a gaseous medium.

In other words, emission from a gas at temperature T_g contained in a hemisphere of radius L to a surface having unit area placed at the base of the hemisphere is $\epsilon_g \sigma T_g^4$. ϵ_g is a function of gas temperature T_g, total pressure p, the partial pressure p of the participating species, and the radius of the hemisphere L.

The emissivities in the form of charts were first proposed by Hottel and Sarofim [66] and later were refined by Leckner [67]. Modest [65] recommends the following empirical expression by Leckner to estimate the total emissivities for H_2O and CO_2.

$$\epsilon_0 \left(p_a L (\text{bar cm}), p = 1\,\text{bar}, T_g(\text{K}) \right) = \exp \left[\sum_{i=0}^{M} \sum_{j=0}^{N} C_{ji} \left(\frac{T_g}{1000} \right)^j \left(\log_{10} (p_a L) \right)^i \right]$$

(4.1.256)

Here ϵ_0 is the emissivity for the limiting case when partial pressure of the absorbing species (H_2O, CO_2) goes to zero. The emissivities at other pressures and partial pressure of absorbing species are then found from

$$\frac{\epsilon \left(p_a L, p, T_g \right)}{\epsilon_0 \left(p_a L, 1\,\text{bar}, T_g \right)} = 1 - \frac{(a-1)(1-P_E)}{a+b-1+P_E} \exp \left(- \left[\log_{10} \frac{(p_a L)_m}{p_a L} \right]^2 \right)$$

(4.1.257)

The empirical parameters for the above two equations for H_2O and CO_2 are tabulated in Tables 4.1.7 and 4.1.8.

In a gas where both H_2O and CO_2 are present, additionally a correction factor needs to be introduced, as the radiation bands of these two gases partially overlap. These corrections are given as

$$\epsilon_{CO_2 + H_2O} = \epsilon_{CO_2} + \epsilon_{H_2O} - \Delta\epsilon \left(p_{H_2O} L,\ p_{CO_2} L \right)$$

(4.1.258)

$$\Delta\epsilon \left(p_{H_2O} L,\ p_{CO_2} L \right) = \left\{ \frac{x_{H_2O}}{10.7 + 101 x_{H_2O}} 0.0089 x_{H_2O}^1 0.4 \right\} \left(\log_{10} \left(\left(p_{H_2O} + p_{CO_2} \right) L \right) \right)^{2.76}$$

where x_{H_2O} is the mole fraction of water vapor in the gas.

The total absorptivity α_g is equal to the total emissivity ϵ_g for a given temperature T_g. In real systems, the source of radiation can be at temperature T_s and gas may be at another temperature T_g; the absorptivity depends on both the temperature of the radiating source T_s as well as the temperature of the gas T_g.

The absorptivity of gases at temperature T_g from gray surface at temperature T_s can be calculated from

$$\alpha \left(p_i, L, p, T_g, T_s \right) = \left(\frac{T_g}{T_s} \right)^{1/2} \epsilon \left(p_i, L, \frac{T_s}{T_g}, p, T_s \right)$$

(4.1.259)

Table 4.1.7 Correlation constants for the determination of the total emissivity for water vapor using equations (4.1.256) and (4.1.257)

M,N			2,2		
C_{00}	C_{01}	C_{02}	−2.2118	−1.1987	0.035596
C_{10}	C_{11}	$C_{12}4$	0.85667	0.93048	−0.14391
C_{20}	C_{21}	C_{22}	−0.10838	−0.17156	0.045915
P_{E}			$\left(p+2.56p_{\mathrm{a}}/\sqrt{T_{\mathrm{g}}/1000}\right)$		
$(p_{\mathrm{a}}L)_{\mathrm{m}}$			$13.2(T_{\mathrm{g}}/T)^2$		
a			$2.144\left(T_{\mathrm{g}}<750\right)$ $1.888-2.053\log_{10}\left(T_{\mathrm{g}}/1000\right),\;\;T_{\mathrm{g}}>750$		
b			$1.10/(T_{\mathrm{g}}/100)^{1.4}$		
c			0.5		

Table 4.1.8 Correlation constants for the determination of the total emissivity for CO_2 using equations (4.1.256) and (4.1.257)

M,N				2,3			
C_{00}	C_{01}	C_{02}	C_{03}	−3.9893	2.7669	−2.1081	0.39163
C_{10}	C_{11}	$C_{12}4$	C_{13}	1.2710	−1.090	1.0195	−0.21897
C_{20}	C_{21}	C_{22}	C_{23}	−0.23678	0.19731	−0.19544	0.044644
P_{E}				$(p+0.28p_{\mathrm{a}})$			
$(p_{\mathrm{a}}L)_{\mathrm{m}}$				$0.054/\left(T_{\mathrm{g}}/T\right)^2,\;\;T_{\mathrm{g}}<700$ $0.225\left(T_{\mathrm{g}}/T\right)^2,\;\;T_{\mathrm{g}}>700$			
a				$1.0+0.1/(T_{\mathrm{g}}/1000)^{1.45}$			
b				0.23			
c				1.47			

Emissivities and absorptivities of gas mass of shapes other than hemispheres are extended using a concept of mean beam length, L_{e}, where L_{e} is the equivalent radius of the hemispherical gas mass whose emissivity or absorptivity is the same as that of the gas mass of interest. The mean beam lengths for various gas geometries are given in Table 4.1.9.

The radiation heat rate from a gas mass to an adjoining surface of area A

$$\dot{q}=A\epsilon_{\mathrm{g}}\sigma T_{\mathrm{g}}^4 \tag{4.1.260}$$

Table 4.1.9 Mean beam lengths, L_e, for various gas geometries [38]

Geometry	Characteristic Length	L_e
Sphere (radiation to the surface)	Diameter (D)	0.65 D
Infinite circular cylinder (radiation to the curved surface)	Diameter (D)	0.95 D
Semi–infinite circular cylinder (radiation to base)	Diameter (D)	0.65 D
Circular cylinder of equal height and diameter (radiation to entire surface)	Diameter (D)	0.60 D
Infinite parallel planes (radiation to planes)	Spacing between planes (L)	1.80 L
Cube (radiation to any surface)	Side (L)	0.66 L
Arbitrary shape of volume V (radiation to surface area A)	V/A	3.6 V/A

4.1.21. MASS TRANSFER

Engineering materials, more often than not, are multiphase materials; each phase is a solution of many chemical constituents present as different atomic, molecular, or ionic species. Properties of materials depend on size, shape, and distribution of phases, as well as composition of chemical constituents and their distribution in each phase. Process metallurgists aim at designing processes to achieve desired distributions of phases in terms of size and shape, as well as the constitution of each phase, so that materials with desired properties can be produced consistently. Hence, understanding transport of chemical constituents within a phase and across different phases is of great importance for a process engineer. The subject of mass transport addresses the transport of chemical constituents within a phase as well as across phases. Often associated with these transports of chemical constituents are chemical reactions and phase transitions. Thus, for analyzing engineering processes, a knowledge of the principles of chemical kinetics and phase transformations is needed, together with the principles of mass transport. In this section, the primary focus is on the transport of chemical constituents. A separate section with a focus on chemical kinetics is presented at the end of this chapter.

Sugar added to a cup of tea is a common example of mass transfer. The dissolution of sugar in tea can be enhanced by stirring the tea with a spoon. The time for dissolution also depends on the size and shape of the sugar crystals being added. Deoxidation of liquid steel using aluminum is an example from steel making. In this process, the added solid aluminum melts and dissolves in the steel bath and is then distributed in the bath. The dissolved aluminum chemically reacts with the dissolved oxygen in steel to produce billions of nonmetallic alumina particles as a second phase. The efficiency of the

deoxidization process depends on ensuring proper delivery of aluminum by maintaining adequate flow in the bath by Ar purging, and on controlling the temperature of the bath, metal, and slag chemistry. The mechanism of sugar dissolution or aluminum being distributed in the liquid occurs through both bulk flow of the fluid (advection) as well as molecular interactions (diffusion). These mechanisms are similar to the mechanisms of heat and momentum transfer discussed earlier. However, the diffusive mass transfer is in one aspect distinct from diffusive heat and momentum transport. This arises from the fact that different chemical species travel at different velocities. These differences in velocities of chemical species can result in a net bulk flow, even in the absence of any mechanical driving force.

The driving force for diffusive transport of chemical species arises from difference in thermodynamic chemical potential. Therefore, anything that can bring about a change in chemical potential can result in mass transfer driving the system toward equilibrium. Differences in concentration of species are the obvious source of potential difference leading to what is termed as ordinary diffusion. Driving forces can also be due to differences in pressure (pressure diffusion), temperature (thermal diffusion), electric field in case of ions (forced diffusion), etc. This section deals with only the ordinary diffusion—that which is driven by concentration differences.

### 4.1.21.1. Fick's Law of Diffusion

As the mechanism of diffusive transport of mass is similar to that of heat, the rate equation of mass transport is also similar to that of Fourier's law of conduction. The rate equation, known as Fick's law, is stated for a binary solution containing species "A" and "B" as

$$j_A = \rho \mathbb{D}_{AB} \nabla m_A \tag{4.1.261}$$

or

$$J_A^* = -C\mathbb{D}_{AB}\nabla x_A \tag{4.1.262}$$

Here, j_A is the mass flux in kg s^{-1} m^{-2}, ρ is density, and m_A is the mass fraction of species "A" in the solution. $\mathbb{D}_{AB}$ is the phenomenological constant, analogous to thermal conductivity, and is called the binary diffusion coefficient. The law can be also written in terms of molar transport where J_A^* is molar flux, C denotes the molar density or total molar concentration, and x_A denotes the mole fraction of "A" in the binary solution. The value of $\mathbb{D}_{AB}$, with the units of m^2 s^{-1}, is the same in both the equations. Unlike conduction, however, mass diffusion often involves simultaneous transport of two or more species in a solution. Fluxes of each species can be different in a solution. This can lead to seemingly paradoxical situations, unless Equations (4.1.261) and (4.1.262) are interpreted correctly.
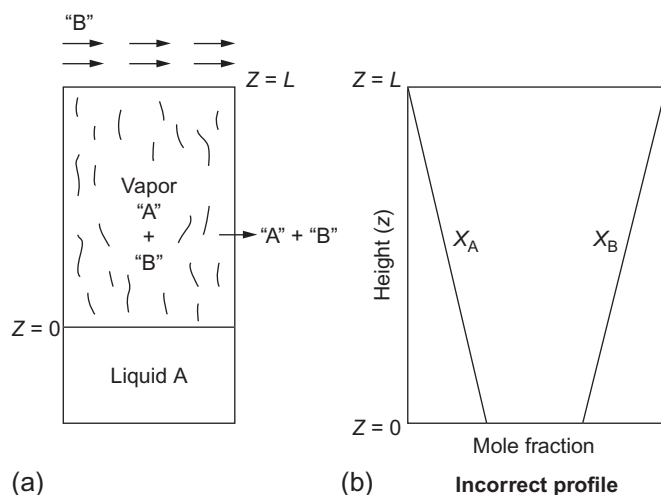
Figure 4.1.61 Stefan experiment on evaporation through a gas column: (a) experimental set up and (b) incorrect composition profile.

An experiment on evaporation of a liquid and the consequent diffusion of the vapor through a seemingly stagnant gas, referred to as Stefan's experiment [5], elucidates the above observation.

Consider a jar containing a liquid "A" up to a height $z=0$ as shown in Figure 4.1.61a. The top of the jar is open; a pure gas "B" flows across the entrance, so that any vapor of species A reaching the top is swept away, so that the concentration of "A" at the top ($z=L$) remains close to zero. Evaporation of "A" is slow, and the level of the liquid is kept at $z=0$ (say by connecting it to a larger reservoir). The liquid would evaporate, and the vapor would diffuse through the "apparently" stagnant gas column of B to escape at the top. Since the pressure everywhere is the same as the atmospheric pressure and the gas mixture is ideal, the total molar concentration of gas in the column is constant. The concentration of "A" at $z=0$ is near saturation value, and is zero at $z=L$, leading to a gradient in x_A as shown in Figure 4.1.61b. Since $x_A + x_B = 1$ (or $C_A + C_B = C = \frac{P}{RT}$), there is an inverse gradient in x_B.

Equation (4.1.262) would indicate that there is an inward flux of "B." But if "B" is insoluble in the liquid, this is impossible! Hence the contradiction. A careful examination of the physical situation would reveal that there is a nonzero flux of "A" outward, and a stagnant "B," leading to a net molar flux of gas outward. A careful measurement with a Pitot tube should reveal an outward velocity of gas, however small. Molecular diffusion, as given by Equations (4.1.261) and (4.1.262), should be interpreted as the fluxes relative

---

[5] This experiment is named after famous Slovene physicist, mathematician, and poet, Joseph Stefan, who conducted a large number of experiments on evaporation.

to this gas mixture moving at this net velocity. In this experiment described above, the species "B" does not have a net inward flow with respect to the stationary coordinates.

Let us denote the molar flux of "A" and "B" with respect to the stationary frame of reference (in this case the tube) as N_A'' and N_B'', respectively. Since the flux is equal to velocity times concentration, then

$$N_A'' = C x_A v_A \quad \text{and} \quad N_B'' = C x_B v_B$$

Then the average velocity of the gas mixture or simply the mixture velocity would be

$$C v^* = C x_A v_A + C x_B v_B = \left(N_A'' + N_B'' \right)$$
$$v^* = \left(N_A'' + N_B'' \right) / C$$

The molar fluxes with respect to the frame moving with the mixture velocity can then be written as

$$J_A^* = C x_A \left(v_A - v^* \right) \quad \text{and} \quad J_B^* = C x_B \left(v_B - v^* \right)$$

Thus Fick's law can be applied to the fluxes in this frame of reference to give

$$J_A^* = C x_A \left(v_A - v^* \right) = - C \mathbb{D}_{AB} \nabla x_A \qquad (4.1.263)$$

Please note that in the frame moving with the mixture velocity, the flux of species "A" and "B" should be equal and opposite, i.e., $J_A^* + J_B^* = 0$. In a binary mixture, $x_A + x_B = 1$, therefore, $\mathbb{D}_{BA} = \mathbb{D}_{AB}$.

In terms of molar fluxes N_A'' and N_B'', the above equation can be written as

$$N_A'' - x_A \left(N_A'' + N_B'' \right) = - C \mathbb{D}_{AB} \nabla x_A \qquad (4.1.264)$$

or

$$N_A'' = - C \mathbb{D}_{AB} \nabla x_A + x_A \left(N_A'' + N_B'' \right)$$

In a similar way, Fick's law can also be defined in terms of mass flux instead of molar flux as

$$j_A = \rho m_A \left(v_A - v \right) = - \rho \mathbb{D}_{AB} \nabla m_A$$

where

$$v = m_A v_A + m_B v_B = \left(n_A'' + n_B'' \right) / \rho$$

and hence

$$n_A'' = \rho \mathbb{D}_{AB} \nabla m_A + x_A \left(n_A'' + n_B'' \right) \qquad (4.1.265)$$

Equations (4.1.264) and (4.1.265) are the general equations of binary diffusion with respect to stationary coordinates. The second term on the RHS is often determined by

the physical situation. Let us revisit the Stefan experiment with these formulations. Since "B" is insoluble in liquid "A," $N_B'' = 0$. Applying this to Equation (4.1.264)

$$N_A'' = -C\mathbb{D}_{AB}\nabla x_A + x_A N_B''$$
$$(1 - x_A)N_A'' = -C\mathbb{D}_{AB}\frac{dx_A}{dz}$$
$$N_A'' = -C\mathbb{D}_{AB}\frac{1}{1 - x_A}\frac{dx_A}{dz}$$

At steady state $\frac{dN_A''}{dz} = 0$ (the molar flux $N_A'' = $ constant).

$$\frac{d}{dz}\left(C\mathbb{D}_{AB}\frac{1}{1 - x_A}\frac{dx_A}{dz}\right) = 0$$

The differential equation can be solved using boundary conditions at $z = 0$ and $z = L$. At $z = 0$, i.e., the liquid–gas interface, thermodynamic equilibrium can be assumed. Let us denote the equilibrium mole fraction at the interface as x_A^0.

At $z = L$, the composition of gas is imposed externally and let it be denoted as x_A^L. For example, if pure gas "B" is flowing at flow rates much larger than the evaporation rate, x_A^L can be taken to be zero.

Using the above two boundary conditions, the solution would be

$$\frac{1 - x_A}{1 - x_A^0} = \left(\frac{1 - x_A^L}{1 - x_A^0}\right)^{z/L} \tag{4.1.266}$$

$$N_A'' = \frac{C\mathbb{D}_{AB}}{L}\ln\left(\frac{1 - x_A^L}{1 - x_A^0}\right) \tag{4.1.267}$$

The variation of the mole fraction along the gas column as illustrated in Figure 4.1.62b is nonlinear. Please note that in the frame moving with mixture velocity (v^*), the flux, J_B^* has to be equal and opposite to the flux J_A^*. Hence on the stationary frame, the flux, N_B'' is given by

$$N_B'' = -C\mathbb{D}_{AB}\nabla x_B + x_B\left(N_A'' + N_B''\right)$$
$$= C\mathbb{D}_{AB}\nabla x_A + x_B\left(N_A'' + N_B''\right)$$
$$N_B''(1 - x_B) = C\mathbb{D}_{AB}\nabla x_A + (1 - x_A)N_A'' = 0$$

An example of stagnant layer diffusive mass transfer is the evaporation of zinc from hot galvanized sheets in stagnant air.

A similar effect, of the overall flux on the flux of individual species, manifests itself as the "Kirkendall effect" in diffusion of substitutional elements in solid solutions. One may observe the overall flux as leading to marker movements in diffusion couples, or as leading to generation of pores. In view of the structure of solids, however, the phenomenon is treated differently for solids.
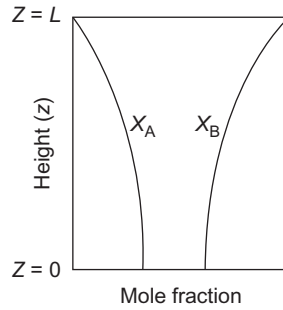
Figure 4.1.62 Stefan experiment on evaporation through a gas column: composition profile.

4.1.21.2. Binary Diffusivities

The mass diffusivities, $\mathbb{D}_{AB}$, for binary gas mixtures are functions of temperature and pressure. These can be estimated, especially for nonpolar gases using the kinetic theory of gases. Bird *et al.* [1] recommend the following correlations based on Lennard Jones parameters:

$$\mathbb{D}_{AB} = 1.8583 \times 10^{-7} \frac{\sqrt{T^3 \left(\frac{1}{M_A} + \frac{1}{M_B}\right)}}{p\sigma_{AB}^2 \Omega_{\mathbb{D}_{AB}}} \tag{4.1.268}$$

where $\mathbb{D}_{AB}$ is in $m^2 \, s^{-1}$, T is temperature in K, M_A and M_B are molecular weights of gas species A and B, p is pressure in atm., and σ_{AB} and $\Omega_{\mathbb{D}_{AB}}$ are the Lennard Jones parameters. For determining the Lennard Jones parameters, please refer to Ref. [1].

As the structure of liquids and solids are complex, there are no generic correlations available to estimate the binary diffusivities at present; experimental data for specific systems are the most reliable source. Unlike gases, the diffusivities in liquids and solids increase with increasing temperature; in general, these are found to be thermally activated processes and hence can be represented using Arrhenius-type relations.

4.1.21.3. Multicomponent Diffusion

Multicomponent diffusion in ideal gases is described by Stefan–Maxwell equations [1]

$$\nabla x_i = \sum_{j=1}^{n} \frac{1}{C\mathbb{D}_{ij}} \left(x_i N_j'' - x_j N_i''\right) \tag{4.1.269}$$

For a binary system, this equation will simplify to Equation (4.1.264). For a multicomponent solution, analogous relations can be written as

$$N_j'' = -C\mathbb{D}_i\nabla x_i + x_i\sum_{j=1}^{n} N_j'' \tag{4.1.270}$$

where $\mathbb{D}_i$ is the diffusivity of species "i" in the multicomponent solution. From the above equations, the multicomponent diffusivity $\mathbb{D}_{im}$ can be related to the binary diffusivities as

$$\frac{1}{C\mathbb{D}_i} = \frac{\sum_{j=1}^{n}\left(1/C\mathbb{D}_{ij}\right)\left(x_i N_j'' - x_j N_i''\right)}{N_i'' - x_i\sum_{j=1}^{n} N_j''} \tag{4.1.271}$$

Please note that $\mathbb{D}_i$ is dependent on position as it changes with composition. Special cases can be deduced for which the expression for $\mathbb{D}_i$ becomes simple: For dilute solutions $(x_2, x_3, \ldots, x_n \rightarrow 0)$ in solvent $(x_1 \rightarrow 1)$:

$$\mathbb{D}_i = \mathbb{D}_{i1} \tag{4.1.272}$$

If all binary diffusivities are same ($\mathbb{D}_{ij}$s are same):

$$\mathbb{D}_i = \mathbb{D}_{ij} \tag{4.1.273}$$

For systems wherein species 2,3,...,n move with the same velocity or for a stationary system $\left(\sum_{j=1}^{n} N_j'' = 0\right)$:

$$\frac{1 - x_1}{C\mathbb{D}_1} = \sum_{j=2}^{n} \frac{x_i}{D_{1j}} \tag{4.1.274}$$

In systems where $\mathbb{D}_i$ varies significantly, a linear variation approximation with composition has given satisfactory results [1].

4.1.21.4. Diffusion Equation for Stationary Media: Steady and Transient

In dilute systems, where the solute concentrations are significantly small, the bulk flow arising out of diffusive mass transfer can be considered insignificant. Additionally, systems wherein the net sum of the fluxes of species is zero $\left(\sum_{j=1}^{n} N_j'' = 0\right)$, for example, equi-molar counter current diffusion of CO and CO_2 through a porous product layer during the reduction of a solid metal oxide to metal, the medium is stationary. In such cases, the Equation (4.1.270) reduces to

$$N_i'' = -C\mathbb{D}_i\nabla x_i \tag{4.1.275}$$

This equation is analogous to the heat conduction equation, Equation (4.1.134). The molar conservation of species "i" in a stationary medium can be written as

$$C\frac{\partial x_i}{\partial t} = -\nabla\cdot N_i'' + \dot{G}_i''' \tag{4.1.276}$$

where $\dot{G}_i'''$ is the rate of generation of species "i" (in mol m^{-3} s^{-1}) that can occur through chemical reactions and nuclear processes. Substituting the diffusion equation into the conservation equation:

$$C\frac{x_i}{t} = C\nabla\cdot(\mathbb{D}_i\nabla x_i) + G_i''' \tag{4.1.277}$$

1D transient diffusion equations without a generation term in Cartesian, cylindrical, and spherical coordinates are

$$\frac{\partial x_i}{\partial t} = \frac{\partial}{\partial z}\left(\mathbb{D}_i\frac{\partial x_i}{\partial z}\right) \tag{4.1.278}$$

$$\frac{\partial x_i}{\partial t} = \frac{1}{r}\frac{\partial}{\partial r}\left(r\mathbb{D}_i\frac{\partial x_i}{\partial r}\right) \tag{4.1.279}$$

$$\frac{\partial x_i}{\partial t} = \frac{1}{r^2}\frac{\partial}{\partial r}\left(r^2\mathbb{D}_i\frac{\partial x_i}{\partial r}\right) \tag{4.1.280}$$

Equation (4.1.276) is analogous to the general conduction equation, Equation (4.1.138). Hence, the solutions for diffusion problems in stationary media are analogous to those in conduction problems.

For example, steady diffusion of a species "i" through a cylindrical wall, with no species generation is governed by

$$\frac{1}{r}\frac{\partial}{\partial r}\left(r\mathbb{D}_i\frac{\partial x_i}{\partial r}\right) = 0$$

with the boundary conditions:at $r=r_1, x_i=x_i^1$ and at $r=r_2, x_i=x_i^2$. The solution is

$$N_i = \frac{C\left(x_i^1 - x_i^2\right)}{\left(\ln(r_2/r_1)/(2\pi L\mathbb{D}_i)\right)}$$

Similarly, the transient diffusion through a semi-infinite wall with a constant $\mathbb{D}_i$ is analogous with Equation (4.1.164) governed by:

$$C\frac{\partial x}{\partial t} = C\mathbb{D}_i\frac{\partial^2 x_i}{\partial z^2}; \quad t>0; 0<z<\infty;$$

Initial condition at $(t=0, 0<=z<=\infty)x_i = x_i^0$
Boundary condition 1 at $(t>0, z=0)x_i = x_i^s$
Boundary condition 2 at $(t>0, z\to\infty)x_i = x_i^0$

The concentration profiles are given by (see Equation 4.1.165)

$$\frac{x_i(z,t) - x_i^s}{x_i^0 - x_i^s} = \text{erf}\left(\frac{z}{2\sqrt{\mathbb{D}t}}\right) \tag{4.1.281}$$

Other cases of transient diffusion through plane walls, cylindrical rods, and spheres can be similarly dealt with as given in Table 4.1.10.

When the overall molar concentration C is relatively constant, the diffusion equation can be written in terms of concentrations. For example, for 1D diffusion, one can write the flux as:
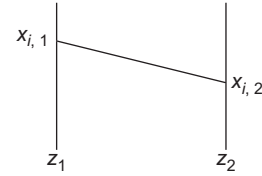
$$N_{i,x}'' = -\mathbb{D}_i\frac{\partial C_i}{\partial x} + x_i\sum_{j=1}^{n} N''_{j,x} \tag{4.1.282}$$

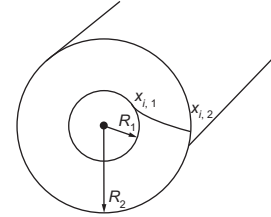In process metallurgy literature, this is the form in which the diffusion equation is often used.

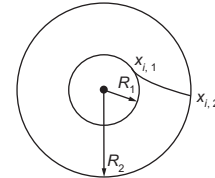**Table 4.1.10** Concentration profiles for 1D diffusion: stationary media

Steady state

$N_i = AN_i'' = \dfrac{C\left(x_i^1 - x_i^2\right)}{(z_2 - z_1)/\mathbb{D}_iA}$ (Planar)

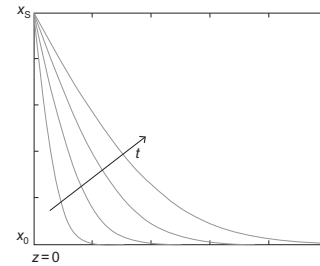$N_i = \dfrac{C\left(x_i^1 - x_i^2\right)}{\dfrac{\ln(R_2/R_1)}{2\pi L\mathbb{D}_i}}$ (Cylindrical)

$N_i = \dfrac{C\left(x_i^1 - x_i^2\right)}{\dfrac{(1/R_1 - 1/R_2)}{4\pi\mathbb{D}_i}}$ (Spherical)

Transient semi-infinite

$\dfrac{x_i(z,t) - x_i^s}{x_i^0 - x_i^s} = \text{erf}\left(\dfrac{z}{2\sqrt{\mathbb{D}_it}}\right)$

$N_i''(z=0) = \dfrac{C\mathbb{D}_i\left(x_i^s - x_i^0\right)}{\sqrt{\pi\mathbb{D}_it}}$ (Planar)

4.1.21.5. Convective Mass Transfer

Convective mass transfer refers to transfer of a species, with respect to a solution of two or more species, in a flowing fluid. As in the case of heat transfer (Section 4.1.19), a species can be transported due to the movement of the fluid particle itself (advection) in addition to diffusion due to a concentration gradient. There are again, as in heat transfer, two situations of engineering interest:

– Concentration variations within a flowing fluid body, as in distributing alloying elements within a steel bath held in a ladle with argon stirring.
– Rate of transfer of species to/from an interface across which a fluid, containing the species of interest, is flowing, as in the case of the transfer of sulfur from the slag/metal interface to the bulk of the slag.

Rigorous treatment of both cases needs solutions of convective transport equations, along with the equations to describe fluid flow. The generalized convective species transport equation can be deduced from the diffusion equation by replacing the partial time derivative with a substantial or total derivative (Lagrangian in place of Eulerian view point)

$$\frac{DC_i}{Dt} = \frac{C_i}{t} + \overrightarrow{v} \cdot \nabla C_i = \nabla \cdot (\mathbb{D}_i \nabla C_i) + \dot{G}_i''' \qquad (4.1.283)$$

This equation is analogous to Equation (4.1.169) for convective heat transfer. Application to complex systems needs computational techniques to be adopted.

Interface mass transfer is in general handled through correlations as was done in the case of heat transfer. One defines a mass transfer coefficient as:

$$N_i''|_s = Ck_{m,i}(x_i^s - x_i^{bulk}) \quad \text{or} \quad N_i''|_s = k_{m,i}(C_i^s - C_i^{bulk}) \qquad (4.1.284)$$

where N'' is the molar flux and x_i^s and x_i^{bulk} are the mole fraction of species "i" at the interface and that in the bulk away from the interface. C_i's are the corresponding molar concentrations.

The mass transfer coefficient is nondimensionalized into the Sherwood number:

$$Sh = \frac{k_{m,i}L}{\mathbb{D}_i} \qquad (4.1.285)$$

where L is the characteristic dimension for the system. The Sherwood number is analogous to the Nusselt number (some authors use the term Nu_m in place of Sh).

By dimensional analysis it can be shown that the Sherwood number is a function of Reynolds number, and the Schmidt number defined as

$$Sc = \frac{\mu/\rho}{\mathbb{D}_i} = \frac{v}{\mathbb{D}_i} \qquad (4.1.286)$$

Schmidt number is the ratio of momentum diffusion to mass diffusion and is analogous to Prandtl number, $Pr = \frac{v}{\alpha}$.

The Chilton–Colburn analogy given in Equation (4.1.185) can be extended to mass transfer:

$$\frac{f}{2} = \frac{Nu}{Re \cdot Sc} Sc^{2/3} = \frac{Sh}{Re\, Sc^{1/3}} \qquad (4.1.287)$$

The Chilton–Colburn analogy holds for many geometrically simple systems, especially between heat and mass transfer. For example, for flow of a fluid past a sphere, where mass transfer of a species takes place between the fluid and the sphere surfaces, the simple correlation commonly used is

$$\overline{Sh}_D = 2.0 + 0.6 Re_D^{1/2} Sc^{1/3} \quad \text{(see Equation 4.1.204)} \qquad (4.1.288)$$

Note that correlations developed specifically for mass transfer should be preferred over those obtained using the analogy given in Equation (4.1.287). Detailed discussion on the empirical correlations for various situations is beyond the scope of this chapter, and readers may refer to books on mass transfer.

The following example of reaction of a porous solid with a gaseous species elucidates several of the concepts presented above.

Example 4.1.15
Topochemical Model for Gas–Solid Reaction

Consider a reducing gas, say a mixture of H_2 and H_2O, reacting with a spherical pellet of NiO (Figure 4.1.63a). Once the solid oxide at the surface is reduced, reaction can only proceed if H_2 diffuses into the pellet and the product H_2O diffuses out. Alternatively O
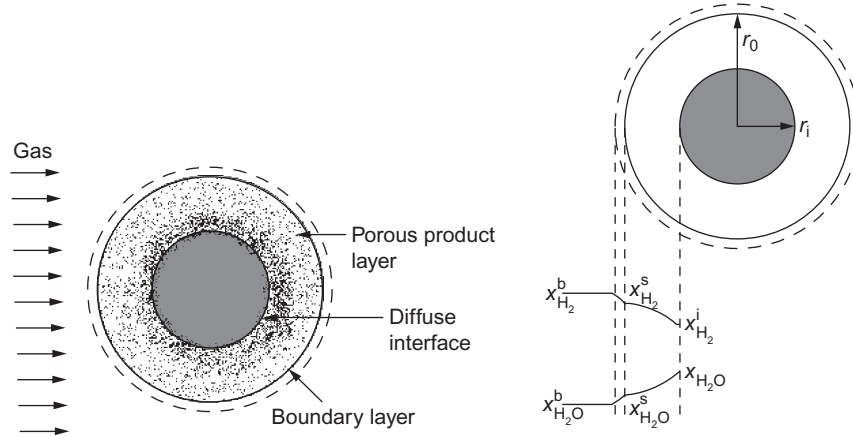
Figure 4.1.63 Gas–solid reaction in a spherical pellet. (a) General schematic showing a diffuse reaction interface and (b) schematic showing a sharp interface for the topochemical model.

has to diffuse out through the solid, which is extremely slow. Solid state diffusion of H_2/H_2O through solid product Ni is also extremely slow. If the initial pellet itself, or at least the product Ni, is porous, diffusion can take place through the gas in the pores, since gas phase diffusion coefficients are several orders of magnitude higher than those in the solid phase.

In porous pellets, therefore, reaction can proceed inside the pellet at reasonable rates. At any spherical cross section inside the pellet, H_2 arriving by diffusion from outside is partly consumed by the reduction reaction. The remaining hydrogen can diffuse further in. The reaction at any instant of time, in general, would be taking place over a diffuse region (Figure 4.1.63a).

Under certain conditions, the region of reaction can be thin enough to be approximated as being a sharp interface. This would happen primarily in either or both of the following conditions: (1) The starting oxide pellet is dense, i.e., the porosity is very low, and the product layer that forms is comparatively porous. The rate of diffusion through the unreacted core of the particle would then be negligibly low compared to that of the diffusion in the outer product layer and the chemical reaction. (2) The chemical reaction at the interphase is extremely fast compared to pore diffusion. The gas arriving at the interface by diffusion through the product layer is almost entirely consumed in a thin interface layer, leaving little H_2 to diffuse further in.

Under these conditions, one can approximate the interface layer to be a sharp surface, with a radius, r_i, which is continuously shrinking (Figure 4.1.63b). Various reaction models can be constructed to describe this process. A comparatively simple is the shrinking core model or the topochemical model. The model assumes that there is no overall change in the radius r_o of the pellet as the reaction proceeds, and the chemical reaction is of first order but reversible. This is described below.

There are five different rate processes that need to take place in series for the reaction to continue:

(1) Diffusion of H_2 from bulk gas to the pellet surface at $r = r_o$ by convective mass transfer.

(2) Diffusion of H_2 from the pellet surface at $r = r_o$ to the reaction interface at $r = r_i$.

(3) Chemical reaction at the interface: $NiO(s) + H_2(g) = Ni(s) + H_2O(g)$.

(4) Diffusion of H_2O from the reaction interface at $r = r_i$ to the pellet surface at $r = r_o$.

(5) Diffusion of H_2O from the pellet surface to the bulk gas by convective mass transfer.

The overall rate of reaction will be decided by the rates of the above steps. The process, as such, is in an unsteady state, since the interface radius r_i is continuously decreasing. The rate equations can, however, be written for each of the steps under the pseudosteady–state approximation: the rate of change of r_i is very slow and therefore each of the processes is very close to steady state that would be obtained for any given r_i.

Then the rate of reaction for a pellet at any instant of time is given by (refer to Figure 4.1.63c)

$$N_{H_2} = \left(4 \cdot \pi \cdot r_o^2\right) \cdot k_{m,H_2} \cdot C \cdot \left(x_{H_2}^b - x_{H_2}^s\right) \quad \text{(step a)}$$

$$= \frac{C \cdot \left(x_{H_2}^s - x_{H_2}^i\right)}{\dfrac{1/r_i - 1/r_o}{4 \cdot \pi \cdot \mathbb{D}_{H_2,\,\text{eff}}}} \quad \text{(step b)}$$

$$= \left(4 \cdot \pi \cdot r_i^2\right) \cdot k_r \cdot C \cdot \left(x_{H_2}^i - x_{H_2O}^i / K_{eq}\right) \quad \text{(step c)}$$

$$= \frac{C \cdot \left(x_{H_2O}^i - x_{H_2O}^s\right)}{\dfrac{1/r_i - 1/r_o}{4 \cdot \pi \cdot \mathbb{D}_{H_2O,\,\text{eff}}}} \quad \text{(step d)}$$

$$= \left(4 \cdot \pi \cdot r_o^2\right) \cdot k_{m,H_2O} \cdot C \cdot \left(x_{H_2O}^s - x_{H_2O}^b\right) \quad \text{(step e)}$$

In the above, C is the total molar concentration ($= P_{\text{total}}/RT$), k_{m,H_2} and k_{m,H_2O} are convective mass transfer coefficients, k_r is the chemical reaction rate constant, and K_{eq} is the equilibrium constant for the reaction. $\mathbb{D}_{H_2,\,\text{eff}}$ and $\mathbb{D}_{H_2O,\,\text{eff}}$ are effective diffusivities in the porous product considering the product to be a homogeneous phase. Since the entire cross section of the pellet is not available for gaseous diffusion, and the path that hydrogen has to follow is tortuous, $\mathbb{D}_{i,\,\text{eff}}$ is less than the $\mathbb{D}_i$ defined for the homogeneous gas phase. $\mathbb{D}_{i,\,\text{eff}}$ is normally calculated as $\mathbb{D}_i \cdot \epsilon / \tau$, where ϵ is the porosity (<1) and τ is the tortuosity (>1).

Note that the pore diffusion as well as the gas phase mass transfer is equimolar counter diffusion, since 1 mol of H_2 generates 1 mol of H_2O. Further if the gas is a binary mixture, $\mathbb{D}_{H_2} = \mathbb{D}_{H_2O}$ and $k_{m,H_2} = k_{m,H_2O}$.

From the above series of equations, the intermediate mole fractions can be eliminated to give the instantaneous rates in terms of the bulk gas composition, which is measurable:

$$\text{Rate} = N_{H_2} = -N_{H_2O} = \frac{\left(C\left(x_{H_2}^b - x_{H_2O}^b / K_{eq}\right)\right)}{\left(\dfrac{1}{4 \cdot \pi \cdot r_o^2 \cdot k_{m,H_2}} \cdot \left(1 + \dfrac{1}{K_{eq}}\right) + \dfrac{1/r_i - 1/r_o}{4 \cdot \pi \cdot \mathbb{D}_{H_2,\,\text{eff}}} \cdot \left(1 + \dfrac{1}{K_{eq}}\right) + \dfrac{1}{4 \cdot \pi \cdot r_i^2 \cdot k_r}\right)} \quad (4.1.289)$$

The mass transfer coefficients are estimated from correlations for flow past a sphere, or flow through a packed bed, etc., as the case may be.

The reduction rate any instant can be related to the rate of change of the interface radius:

$$\text{Rate} = 4 \cdot \pi \cdot r_i^2 \cdot \frac{\partial r_i}{\partial t} \left(\rho_{\text{NiO,molar}}\right) \quad (4.1.290)$$

where $\rho_{\text{NiO,molar}}$ is the apparent molar density of nickel oxide in the original pellet. Equation (4.1.289) when combined with Equation (4.1.290) is a first-order differential equation for r_i, with the initial condition: at $t = 0$, $r_i = r_o$, and can be numerically integrated. At any instant of time, the extent of reaction $F(t)$ is given by:

$$F(t) = 1 - \left(\frac{r_i}{r_o}\right)^3$$

Kinetics of reduction of porous oxide particles is important in several metallurgical processes. In the iron blast furnace, for example, hematite, Fe_2O_3, particles charged at the top of the furnace get reduced to magnetite, Fe_3O_4, and then to wustite, Fe_xO, in the upper part of the furnace. In the middle region, the wustite particles further get reduced to metallic iron, all in solid state. The latter reaction is often treated in a manner similar to what is described in the above example. In the top region on the other hand, the two reactions, hematite-to-magnetite and magnetite-to-wustite, may take place simultaneously inside each pellet, resulting in two reaction fronts one inside the other. This would need more sophisticated treatment. Further, the temperatures of the pellets, and the gas surrounding them, change continuously as they descend in the furnace. A mathematical model describing the processes in the entire furnace, therefore, needs to combine the single pellet reduction rate equation (in differential form) with the overall enthalpy, mass, and species balance equations for complete description.

REFERENCES

[1] R. Bird, W. Stewart, E. Lightfoot, Transport Phenomena, John Wiley & Sons, New York, 1960.
[2] H. Struchtrup, Macroscopic Transport Equations for Gas Flows Approximate Methods in Kinetic Theory, first ed., Springer, Germany, 2005.
[3] O. Reynolds, Philos. Trans. R. Soc. Lond. A 174 (1883) 935.
[4] O. Reynolds, Philos. Trans. R. Soc. Lond. A 186 (1894) 123.
[5] R.I.L. Guthrie, Engineering in Process Metallurgy, Oxford University Press, USA, 1992.
[6] ISO Technical Committee ISP/TC30, I.O. of Standards (ISO 5167-1), Measurement of fluid flow by means of pressure differential devices part 1: orifice plates, nozzles, and venturi tubes inserted in circular cross-section conduits running full, ISO, Geneva, 2003.
[7] C.W. Macosko, Rheology: Principles, Measurements, and Applications (Advances in Interfacial Engineering), first ed., Wiley-VCH, USA, 1994.
[8] S.P. Sutera, R. Skalak, Annu. Rev. Fluid Mech. 25 (1993) 1.
[9] R. Perry, D. Green, Chemical Engineers Handbook, eighth ed., McGraw-Hill, New York, 2008.
[10] L. Moody, N. Princeton, Trans. ASME (Novermber 1944), 671–678.
[11] C.F. Colebrook, J. Inst, Civil Eng. London 11 (1939) 138–156.
[12] S.W. Churchill, Chem. Eng. 84 (1977) 891.
[13] P.R.H. Blasius, Das Aehnlichkeitsgesetz bei Reibungsvorgangen in Flüssigkeiten, Forschungsheft 131 (1913) 1–41.
[14] O. Levenspiel, Engineering Flow and Heat Exchange, Plenum Press, New York, 1984.
[15] E. Achenbach, Exp. Therm. Fluid Sci. 5 (1995) 17.
[16] S. Ergun, Chem. Eng. Prog. 48 (2) (1952) 89.
[17] G.G. Brown, Unit Operations, first ed., Wiley, USA, 1950.
[18] C.Y. Wen, Y.H. Yu, AIChE J. 12 (1966) 610.
[19] W.K. Lewis, E.R. Gilliland, W.C. Bauer, Ind. Eng. Chem. 41 (1949) 1104.

[20] M. Leva, Fluidization, McGraw-Hill, New York, 1959.
[21] D. Kunii, O. Levenspiel, Ind. Eng. Chem. Process Des. Dev. 7 (1968) 481.
[22] G.G. Stokes, Trans. Cambridge Philos. Soc. 9 (1851) 8–106.
[23] J.M. McDonough, Introductory Lectures on Turbulence, University of Kentucky, Lexington, KY, 2007.www.engr.uky.edu/acfd/lctr-notes634.pdf (June 4, 2012).
[24] J.O. Hinze, Turbulence, McGraw-Hill, New York, 1959.
[25] G.T. Chapman, M. Tobak, in: D.L. Dwoyer et al., (Ed.), Theoretical Approaches to Turbulence, Springer-Verlag, 1985, p. 19.
[26] J.W. Deardorff, J. Fluid Mech. 41 (1970) 453.
[27] T.V. Boussinesq, Mém. Prés. Acad. Sci., third ed., vol. XXIIII, Paris, 1877.
[28] L. Prandtl, Z. Angew. Math. Mech. 5 (1925) 136.
[29] B.E. Launder, D.B. Spalding, Mathematical Models of Turbulence, Academic Press, London, 1972.
[30] H. Schlichting, K. Gersten, Boundary Layer Theory, eighth ed., McGraw-Hill, New York, 2000.
[31] D.C. Wilcox, Turbulence Modeling for CFD, DCW Industries Inc., La Canada, 1993.
[32] V. Yakhot, S.A. Orszag, S. Thangam, T.B. Gatski, C.G. Speziale, Phys. Fluids A 4 (1992) 1510.
[33] A.N. Kolmogorov, J. Fluid Mech. 13 (1962) 82.
[34] J. Smagorinsky, Mon. Weather Rev. 91 (1963) 99.
[35] P. Sagaut, Large Eddy Simulation for Incompressible Flows, Springer, Berlin, 2001.
[36] M.N. Ozisik, Heat Conduction, John Wiley & Sons, New York, 1993.
[37] Y.S. Touloukian, Thermophysical Properties of Matter, vols. 1–2, IFI/Plenum, New York, 1970.
[38] F.P. Incropera, D. DeWitt, Fundamentals of Heat and Mass Transfer, fifth ed., Wiley, New York, 2002.
[39] E. Kreyszig, Advance Engineering Mathematics, John Wiley & Sons, New York, 2006.
[40] M.T. Heisler, Trans. ASME 69 (1947) 227.
[41] S. Patankar, Numerical Heat Transfer and Fluid Flow, Hemisphere Publishing Corporation, USA, 1980.
[42] N. Chvorinov, Giesserei 27 (1940) 177.
[43] L. Prandtl, in: A. Krazer (Ed.), Conference: Verhandlungen des dritten internationalen Mathematiker-Kongresses in Heidelberg 1904, Teubner, Leipzig, Germany, 1905, p. 484.
[44] J.D. Anderson, Phys. Today 58 (2005) 42.
[45] R. Hilpert, Forsch. Geb. Ingenieurwes. 4 (1933) 215.
[46] S.W. Churchill, M. Bernstien, J. Heat Transfer 99 (1977) 300.
[47] S. Whitaker, AIChE J. 18 (1972) 361.
[48] W. Ranz, W. Marshall, Chem. Eng. Prog. 48 (1922) 141.
[49] W.M. Kays, Trans. ASME 77 (1955) 1265.
[50] H.Z. Hausen, VDI Beih. Verfahrenstech. 4 (1943) 91.
[51] R.K. Shah, A.L. London, Laminar Flow Forced Convection in Ducts, Academic Press, New York, 1978.
[52] R.H.S. Winterton, Int. J. Heat Mass Transfer 41 (1998) 809.
[53] E.N. Sieder, G.E. Tate, Ind. Eng. Chem. 28 (1936) 1429.
[54] M.S. Bhatti, R.K. Shah, Handbook of Single-Phase Convective Transfer, Wiley-Interscience, Hoboken, NJ, 1987(Chapter 4).
[55] R.H. Norris, Augmentation of Convective Heat and Mass Transfer, ASME, New York, 1970.
[56] R.A. Seban, T.T. Shimazaki, Trans. ASME 73 (1951) 803.
[57] A. Cramb (Ed.), The Making, Shaping and Treating of Steel, 11th ed., Association for Iron & Steel Technology, 2003.
[58] L. Rayleigh, Philos. Mag. 1 (1876) 257.
[59] S.W. Churchill, H.H.S. Chu, Int. J. Heat Mass Transfer 18 (1975) 1323.
[60] J.R. Lloyd, W.R. Moran, J. Heat Transfer 96 (1974) 443.
[61] E. Radziemska, W.M. Lewandowski, Appl. Energy 68 (2002) 347.
[62] S.W. Churchill, H.H.S. Chu, Int. J. Heat Mass Transfer 18 (1975) 1049.
[63] S.W. Churchill, in: G.F. Hewitt (Exec. Ed.), Heat Exchanger Design Handbook, Section 2.5.7, Begell House, New York, 2002.
[64] M. Planck, The Theory of Heat Radiations, Dover Publications, New York, 1959.
[65] M.F. Modest, Radiative Heat Transfer, Academic Press, California, 2003.
[66] H.C. Hottel, A.F. Sarofim, Radiative Transfer, McGraw-Hill, New York, 1967.
[67] B. Leckner, Combust. Flame 19 (1972) 33.